Modeling Paleorecharge on the Yucatan Peninsula, Mexico

by

Stephanie Van Pelt

B.Sc., Simon Fraser University, 2015

Thesis Submitted in Partial Fulfillment of the
Requirements for the Degree of
Master of Science

in the

Department of Earth Science

Faculty of Science

© Stephanie Van Pelt 2016

SIMON FRASER UNIVERSITY

Summer 2016

Approval

Name: **Stephanie Van Pelt**

Degree: **Master Science (Earth Sciences)**

Title: ***Modeling Paleorecharge on the Yucatan Peninsula, Mexico***

Examining Committee: **Chair:** Dr. Doug Stead
                                       Professor

Dr. Diana Allen
Senior Supervisor
Professor

Dr. Karen Kohfeld
Supervisor
Associate Professor

Dr. Dirk Kirste
External Examiner
Associate Professor

Date Defended/Approved: August 15, 2016

Abstract

The decline of the Mayan Civilization is thought to be caused by a series of droughts that affected the Yucatan Peninsula during the Terminal Classic Period (TCP) 800-1000 AD. This study modeled groundwater recharge for the TCP and the historical period (1979-2005). Precipitation was reconstructed using proxy data for the Yucatan Peninsula. Drought periods were identified, but the annual time scale for the proxy data precluded their use for recharge modeling. A daily time series representative of the TCP climate was thus generated using a novel backward shift factor approach using output from the Community Climate System Model Version 4 (CCSM4). Shift factors (for precipitation and temperature) were applied to observed precipitation data for recharge modeling. Average annual recharge was 1.7% higher during the TCP, and the majority of this higher recharge occurred during the wet season. These changes indicate the Yucatan Peninsula may have been susceptible to dry season droughts.

Keywords: recharge; paleoclimate; proxy data; climate change; shift factors; Yucatan Peninsula

Acknowledgements

Table of Contents

List of Tables

List of Figures

Chapter 1.   Introduction

1.1. Study Context

Once the most powerful civilization in Mesoamerica, the Mayan civilization suffered a massive population decline during a 150-year series of droughts during the Terminal Classic Period (TCP) (800-950 C.E.). Previous studies have found evidence of drought using paleoproxy studies (Curtis, 1998; Curtis et al., 1996; Hodell et al., 1995; Hodell et al., 2005a; Medina-Elizalde et al., 2010; Stahle et al., 2011). This drought period is thought to be the result of interactions between climate cycles, such as the El-Niño Southern Oscillation (ENSO), the Pacific Decadal Oscillation (PDO), and Atlantic Multi-decadal Oscillation (AMO). If dry phases occurred in more than one of these climate cycles at one time, this may have resulted in an amplified dry period and caused enough strain on the environment that the Mayans became unable to support themselves. These climate cycles still exist on the Yucatan Peninsula, causing annual precipitation in the area to vary naturally by nearly 600 mm/year on average (Gondwe et al., 2010). If droughts did occur during the TCP due to natural climate variability, similar climate conditions are likely to occur again in the future climate.

The idea of droughts during the TCP was first introduced and accepted by Gunn and Adams (1981), who suggested that the periods of global warming seen in paleoclimate records corresponded to periods of dryness on the Yucatan Peninsula, and that major growth and decline periods of the Mayan civilization coincided with cool and warm phases of global temperatures. However, Dahlin (1983) states that the idea of climatic changes affecting the Maya civilization was first introduced by Huntington (1917), but was refuted by numerous climatologists who stated there was little evidence of climatic changes on the Yucatan Peninsula. The relationship of culture and climate was further explored by Folan et al. (1983), who compared archaeological evidence of wet and dry periods to the timing of global warm and cool phases. That study found that

1

development of some of the major cities on the Yucatan, such as Chichen Itza, occurred during wet, cool phases, and that evidence of large changes in the lake levels on the Yucatan suggested that the amount of precipitation on the Yucatan varied widely. While many of the cities studied showed evidence of growth during cool periods and decline during warm, dry periods, some cities (such as Chichen Itza, La Quemada, Monte Alban, and Cholula) appear to have survived during the dry period that is thought to have occurred during the TCP (Gunn and Adams, 1981).

The first lake sediment core used to reconstruct the past climate on the Yucatan Peninsula was analyzed in Hodell et al. (1995). This record of the oxygen isotope composition of shell carbonates combined with the density of the lake sediment was used to infer changes in the moisture conditions on the Yucatan, and provided evidence of dry periods during the TCP. Since then, numerous studies of proxy records from the Yucatan Peninsula claim to show evidence of dry conditions occurring on the Yucatan at the time (e.g. Curtis, 1998; Curtis et al., 1996; Hodell et al., 1995; Hodell et al., 2005a; Medina-Elizalde et al., 2010; Stahle et al., 2011).

This study will use existing paleoproxy records to attempt to quantify precipitation amounts during the TCP for the Yucatan Peninsula, Mexico. Output from General Circulation Models (GCMs) will be used to reconstruct a daily climate record spanning the TCP, with the ultimate goal of using this paleoclimate time series to model the recharge conditions that would have existed during the period. This paleorecharge model will be compared to a recharge model representing the current climate conditions, to determine if recharge on the Yucatan Peninsula has changed between these two periods. The results of this research can be compared to future climate projections for the Yucatan Peninsula as a means to inform water management under future climate scenarios, as well as be compared to the published proxy records from the Yucatan Peninsula in order to explore the possibility of droughts during the TCP.

1.2. Background

Paleoproxy studies

Numerous studies have examined the paleoclimate of the Yucatan Peninsula and the surrounding areas using paleoclimate indicators to reconstruct temperature or precipitation. Medina-Elizalde et al. (2010) used the $\delta^{18}O$ record of a speleothem (stalagmite) found in northwest Yucatan Peninsula to reconstruct precipitation spanning the past 1500 years. In order to reconstruct precipitation from speleothem $\delta^{18}O$, the temperature of formation was assumed to be stable. The reconstructed precipitation record was significantly correlated to the annual observed precipitation from a composite precipitation record of three stations on the Yucatan Peninsula (from 1965-1995), indicating that the speleothem $\delta^{18}O$ produced a reasonable record of past precipitation. The speleothem recorded changes in the moisture conditions on the Yucatan, including a dry period from 810 to 938 C.E., with rainfall amounts up to 52% less than the current annual mean precipitation. The high resolution of the speleothem during the TCP shows that the drought period may have consisted of a series of up to eight droughts, separated by relatively wet conditions (Medina-Elizalde et al, 2010).

This evidence is supported by the results of other paleoclimate studies in the area. Analysis of sediment cores from Lake Chichancanab in the central Yucatan Peninsula concluded that a dry period existed from 800 to 1000 C.E. The study used the abundance of calcite and gypsum in the sediment to determine the past ratios of evaporation to precipitation, assuming that a high evaporation to precipitation (E/P) ratio occurred during periods of high aridity, which corresponded to a high amount of gypsum compared to calcite (Hodell et al, 1995). A follow up study by Hodell et al. (2005a) looked at the density record of a sediment core, also from Lake Chichancanab, to obtain a higher resolution climate record. That study revealed that the dry period experienced during the TCP was not a 150 year "mega-drought", as was previously thought, but a series of droughts alternating with wetter periods that occurred about every 50 years, similar to the conclusions made by Medina-Elizalde et al. (2010).

These studies both seem to correlate well with another sediment core study from Lake Punta Laguna on the eastern Yucatan Peninsula. The $\delta^{18}O$ in ostracods and

gastropods in the lake sediments were analysed to determine the E/P ratio (Curtis et al., 1996). The analysis of $\delta^{18}O$ in ostracods and gastropods assumes that the shells of the organisms, which are composed of calcite, formed in isotopic equilibrium with the lake water, and that the lake water $\delta^{18}O$ composition is dependent on the amount of evaporation, which is considered to be a proxy for moisture conditions (Heaton et al., 1995). The authors observed that the period from 585 to 1391 C.E. had the highest oxygen isotope values of the entire record, with peaks at 862, 986, and 1051 that alternated with slightly wetter periods. Again, this evidence supports a period of aridity during the Mayan collapse (Curtis et al., 1996).

The above studies are considered by Medina-Elizalde and Rohline (2012) to have the most accurate dates and highest resolution of all of the reconstructed climate records for the Yucatan Peninsula. These studies had a sample resolution ranging from 1 to 28 years. Data from these studies were summarized by Medina-Elizalde and Rohling (2012), who used an isotope mass balance model to determine how a lake in the Yucatan Peninsula responded to seasonal variations in precipitation over different time periods in the paleoclimate record (Figure 1.1). The model reasonably replicated lake level variations during modern conditions. The first paleoclimate scenario caused Lake Chichancanab to run dry in 14 years, which is less time than the longest recorded drought period. However, a second scenario, which only decreased the amount of summer precipitation, was able to more accurately reflect the expected changes in Lake Chichancanab and Lake Punta Laguna. Additionally, the authors note that since in the modern climate, "light" isotope values (which represent summer precipitation) represent an absence of extreme precipitation events, the Terminal Collapse droughts could have been related to a reduction in the number of these types of summer rain events.
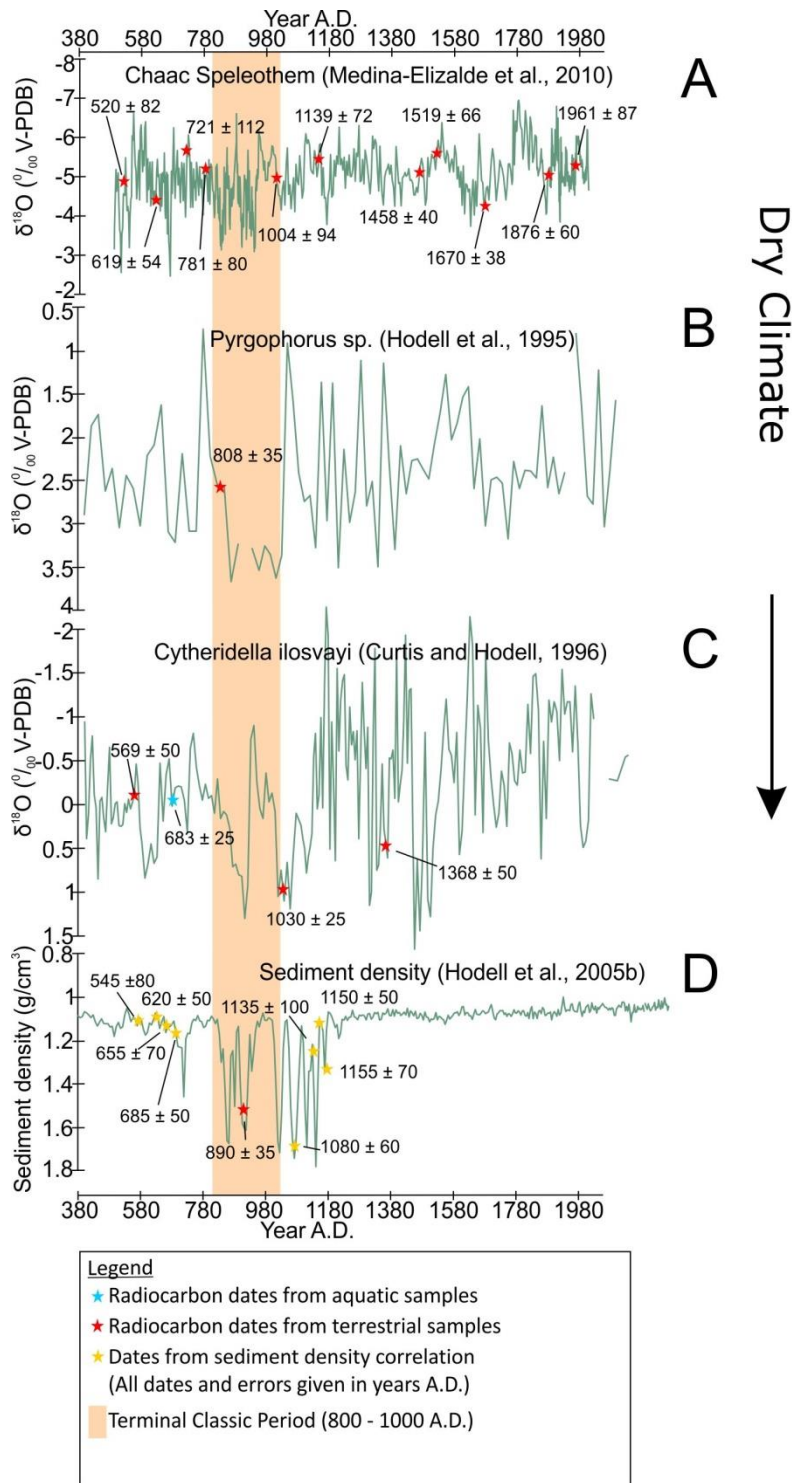
Figure 1.1   Climate proxy records for the Yucatan Peninsula from studies by (a) Medina-Elizalde et al. (2010); (b) Hodell et al. (1995); (c) Curtis et al. (1996); and (d) Hodell et al. (2005a). These records are considered the best proxy records of this period, and show similar variation in precipitation.

Fossil pollen data from the Northern Yucatan Peninsula (Tecoh cave, Ria Lagartos, and Lake Chichancanab) have also been used to reconstruct a precipitation record. Carrillo-Bastos et al. (2013) collected pollen data and used a transfer function to relate the modern environmental conditions to modern pollen samples. A transfer function was created, and used to reconstruct precipitation reasonably well for higher values of precipitation. At lower precipitation values, the model was slightly less accurate and tended to overestimate precipitation. Precipitation values reconstructed from the pollen record showed that the driest period occurred from 50 B.C. to 500 A.D. This time period is earlier than the TCP, but a drought was recorded at 800 A.D., which is in accordance with the previously mentioned studies. However, since the model overestimates lower precipitation values, the calculated reduction in precipitation was only 18%, as opposed to 36-52% recorded by the speleothem in the study by Medina-Elizalde (2012).

The Cariaco Basin (north of South America) has also been used as an analog for the Mayan Lowlands, due to the control on the climate of the Intertropical Convergence Zone (ITCZ) in both of these areas. Both the Yucatan Peninsula and the Cariaco Basin sit at the northernmost extent of the ITCZ, so the climate in both areas is thought to be affected similarly by the convective belt (Haug et al., 2001). Studies by Haug et al. (2001, 2003) in the Cariaco Basin used titanium and iron concentrations as proxies for rainfall, arguing that when the ITCZ is located over the Cariaco Basin (during the summer), higher amounts of rainfall cause terrigenous material to be carried to the coast, in runoff or in river water. Therefore, aridity would be represented in the sediment cores as low iron and titanium contents. However, this record showed that the most arid period in the Holocene was during the Little Ice Age (1400- 1750 C.E.) and not during the TCP, as determined from previous paleoclimate studies (Medina-Elizalde et al, 2010). These timing discrepancies suggest that there could be some differences in climate between the Cariaco Basin and the Yucatan Peninsula that are not controlled by the ITCZ (Haug et al., 2003).

The paleoclimate has also been reconstructed using tree rings as a proxy for the Palmer Drought Severity Index (PDSI). The PDSI is a measurement of soil moisture that is based on observed temperature and precipitation data, both of which are parameters

that affect the growth of tree rings (Stahle et al., 2011). A comparison of this tree ring reconstruction to climate cycle indices showed evidence of being influenced by the AMO, PDO and ENSO climate cycles, and found that in the modern PDSI record, June PDSI was highly correlated to ENSO (Stahle et al., 2012). Interestingly, although the record is from central Mexico (east of the Yucatan Peninsula), it appears to be correlated with the droughts of the TCP on the Yucatan Peninsula, with distinct negative PDSI values from 897 to 922 A.D, with additional droughts at 810 and 860 A.D. Inconsistencies between this record and previous proxy studies of the Yucatan could indicate that droughts during the TCP occurred throughout Mexico, but at slightly different times (Stahle et al., 2011). However, some variation in the drought dates calculated by all studies is expected, due to the differences in resolution of the proxy records, dating techniques, and responses to climatic factors (Medina-Elizalde et al., 2010).

Climate variability

The main control on Yucatan climate is the ITCZ, a belt of converging trade winds and rising air located around the equator. At its most southern point, the ITCZ lies over the Venezuelan coast, while at its northernmost point it lies over the Cariaco Basin (Haug et al., 2003). Shifts in the ITCZ cause seasonal precipitation variations; a northward shift during the summer/fall increases precipitation in the Caribbean, creating the wet season (Haug et al., 2003). Shifts in the mean position of the ITCZ, which can be inferred from iron and titanium signals in sediment cores from the Cariaco Basin, likely occur over a longer time scale as well, contributing to century-long wet and dry regimes (Haug et al., 2003).

The ITCZ is affected by the El Niño Southern Oscillation (ENSO). ENSO events typically occur every two to seven years, with warm phases (El Niño) occurring more often than cold phases (La Niña) (McPhaden et al., 2006). A typical ENSO event lasts six to eighteen months (Mantua, 2002). These events cause changes in the atmospheric and oceanic circulation in the equatorial Pacific Ocean; during the warm phase, a weakening of the northeast and southeast trade winds causes warm water of the western Pacific to migrate further east, promoting convection in the east-central Pacific (Goosse et al., 2008). During an El Niño year, the Yucatan Peninsula

7

experiences higher amounts of precipitation and slightly cooler temperatures in the Northern hemisphere winter (the dry season during neutral years). These abnormal weather patterns are caused by the movement of the ITCZ south of its regular winter position, displacing the jet stream hundreds of kilometers to the south and allowing storms to reach farther south (Pavia et al., 2006). Therefore, the timing of precipitation is affected by El Niño events, so that more precipitation falls during the winter and there is a decrease of precipitation during the summer. The Yucatan usually receives most of its precipitation during the summer, so the change in the timing of precipitation can cause mid-summer droughts (Cabrera et al., 2010). La Niña years have the opposite effect on the Yucatan, producing more rain in the summer and less in the winter, but the anomalies are somewhat less pronounced (Pavia et al., 2006).

The Pacific Decadal Oscillation (PDO) has a similar effect on Yucatan climate, but on a longer time scale, with PDO regimes lasting 20 to 30 years. Unlike ENSO, which has a neutral phase, PDO regimes are either positive or negative and are determined by sea surface temperature (SST) anomalies in the interior, northern area of the Pacific Ocean and the Pacific Coast (Mantua, 2002). PDO and ENSO interact by enhancing or cancelling out the effect of the other. For example, an El Niño year during a positive PDO regime would have more extreme climate anomalies than an El Niño year during a negative PDO regime, and would produce a year with a drier than usual summer, and a wetter winter (Pavia et al., 2006).

Other climate systems also have the potential to affect Yucatan climate. The Atlantic Multidecadal Oscillation (AMO) affects much of the Northern Hemisphere and has a cycle of about 65-80 years. The positive phase is related to high SSTs along the Pacific Coast and is coincident with a northward shift of the ITCZ, allowing for more evaporation in the North Atlantic Ocean and increased precipitation in the Caribbean Sea (Fensterer et al., 2012). The Madden Julian Oscillation (MJO) is a seasonal wave that occurs in the tropics and affects SSTs, wind speeds and direction, cloud formations, and precipitation. A MJO cycle lasts between 30 and 100 days, and stronger MJO cycles seem to occur during weak La Niña years or years where ENSO is neutral, and so can contribute to the effects of an ENSO cycle. The active phase of the MJO is characterized by a strong center of precipitation and convection that propagates

eastward in the middle Indian and western Pacific Oceans. The MJO is also one of the main drivers of monsoons in Asia, North and South America, and Australia, as well as tropical cyclone activity in the Gulf of Mexico (Zhang, 2005).

General Circulation Models and shift factors

With global climate change becoming an increasing concern, groundwater studies are increasingly focused on modeling the effects of climate change on the hydrologic cycle. General Circulation Models (GCMs) are often used in these studies to generate climate data for future climate scenarios. GCMs produce data for specified climate variables (such as temperature and precipitation), which are typically reported as relative and absolute changes from a 30-year baseline period. The baseline period coincides with the historical period (1979-2005), and the relative and absolute changes in the climate variables are reported as monthly or seasonal "shift factors".

However, GCM output cannot be used at a local scale, as large uncertainties in GCM output at regional scales can affect the reliability of the results (Hewitson et al., 2014). Regional climate projections can be generated by downscaling the GCM data to the regional scale, which can be achieved through a number of different methods. Regional climate models (RCMs) are similar to GCMs, but they operate at a higher resolution. RCMs simulate the climate at the local scale using more detailed data of the physiography of an area as well as the GCM output for that area, which allows the model to predict the local climate more accurately. Data can also be downscaled using statistical methods, using, for example, Statistical DownScaling Model (SDSM) (Wilby et al., 2002). These methods find statistical relationships between the GCM data and observed climate data and use these relationships to predict the local climate (Wilby et al., 2002). Stochastic weather generators can be used to downscale data. A stochastic weather series representing the historical period is adjusted by applying the shift factors derived from GCM data to produce a stochastic weather series representing some future time period. Stochastic weather generators can generate a long term weather series for an area that is statistically the same, albeit shifted for specific climate parameters (e.g. temperature, precipitation), as observed weather data for that area (Semenov and Barrow, 2002). Finally, shift factors may also be applied directly to an observed climate

time series, by linearly interpolating monthly shift factors between the middle of each month.

Modeling recharge

Understanding groundwater recharge is a vital component in creating a well-developed water balance of a watershed or aquifer. Recharge studies are divided into the land-surface zone, unsaturated zone, and saturated zones. Unsaturated zone studies are usually conducted for a semi-arid region such as the Yucatan Peninsula, because the unsaturated zone is generally thicker than in humid climates and because such unsaturated zone studies can be used to estimate recharge on a smaller scale than land-surface studies (Scanlon et al., 2002). Quantifying recharge can be complex, as it can vary spatially due to differences in vegetation, soil, and climate (Smerdon et al., 2010). Numerous approaches have been used to account for this spatial variability in recharge, including dividing a single watershed into recharge zones (Scibek and Allen, 2006). However, recharge can also vary temporally, as recharge rates are often directly linked to seasonal precipitation. Recharge is often estimated in terms of annual recharge rates, while in reality the majority of recharge may occur from a few large rainfall events throughout the year (de Vries and Simmers, 2002). To address the complexities associated with estimating recharge, numerical modeling approaches are being used increasingly in groundwater resource assessments or in contamination studies, although recharge modeling for groundwater resources assessments has been questioned by some, who argue that models may not accurately simulate soil moisture conditions in the unsaturated zone, which can affect recharge rates (Scanlon et al., 2002; Sorenson et al., 2014).

Numerical modeling codes for unsaturated flow calculate recharge by solving the Richards' equation, a modification of Darcy's Law created for flow through unsaturated porous media:

$$\frac{d\theta}{dt} = \frac{d}{dz}\left[K(\theta)\left(\frac{d\psi}{dz} + 1\right)\right] \tag{1.1}$$

where θ is the moisture content, t is time, z is the elevation, K is hydraulic conductivity, and ψ is the matric potential (negative pressure head or soil tension). These models are

restricted to smaller study areas, and can only consider one-directional flow down to a depth of about 15 m. Uncertainty in these models is related to uncertainty in the collected data, such as K and θ of the soil. These models are often calibrated by comparing the resulting recharge estimates to field data (Scanlon et al., 2002). Other codes, such as the United States Environmental Protection Agency's (USEPA) Hydrologic Evaluation of Landfill Performance (HELP) model (Schroeder et al., 1994), have also been used in recharge modeling (e.g. Jyrkama and Sykes, 2007; Scibek and Allen, 2006). This quasi two-dimensional model calculates the water balance for a soil percolation column. For spatial recharge, GIS methods have been used to map HELP model results based on different combinations of soils and their thicknesses (e.g. Scibek and Allen, 2006).

1.3. Research objectives

In recent years, many groundwater studies have attempted to model future recharge using the shift factor approach (e.g. Allen et al., 2004; Allen et al., 2010; Jyrkama and Sykes, 2007; Scibek and Allen, 2006). This thesis proposes that a backwards shift factor approach can be applied in the reverse sense to generate a climate time series representative of the paleoclimate of a region for input to a recharge model.

The purpose of this study is to compare historical recharge on the Yucatan Peninsula to paleorecharge. This goal will be achieved by answering two research questions, which are divided into three objectives..

Question 1: Was the paleoclimate of the Terminal Classic Period in the region of the Yucatan Peninsula different from the current climate (1980-2010)?

- Objective 1: Synthesize and compare paleoproxy data for the Yucatan Peninsula.

Question 2: Was paleorecharge different from current recharge?

- Objective 2: Produce daily climate time series for the paleoclimate, with focus on the time period from 800-1000 AD (The Terminal Classic Period).

- Objective 3: Use paleoclimate and historical climate data to simulate recharge for a watershed on the Yucatan Peninsula.

1.4. Study area

The Yucatan Peninsula is located in southeast Mexico, south of the Gulf of Mexico (Figure 1.2). The Mayans lived in an empire which covered much of Central America and extended from the Yucatan Peninsula to Guatemala and Belize, as well as parts of Honduras, El Salvador and the Mexican states of Chiapas and Tabasco (Turner and Sabloff, 2012). The northern Yucatan Peninsula, where the topography is relatively flat, is known as the Mayan Lowlands, and is the focus for this study, as well as past proxy studies.
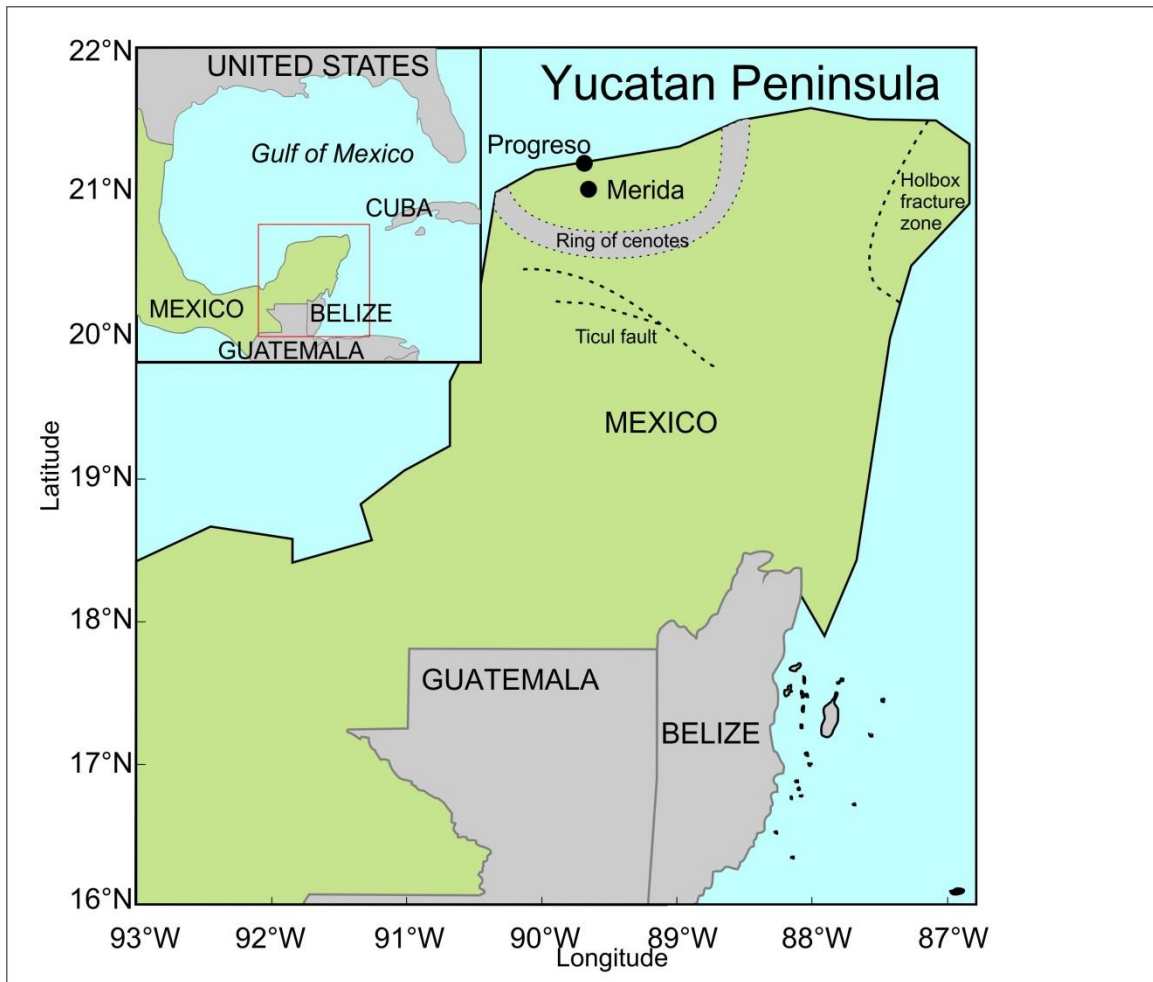
Figure 1.2   Location map of the Yucatan Peninsula. The focus of this study is on the northern half of the Yucatan Peninsula, although the Mayan empire extended south into Guatemala and Belize. Faults and fault zones are indicated with a dashed line; the Ring of Cenotes is shaded in grey with a dashed outline.

The Yucatan Peninsula is characterized by the uneven, but generally flat landscape that is typical of karst topography. Elevations gradually increase towards central Yucatan, with maximum elevations of up to 300 m found in the southern hilly karst plain (Weidie, 1985). The Yucatan Peninsula consists of over 1500 m of evaporites, limestones, and dolomites that formed throughout the Tertiary. These carbonates are overlain by Upper Cretaceous to Holocene sediments that are nearly horizontally bedded (Gondwe et al., 2010). The carbonates are highly permeable, due to both the high permeability of the limestone and the abundant fracture zones. The peninsula has two major fault zones: the Ticul fault and the Holbox fracture system,

13

which allow for the preferential movement of groundwater and mixing of saltwater and freshwater (Weidie, 1985). In the northern part of the peninsula, a thick layer of calcrete (a calcium carbonate cement, also called caliche) forms on the surface due to the alteration of exposed carbonates and acts as an aquitard (Perry et al., 2003). The calcrete precipitates where fresh groundwater discharges into the coastal saline zone (tsekel zone), as it is subjected to intense evaporation and the loss of CO_2, leading to the formation of a dense calcite (Socki et al., 2004). This calcrete layer extends out into the Gulf of Mexico, creating a higher hydraulic head at the coast. Groundwater flows either above or below this layer to reach the coast, and discharges at numerous locations into the Gulf of Mexico as submerged freshwater springs (Perry et al., 2003).

Groundwater flow is further complicated by the Ring of Cenotes, a semi-circular feature in northwest Yucatan that is thought to have formed from preferential dissolution along underlying fractures created by the Chicxulub impact crater (Perry et al., 1992). Farther away from the coast, the aquitard becomes fractured and allows for rapid infiltration. The Ring of Cenotes channels the groundwater towards the coast, such that high groundwater discharge occurs at the two points where the structure intersects the coastline, Estuario Celestun and Bocas de Dzilam. These areas remain points of high groundwater discharge despite the presence of strong ocean currents and high sedimentation rates along the shore (Perry et al., 1995).

Weathering of the pure carbonates at the surface creates little to no soil. However, a thin layer of a softer, magnesium-poor calcite, known as sascab, forms beneath the calcrete layer at the coast due to the infiltration of water (Perry et al., 2003). Soil is thickest (over 1 m) at the base of clay-lined karst depressions, known as aguadas. The thin soil cover allows water to rapidly infiltrate through the fractures in the calcrete layer, ultimately leading to the limited surface water seen on the Yucatan and high recharge rates (Perry et al., 2003). Soils throughout the Yucatan Peninsula consist of predominantly Leptosols, with some Cambisols, Luvisols, Vertisols, and Nitosols (Bautista et al., 2011).

The majority of the Yucatan Peninsula has a tropical climate, with vegetation ranging from tropical deciduous to tropical evergreen forest with savannahs at the coasts

(Bautista et al., 2011). Average annual precipitation ranges from 840 to 1500 mm per year, 75% of which falls during the wet season (May to October) in the form of tropical storms (Gondwe et al., 2010). July and August receive less precipitation than other months during the wet season (Medina-Elizalde et al., 2010). The average annual precipitation increases across the peninsula from north to south, so that the northern part of the peninsula has a semi-arid climate while the south is semi-humid (Bautista et al., 2010). The average monthly temperatures range from 23 to 27°C, and the average air temperature near Merida is 26°C (Gondwe et al., 2010; Medina-Elizalde et al., 2010).

1.5. Organization of thesis

This thesis is organized in traditional chapter format.

- Chapter 1: Introduction to the thesis, including the background, purpose and objectives
- Chapter 2: Precipitation reconstructions from paleoproxy data for the Yucatan Peninsula
- Chapter 3: Approach for producing a daily climate time series for the Terminal Classic Period
- Chapter 4: Recharge modeling
- Chapter 5: Limitations, conclusions, and recommendations
  - Appendix A: Graphs for all proxy data sets used for qualitative analysis
  - Appendix B: LARS-WG output
  - Appendix C: Recharge model sensitivity analysis
  - Appendix D: Climate variability on the Yucatan Peninsula

Two scientific papers are in preparation. Paper 1 focuses on the precipitation reconstructions described in Chapter 2, and Paper 2 integrates the methodology and results described in Chapters 3 and 4 related to the recharge modeling. Both papers will be co-authored by Drs. Allen and Kohfeld, who supervised my research.

Chapter 2.   Precipitation reconstructions from paleoproxy data for the Yucatan Peninsula

2.1. Introduction

Proxy records are useful tools for providing insight into the past climate. Climate records of the past can be inferred from terrestrial processes (such as sediment deposition) and organisms that existed during that time. For example, the amount of precipitation can be inferred from some property of the proxy that is sensitive to precipitation changes, such as $\delta^{18}O$, the ratio of calcite to gypsum in sediment, or tree growth (Curtis and Hodell, 1996; Curtis et al., 1998; Hodell et al., 1995; Hodell et al., 2005a; Hodell et al., 2005b; Medina-Elizalde et al., 2010; Stahle et al., 2011).

Multiple efforts have been made to reconstruct climate of the Yucatan Peninsula during the Terminal Classic Period (TCP, 800-1000 AD), a period of extensive droughts (Curtis and Hodell, 1996; Curtis et al., 1998; Hodell et al., 1995; Hodell et al., 2005; Hodell et al., 2005b; Medina-Elizalde et al., 2010; Stahle et al., 2011). Many of these studies have provided qualitative reconstructions of changes in precipitation and evaporation, although not all of the studies suggest the same timing and extent of drought during the TCP. The first quantitative estimate of precipitation reconstructed for the TCP was based on a statistical relationship derived using observed precipitation data from an instrumental record and the oxygen isotope ($\delta^{18}O$) composition of calcite extracted from a speleothem near Merida, Mexico (Medina-Elizalde et al., 2010). This method provided the basis for this study for reconstructing precipitation from seventeen proxy records from the Yucatan Peninsula.

Reconstructing regional climate patterns using proxy data is by nature uncertain. First, these records rarely have higher than annual resolution, and more often have measurements only every few years. Second, age determination for these records is

16

based on the development of adequate age models determined from radiocarbon dating techniques that also have uncertainty associated with them (Ohno et al., 1993). Third, establishing regional patterns depends on having an adequate spatial coverage of records. Finally, the ability to quantitatively translate environmental data into variables such as precipitation depends on statistical correlations, which can oversimplify the relationship between the proxy and climate. When put together, these uncertainties may make a proxy a useful, *qualitative* indicator of climate change, but translating proxy changes into a quantitative reconstruction may prove more challenging.

The goal of this study is to use the paleo-record to reconstruct changes in precipitation, using seventeen proxy records from the Yucatan Peninsula. Evidence from tree rings, speleothems, as well as gastropods, ostrocods and mineralogical changes found in lake sediments, was used to evaluate changes in precipitation. This comparison of the available proxy records aims to examine some of the uncertainties associated with reconstructing total annual precipitation and to determine the suitability of these proxy records for providing quantitative reconstructions of precipitation.

Available proxy data:

Previous studies on the Yucatan Peninsula have made their proxy records available, including the age models used by the authors (Table 2.1). Seventeen records, which are thought to represent changes in precipitation, were collected from six sites on the Yucatan Peninsula and surrounding areas.

Table 2.1 Proxy data collected from the Yucatan Peninsula (and surrounding area) for analysis. The locations and types of proxy are recorded for each site. The historical period refers to the modern portion of the proxy record used for precipitation reconstructions (1900-2002).

Site	Location (Latitude, Longitude)	Elevation (masl)	Type of Proxy	Proxy name	Sample resolution	Dating method	Historical data available	Source
Aguada X'Caamal*	20.60°N, 89.70°W	-	Ostracod $\delta^{18}O$	*D. stevensoni*	3-10 years	Radiocarbon	Yes	Hodell et al. 2005a
Aguada X'Caamal	20.60°N, 89.70°W	-	Gastropod $\delta^{18}O$	Chara	3-10 years	Radiocarbon	Yes	Hodell et al. 2005a
Aguada X'Caamal	20.60°N, 89.70°W	-	$\delta^{18}O$ of calcite encrusted algae	*P. coronatus*	3-10 years	Radiocarbon	Yes	Hodell et al. 2005a
Chichancanab*	19.89°N, 88.78°W	4	Ostracod $\delta^{18}O$	*Cyprinotus sp.*	17-21 years	Radiocarbon	Yes	Hodell et al. 1995
Chichancanab*	19.89°N, 88.78°W	4	Gastropod $\delta^{18}O$	*Pyrgophorus sp.*	17-21 years	Radiocarbon	Yes	Hodell et al. 1995
Chichancanab*	19.89°N, 88.78°W	4	Ostracod $\delta^{18}O$	*Physocypria sp.*	17-21 years	Radiocarbon	Yes	Hodell et al. 1995
Lake Peten-Itza (Guatemala)*	16.92°N, 89.83°W	80	Ostracod $\delta^{18}O$	*Cytheridella ilosvayi*	10-28 years	Radiocarbon and ^{210}Pb	No	Curtis et al. 1998
Lake Peten-Itza (Guatemala)*	16.92°N, 89.83°W	80	Gastropod $\delta^{18}O$	*Cochliopina sp.*	10-21 years	Radiocarbon and ^{210}Pb	Yes	Curtis et al. 1998
Lake Peten-Itza (Guatemala)*	16.92°N, 89.83°W	80	Gastropod $\delta^{18}O$	*Pyrgophorus sp.*	10-52 years	Radiocarbon and ^{210}Pb	No	Curtis et al. 1998
Punta Laguna*	20.63°N, 87.5°W	18	Gastropod $\delta^{18}O$	*Pyrgophorus coronatus*	5-24 years	Radiocarbon	Yes	Curtis and Hodell 1996
Punta Laguna*	20.63°N, 87.5°W	18	Ostracod $\delta^{18}O$	*Cytheridella ilosvayi*	5-24 years	Radiocarbon	Yes	Curtis and Hodell 1996
Chichancanab*	19.89°N,	4	Mineralogical proxy	Sulphur (%S)	16-21 years	Radiocarbon	No	Hodell et al.

Site	Location (Latitude, Longitude)	Elevation (masl)	Type of Proxy	Proxy name	Sample resolution	Dating method	Historical data available	Source
	88.78°W							1995
Chichancanab	19.89°N, 88.78°W	4	Mineralogical proxy	Calcite (%CaCO$_3$)	16-21 years	Radiocarbon	Yes	Hodell et al. 1995
Chichancanab*	19.89°N, 88.78°W	4	Mineralogical proxy	Sediment density	2-6 years	Radiocarbon	Yes	Hodell et al. 2005b
Lake Peten-Itza (Guatemala)*	17.00°N, 89.78°W	80	Mineralogical proxy	Magnetic Susceptibility	5 years	Radiocarbon	Yes	Escobar 2010
Tzabnah Cave, Tecoh	20.74°N, 89.48°W	20	Speleothem δ^{18}O	Speleothem (Chaac)	1-8 years	U-Th dating	Yes	Medina-Elizalde et al. 2010
Barranca de Amealco (Central Mexico)	19.79°N, 91.03°W	2,605	Tree Ring Reconstruction	Palmer Drought Severity Index (PDSI) reconstruction	1 year	Dendro-chronology	Yes	Stahle et al. 2011

*record removed from final precipitation reconstructions (see Section 2.3.2)

The proxy data presented in this study are used to reconstruct precipitation during the TCP. In general, $\delta^{18}O$-type proxies are sensitive to changes in the ratio between evaporation and precipitation (E/P). During dry periods, enrichment of ^{18}O in the lake water from evaporation tends to result in higher values of $\delta^{18}O$ in carbonate minerals (Curtis and Hodell, 1996; Curtis et al., 1998; Heaton et al., 1995; Hodell et al., 1995; Hodell et al., 2005a; Hodell et al., 2012; Medina-Elizalde et al., 2010). This study uses a linear regression approach to reconstruct precipitation, which assumes that the variability in each proxy record is due to changes in E/P.

Changes in temperature also influence the oxygen isotope composition of carbonate during mineral formation, with decreases in temperature resulting in higher values of the $\delta^{18}O$ of calcite (e.g. Kim and O'Neil, 1997). Since the average annual temperature over the tropics for the Holocene is thought to be relatively stable (Curtis and Hodell, 1996; Hodell et al., 2005a), this study assumes that the predominant cause of changes in $\delta^{18}O$ in carbonate proxies is related to changes in the balance of evaporation and precipitation associated with drought (and not to temperature changes). This assumption and others associated with the linear regression technique are further discussed in Section 2.3.3.

Each of the proxy records is thought to be related to E/P in different ways. For $\delta^{18}O$ proxies (ostracods/gastropods in lake sediments and speleothems), this relationship is based on the assumption that carbonate forms in equilibrium with the ambient water (lake water for shells or cave drip water for speleothems). The composition of the water in turn reflects the composition of the inputs and output of the system, which for a closed system will be only precipitation and evaporation (Hodell et al., 2005a). The speleothem record is, of course, formed in a cave instead of a lake, but is expected to reflect mean annual precipitation due to its high correlation with observed precipitation records from the Yucatan Peninsula (Medina-Elizalde et al., 2010). As discussed above, a dry period in the proxy record is reflected by an increase in $\delta^{18}O$.

The sediment density record (Hodell et al., 2005b) and the relative abundance of calcite and sulphur (%CaCO$_3$ and %S records) (Hodell et al., 1995) all use the same principle to relate them to precipitation. These proxies use two different ways to

measure the amount of gypsum ($CaSO_4$) and calcite ($CaCO_3$) to infer past changes in E/P. These are the dominate minerals found in the lake, along with celestite ($SrSO_4$), aragonite ($CaCO_3$) and dolomite ($CaMg(CO_3)_2$). In a closed system saturated with these minerals, changes in E/P affect how much of each mineral precipitates in the lake sediments. A dry climate would cause gypsum to precipitate, causing an increase in %S and a decrease in %$CaCO_3$ (Hodell et al., 1995). Gypsum is denser than calcite, so gypsum-rich layers in the sediment core are recorded as peaks in sediment density (Hodell et al., 2005b).

Magnetic susceptibility of lake sediments is similarly used to infer changes in E/P in a closed system. Escobar et al. (2010) used magnetic susceptibility to show alternating clay and gypsum units in the sediment, which corresponded to both wet and dry periods, respectively. Clay has a high magnetic susceptibility, so a decrease in precipitation is inferred in this record by a decrease in magnetic susceptibility (Escobar et al., 2010).

Finally, the PDSI record (Stahle et al., 2011) is a reconstruction of the PDSI (a measurement of soil moisture) based on tree ring growth. Tree growth from the study site is sensitive to both temperature and precipitation, so the tree ring record is correlated with PDSI, which incorporates both of these. However, to relate this record to moisture changes, the PDSI is assumed to be only correlated to precipitation. A dryer climate in the PDSI record is indicated by decreasing PDSI (negative PDSI).

Proxy data locations:

All sites are located on the Yucatan Peninsula (Figure 2.1), with the exception of the tree ring record by Stahle (2011). This particular record is from Barranca de Amealco, which is at a similar latitude to the Yucatan Peninsula but located in central Mexico. However, this record is also at a much higher elevation than the other records (2,605 masl), so this record may have recorded a much different climate than others on the Yucatan Peninsula.
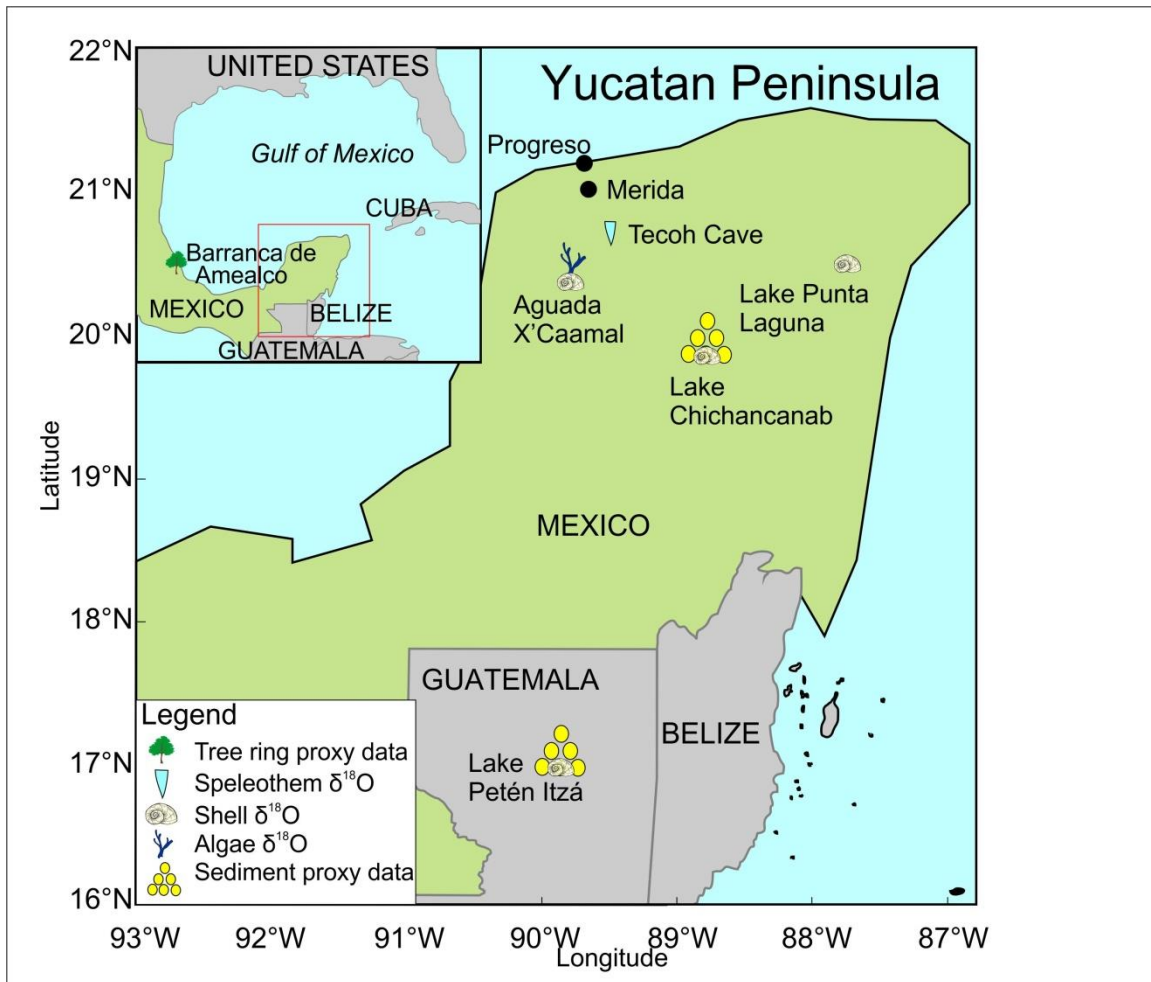
Figure 2.1   Proxy data sites from the Yucatan Peninsula. Multiple proxy data types were found for three of the sites. The composite observed precipitation record is from Merida, Merida Airport, and Progreso. The location of the tree ring record for Barranca de Amealco is shown in the inset map.

A historical record of observed total annual precipitation (the composite observed record) was supplied by Medina-Elizalde (personal communication, 2015) for comparison to the historical period of the proxy records. This record is a combined record from three climate stations on the Yucatan Peninsula (Merida airport, Merida observatory, and Progreso) due to the lack of a full dataset at either station. This record spanned the years 1900-2002.

2.2. Methodology: reconstructing precipitation

Total annual precipitation was reconstructed using a method similar to Medina-Elizalde et al. (2010). This method estimates a statistical relationship between $\delta^{18}O$ and observed total annual precipitation using the instrumental record of total annual precipitation and the modern portion of the proxy records (1900 to 2002). While none of the proxy records had recorded data for every year between 1900 and the present, as many data points as possible were used to create a linear relationship between each proxy record and precipitation. The statistical relationship between observed total annual precipitation and $\delta^{18}O$ was used to reconstruct precipitation for each proxy record (Appendix A). The $\delta^{18}O$ record of *Pyrgophorus coronatus* (Hodell et al., 2005a) is used as an example in the text.

Before estimating the statistical relationship, the $\delta^{18}O$ and the composite observed precipitation records were each smoothed using 3-year triangular smoothing. This smoothing technique takes an average of three years of data, putting more weight on the middle year (Medina-Elizalde et al. 2010). These smoothed records were used to complete a cross correlation analysis using the statistical software R (with the ccf() function), which determines the correlation between the two datasets at different lag times (Figure 2.2). The lag time with the maximum correlation was chosen as the offset between the two datasets. These lag times could be a reflection of uncertainty in the age models, or, in the case of the speleothem record, the amount of time needed for water to infiltrate into a cave and precipitate carbonate (Medina-Elizalde et al., 2010). For carbonate shells in lake sediments, it is expected that there is little to no lag time because the shells reflect the composition of the lake water at the time the shells precipitate, and the shells precipitate instantaneously. If there is a lag time for a shell record, it may suggest that outside processes have affected the $\delta^{18}O$ record.

Figure 2.2   Cross correlation results for gastropod *Pyrgophorus coronatus* δ¹⁸O and the composite observed precipitation record for 1900-2002 (annual). The lag time between datasets coincides with the highest correlation. A negative lag indicates the proxy record lags behind precipitation. The actual lag time is given in years. Correlation is significant at ± 0.5 as shown by the blue horizontal dashed lines.

For the regression analysis, the lag time was incorporated by offsetting either the precipitation or proxy record by the specified lag time. In cases where the lag time was zero, the datasets were left as is. Two proxy records (the speleothem record by Medina-Elizalde et al., 2010 and the PDSI record, Stahle et al., 2011) had an annual resolution during both the historical period and the TCP, meaning that annual proxy data and annual precipitation data were available for the cross correlation and regression analyses. The sample resolutions of all other records during the historical period and the TCP were greater than one year and varied between 2-6 years (sediment density, Hodell et al., 2005b) and 10-52 years (*Pyrgophorus sp.*, Curtis et al., 1998). The subannual resolution in these records means that the actual lag time (in years) was greater than the lag time unit determined from the cross correlation analysis. For example, for *Pyrgophorus coronatus*, the lag time unit was -4, but the sample resolution during the historical portion of the record was 5-6 years (Table 2.2). This means that the δ¹⁸O record actually lagged behind the precipitation record by 22 years. A negative lag time indicates the proxy record is lagged behind the precipitation records (for example, if

24

the lag time is -22, the $\delta^{18}O$ of precipitation in the year 1900 is recorded in the proxy record in the year 1922).

Lag times from the cross correlation analyses range from -22 to +17 years. The majority of lag times were negative, indicating the proxy record was lagged behind the precipitation record. Two of the records had positive lag times (*Pyrgophorus sp.* and *Physocypria sp.*, Hodell et al., 1995), but both of these records had only two modern data points, which may have led to an inaccurate relationship between the proxy and precipitation (as it is impossible for the proxy to reflect the precipitation of a year that has not occurred yet). As mentioned previously, lag times of fossil shell proxies are expected to be 0 or close to 0 years, as fossil shells precipitate instantaneously and reflect the oxygen isotope composition of the lake water they formed in. All fossil shell records had a lag time of 0, with the exception of the *P. coronatus* record (Hodell et al., 2005a), which had a lag time of 22 years. This anomalous lag time could be a result of outside factors affecting the isotopic composition of the lake. The Chara record, which is a calcite encrusted algae record, had a lag time of -6. While this record is an oxygen isotope type record, its oxygen isotope composition may have been controlled by more than just the lake water, as it is formed near a photosynthesizing algae (discussed in Section 2.3.2). The sediment density, magnetic susceptibility, PDSI, and speleothem records all had negative lag times (ranging from -3 to -10 years). These lag times could be related to the process of formation of these proxies, as mentioned above. Although the lag times are dependent on the age models of the proxy records, which themselves have uncertainties (Section 2.3.3), the general agreement in the fossil shell proxies and the negative lag times of the sediment, speleothem, and tree ring proxies all suggest that these are reasonable lag times for these proxy records.

The lagged datasets were then used to create a scatterplot with a linear trendline in MS Excel (Figure 2.3). The regression equation was then used to calculate precipitation (y) from the proxy record value (x) for any year that had a recorded proxy value. At this step, any proxy records that did not have modern data (1900-present) had to be eliminated from the precipitation reconstructions because they could not be used for this method. The average difference between the two datasets was characterized using the Root Mean Squared Error (RMSE) according to:

$$RMSE = \sqrt{\frac{\sum(\text{calculated precipitation}-\text{observed precipitation})^2}{\text{Number of years with proxy data value}}} \qquad (2.1)$$

Table 2.2   **Calculated precipitation using *Pyrgophorus coronatus* δ^{18}O. Bold records indicate those that were used due to the lag time (for example, the 1903 precipitation would be correlated with the 1925 δ^{18}O, which is a lag time of four measured values).**

Year	Smoothed precipitation	Smoothed δ^{18}O	Calculated precipitation
1903	**566**	0.98	961
1908	**795**	0.54	903
1914	**1113**	0.47	893
1920	**845**	-0.01	830
1925	**1050**	**-0.99**	700
1931	**925**	**-0.78**	728
1937	**895**	**0.52**	900
1942	**1048**	**1.14**	982
1948	**978**	**0.99**	962
1953	**991**	**0.84**	943
1959	**874**	**0.94**	955
1965	1018	**1.17**	986
1970	934	**1.04**	969
1976	1018	**0.92**	953
1981	923	**1.30**	1003
lag =	**-22**		
RMSE =	**164 mm/year**	**R^2 =**	**0.47**
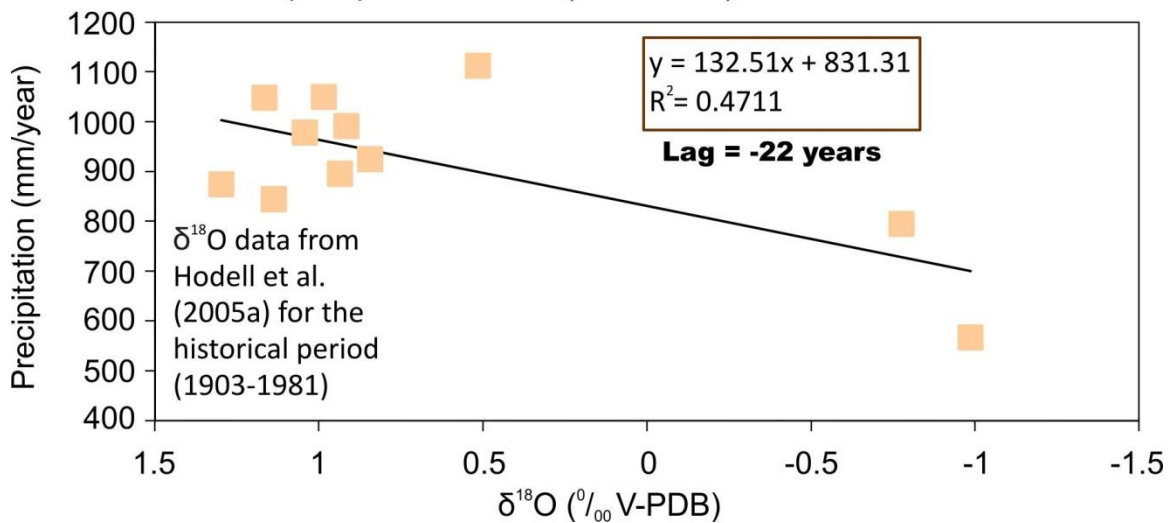
Figure 2.3 Scatterplot and the linear regression of *Pyrgophorus coronatus* δ¹⁸O and the historical precipitation record (1900-2002). The actual lag time is shown in bold. The resulting linear equation is used to calculate annual precipitation for any year where *Pyrgophorus coronatus* δ¹⁸O data are available at this site.

Three criteria were used to determine if the reconstructions produced realistic precipitation values for the Yucatan Peninsula. These criteria were:

- No negative precipitation values throughout the reconstructions;

- No calculated annual precipitations of over 2000 mm/year for more than one year during the proxy record, which would be exceptionally high compared to the modern total annual precipitation for the Yucatan Peninsula, which ranges from 840 to 1500 mm/year (Gondwe et al., 2010);

- A minimum of five data points available for the period 1900-present.

The records that met these criteria were compared to the composite observed annual precipitation record for the period 1981-2004 (Medina-Elizalde, personal communication, 2015).

Finally, the linear equations for each proxy record were used to extrapolate precipitation back to the TCP using the proxy data from the pre-modern period (pre-1900).

2.3.   Results and discussion

2.3.1.   Qualitative comparison of proxy data

Various types of proxy data were used in the proxy data analysis, and each record had a different resolution and time span (data types shown in Figure 2.1). The important similarity between all of the datasets is that the proxies are thought to represent changes in precipitation (or the ratio of evaporation to precipitation). Less precipitation is represented in the proxy records by:

- an increase in $\delta^{18}O$
- an increase in sulphur content and corresponding decrease in $CaCO_3$ content
- an increase in sediment density
- a decrease in magnetic susceptibility
- a decrease in PDSI

A comparison of all collected records from the Yucatan shows that not all of the records agree on the timing or even the existence of, droughts during the TCP (Figure 2.4). The discussion below focuses on those records for which measurements have been made during the TCP.

Six records show evidence of drought conditions during the TCP. These records show distinct troughs in the proxy record (in Figure 2.4), which appear to be considerably different from the later times in the record or include the lowest troughs in the record. The highest $\delta^{18}O$ values in the Chaac speleothem record by Medina-Elizalde et al. (2010) actually precede the TCP and occur years 500 and 600 A.D. (Figure 2.4L), although longer periods of high $\delta^{18}O$ values during the TCP could also indicate droughts. Similarly, the Chara algae record (Hodell et al., 2005a) shows peaks in $\delta^{18}O$ during the TCP, although the highest $\delta^{18}O$ values recorded occur circa 1200AD (Figure 2.4J). Overall higher $\delta^{18}O$ values in the *Pyrgophorus coronatus* record (Curtis and Hodell, 1996) could also indicate droughts (Figure 2.4P). The mineralogy proxy record by Hodell et al. (1995) shows a significant increase in sulphur content and a decrease in $CaCO_3$ during the TCP (Figure 2.4N, Figure 2.4O), and the sediment density record

(Hodell et al. 2005b) shows distinct peaks in sediment density during and after the TCP, which is indicative of a reduction in precipitation (Figure 2.4C). .

Four of the records show periods of aridity around the TCP but not during it. The *Pyrgophorus sp.* record by Hodell et al. (1995) (Figure 2.4Q), the *Cytheridella ilosvayi* record by Curtis et al. (1998) (Figure 2.4A), the *Cochliopina sp.* record by Curtis et al. (1998) (Figure 2.4D), and the *Cytheridella ilosvayi* record by Curtis and Hodell (1996) (Figure 2.4H) all show a distinct increase in $\delta^{18}O$ at the end of the TCP (just after 1000 A.D.), although uncertainty in the age model could place these events during the TCP.

The remaining seven records show no conclusive evidence of drought during the TCP or do not have enough data during the TCP to analyze this time period. The $\delta^{18}O$ of *Physocypria* (Figure 2.4G) and *Cyprinotus sp.* (Figure 2.4M) records (Hodell et al., 1995) have few data during the TCP which prevents them from being useful for this time period. The magnetic susceptibility (Escobar, 2010) (Figure 2.4E), $\delta^{18}O$ of *D. stevensoni* (Figure 2.4K) and *P. coronatus* (Hodell et al., 2005a), and PDSI (Stahle et al., 2011) records show no significant evidence of drier climate during the TCP. These records may show some variations in climate during the TCP, but all have much more distinctive troughs throughout different portions of the record, suggesting that the variations that occur during the TCP are not out of the ordinary range of moisture conditions. The PDSI record (Stahle et al., 2011) may be different because it is not located directly on the Yucatan Peninsula, which would suggest that the Terminal Classic droughts were localized over the Yucatan (Figure 2.4I). As mentioned earlier, this record is also at a higher elevation, and may have a cooler climate than the records found directly on the Yucatan Peninsula. The *P. coronatus* (Hodell et al., 2005a) record is an exception because it has no evidence of drier periods until after the TCP, around 1500 A.D. to the present time (Figure 2.4F). In fact, the $\delta^{18}O$ of *Pyrgophorus sp.* (Curtis et al., 1998) record actually seems to indicate a wetter climate during the TCP, followed by fluctuations between wet and dry climates (Figure 2.4B). These disagreements between the proxy records highlight the need for higher resolution proxy data, as well as emphasize the complexity of the proxy records themselves. While conceptually each of these proxies is connected in some way to changes in precipitation, other factors may

affect the relationship between precipitation and the proxy records (discussed in Section 2.3.3).
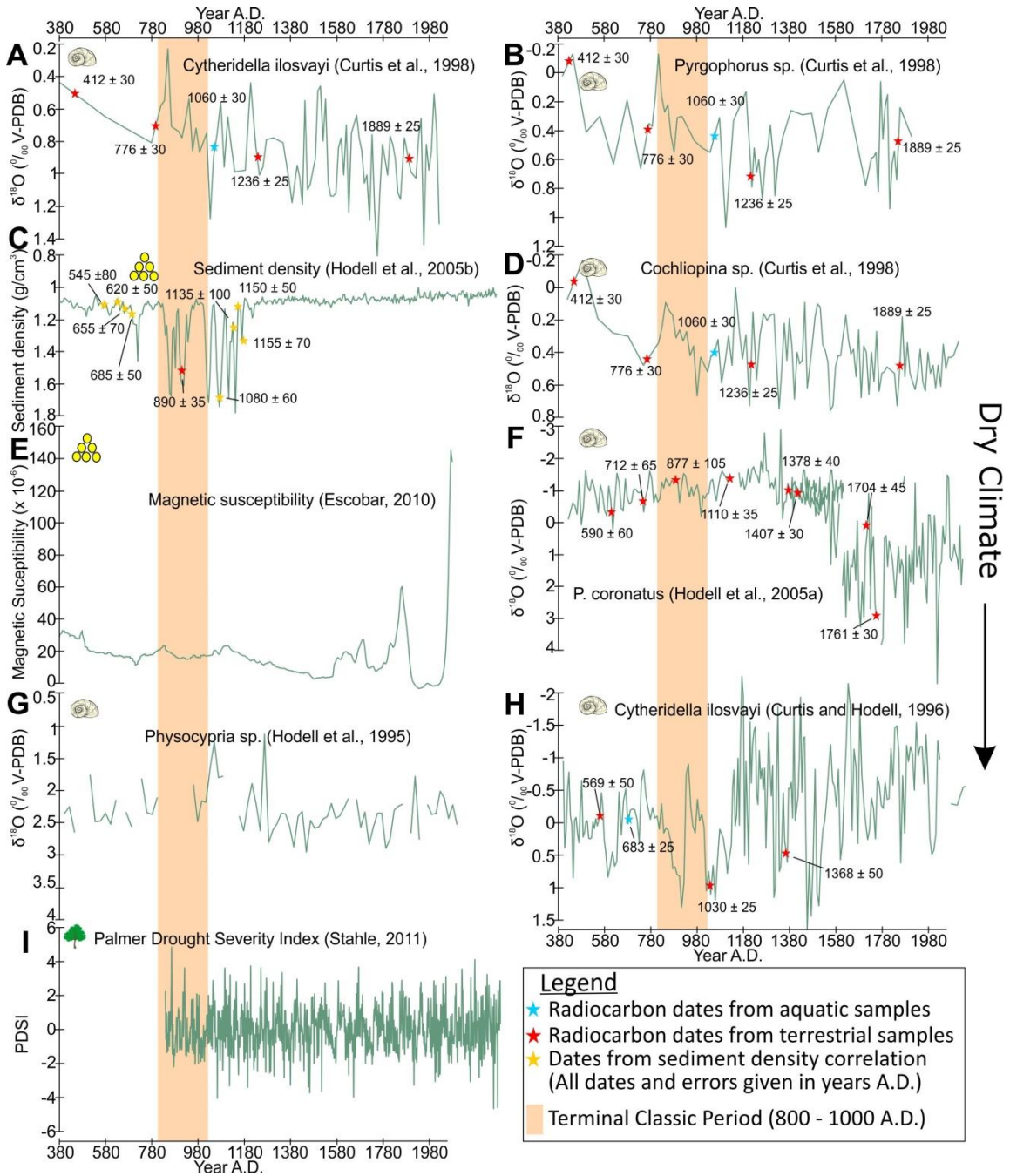
Figure 2.4 A-I. Comparison of all proxy records from 380 A.D. to the present. δ¹⁸O records are indicated by a shell, sediment related proxy records with a mountain, speleothems with an inverted triangle, encrusted algae with seaweed, and tree rings with a tree. The Terminal Classic Period in shaded in peach, and the age dates used by the authors to create the age model for the proxy are indicated with stars. The arrow on the right side shows the tendency for a record to indicate a dry climate.

31
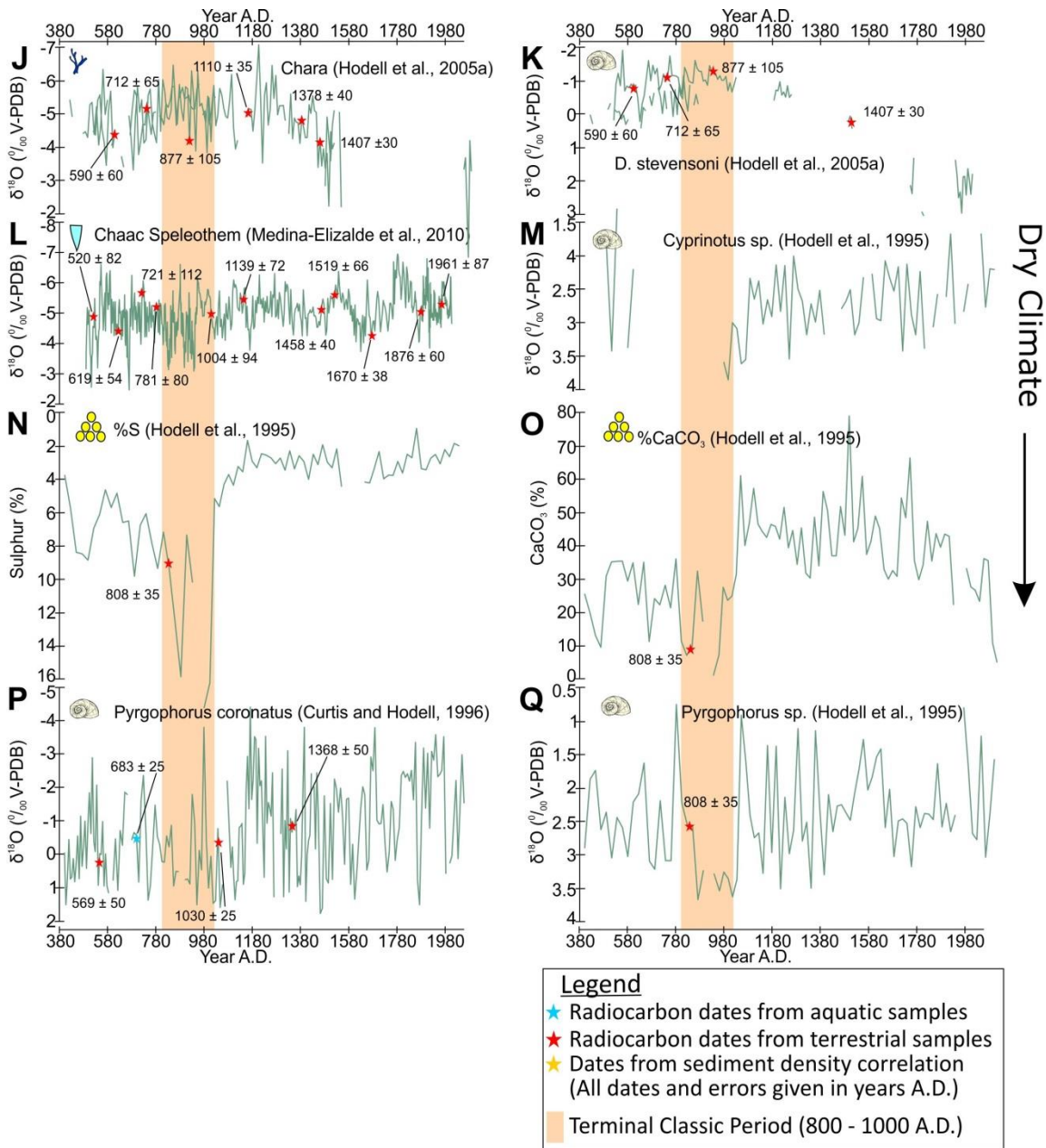
Figure 2.4 **J-Q. Comparison of all proxy records from 380 A.D. to the present.** δ¹⁸O records are indicated by a shell, sediment related proxy records with a mountain, speleothems with an inverted triangle, encrusted algae with seaweed, and tree rings with a tree. The Terminal Classic Period in shaded in peach, and the age dates used by the authors to create the age model for the proxy are indicated with stars. The arrow on the right side shows the tendency for a record to indicate a dry climate.

2.3.2. Reconstructed precipitation

The linear equations found for each proxy record are summarized in Table 2.3. These equations were used to reconstruct total annual precipitation during the TCP for each year where a measurement was available.

Table 2.3 **The linear regression equations for all of the proxy records that were not eliminated. The correlation with the observed precipitation record (1900- 2002) was characterized using R^2 values and the RMSE. n indicates the number of data points for each proxy that fell within the range 1900-2002. For each record, precipitation was calculated for its entire range.**

Author	Equations	R^2	RMSE (mm/year)	Range (mm/year)	Date	n	Lag
Hodell 2005a	*P. coronatus*: y = 132.51x + 831.31	0.4	164	346-1500	1903-1981	11	-4
	Chara: y = -73.99x + 769.26	0.58	70	769-1391	1925-1953	5	-1
Hodell et al. 1995	%CaCO3: y = 3.0663x + 812.98	0.30	30	812-1126	1909-1959	4	0
Escobar 2010	Magnetic susceptibility: y = 1.8942x + 806.7	0.34	143	781-1144	1904-1934	6	-1
Stahle et al. 2011	PDSI: y = -35.893x + 936.29	0.10	135	801-1092	1901-2001	99	-10
Medina-Elizalde 2010	Chaac: y = -198.04x – 48.482	0.45	142	439-1326	1966-1994	29	-7

Eleven reconstructions were removed that did not meet the precipitation criteria for the Yucatan Peninsula. These records were:

- *D. stevensoni* (Hodell et al., 2005a)
- % Sulphur, *Pyrgophorus sp.*, *Physocypria sp.*, and *Cyprinotus sp.* (Hodell et al., 1995)
- Sediment density (Hodell et al., 2005b)

- *Pyrgophorus coronatus* and *Cytheridella ilosvayi* (Curtis and Hodell, 1996)
- *Cochliopina*, *Cytheridella ilosvayi* and *Pyrgophorus sp.* (Curtis et al., 1998)

Three records had no modern data that could be compared with observed precipitation: *Cytheridella ilosvayi* (Curtis et al., 1998), *Pyrgophorus sp.* (Curtis et al., 1998), and % Sulphur (Hodell et al. 1995). Of the other eight records that were excluded, six only had two modern data points: *Pyrgophorus coronatus* and *Cytheridella ilosvayi* (Curtis and Hodell, 1996), *D. stevensoni* (Hodell et al., 2005a), and *Pyrgophorus sp.*, *Physocypria sp.*, and *Cyprinotus sp.* (Hodell et al., 1995). *Cochliopina* (Curtis et al., 1998) had five modern data points, but it was excluded because it calculated negative precipitation values.

The final record removed (sediment density, Hodell et al., 2005b) had sufficient data points during the historical period (31 points), but the range of variability during the historical period was extremely small compared to that during the TCP (a range of approximately 0.1 g/cm^3 near the present compared to a range of nearly 0.8 g/cm^3 during the TCP). Since the linear relationship between total annual precipitation and sediment density was based solely on the modern portion of the record, this dramatic change in variability could mean that sediment density reacted to precipitation differently during the TCP or that some outside factor affected the record during this time. As a result, the modern portion of the record is likely not a good indicator of the past portion of the record. This no-analog situation likely resulted in the negative values for precipitation that were calculated using the statistical relationship.

Observed precipitation today shows that average annual precipitation ranges from 750 and 1500 mm/year, with the majority of years ranging from 850 to 1250 mm/year (Figure 2.5). Combined, the precipitation reconstructions for the TCP have a range of approximately 550 to 1250 mm/year during the TCP. The range of individual reconstructions varies, with the speleothem record (Medina-Elizalde et al., 2010) having the greatest range. The remaining records have ranges of approximately 200 years or less, indicating that they do not represent the annual precipitation variability on the Yucatan Peninsula very well.

The Chara record (Hodell et al. 2005a) was not eliminated, but has a median annual precipitation of 1200 mm/year, which is 200 mm/year above the median of the composite observed record. The higher average annual precipitation is likely a result of the higher $\delta^{18}O$ composition of the *Chara* carbonate. This is likely caused by algae photosynthesis occurring next to the precipitating carbonate, which results in a reduction in the CO_2 of the lake water directly next to the algae and prevents the carbonate from forming in equilibrium with the lake water (Hodell et al., 2005a).

Two of the proxy records (the speleothem record, Medina-Elizalde et al. 2010; the PDSI record, Stahle et al., 2011) were used to reconstruct precipitation for the historical period (1981-2010) as they had data for this period. Both of the historical reconstructions have a lower range compared to their TCP counterparts, which is likely an effect of the smoothing of the record due to the linear approach used to reconstruct precipitation. The median annual precipitation of the speleothem record (Medina-Elizalde et al., 2010) is approximately 75 mm/year lower during the TCP than during the historical period (although some years have higher annual precipitation during the TCP), which indicates that in general there was less precipitation during the TCP. In contrast, the PDSI record (Stahle et al., 2011) has a very similar median annual precipitation during both periods (a decrease of less than 25 mm/year). However, this record is not located directly on the Yucatan Peninsula, and therefore may have less evidence of the TCP droughts.

Only one proxy reconstruction (the *Chara* record) shows a median annual precipitation during the TCP that is higher than that of the composite observed record. As mentioned previously, this record may have anomalously high precipitation values because the carbonate of this record may not have formed at equilibrium with the lake water. The remaining records, then, show moisture conditions similar to the observed climate (the PDSI record, %$CaCO_3$ record, and the magnetic susceptibility record) or dryer conditions than the observed record (the speleothem record and the *Pyrgophorus coronatus* record, Hodell et al., 2005a). While these records do suggest droughts may have existed during the TCP, they do not provide conclusive evidence of a widespread drought on the Yucatan Peninsula. This interpretation differs from that of previous

studies, which inferred TCP droughts from all of these records and claimed that climate change was a driving factor in the collapse of the Mayan civilization.
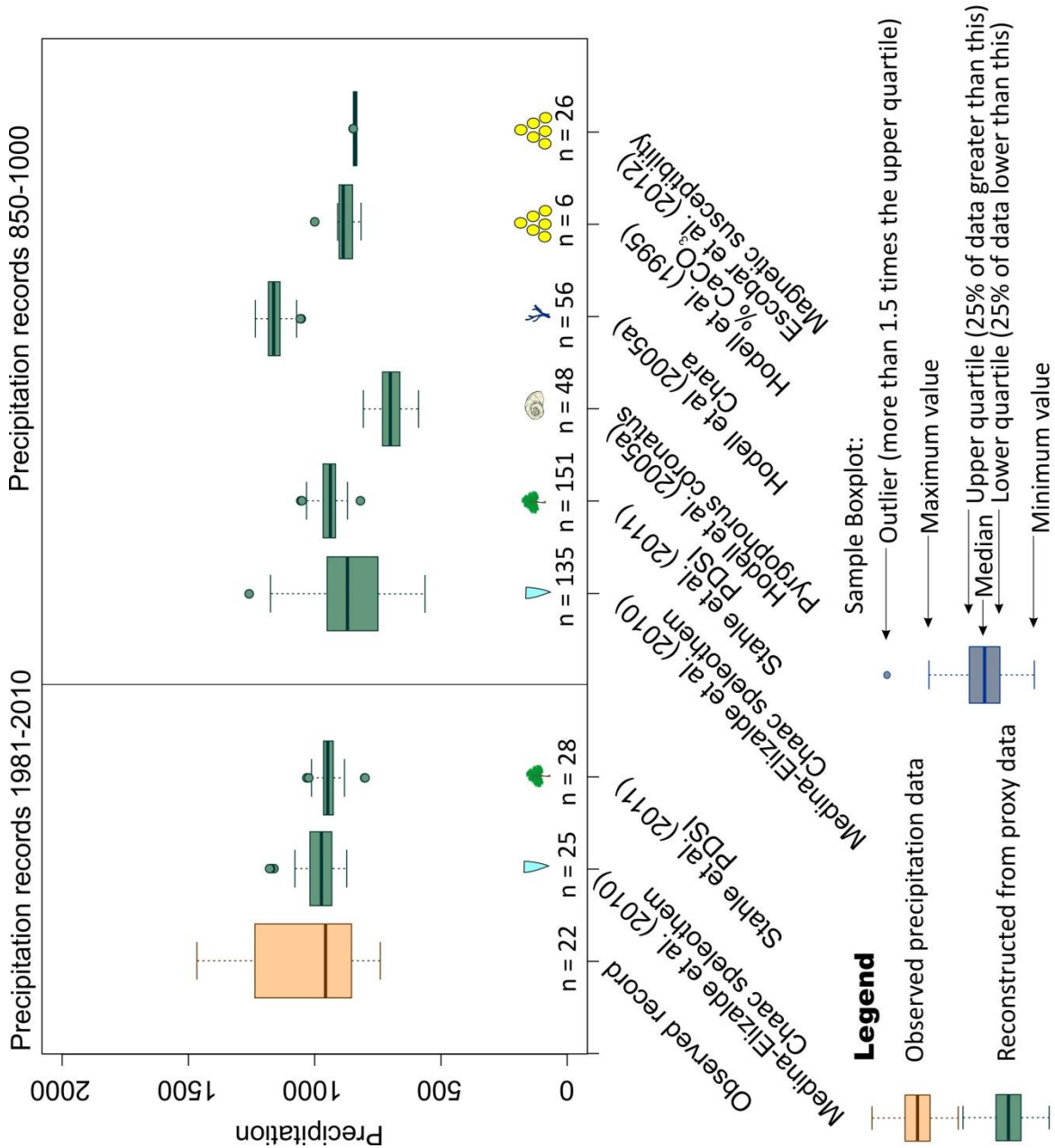
Figure 2.5 Average annual precipitation calculated by the proxy records (excluding eliminated records) compared to observed average annual precipitation. Proxy records with modern data were compared for the period 1981- 2004, while remaining proxy records were compared for 850-1000 AD to represent the TCP. Only one record has annual resolution for the entire record (Stahle et al., 2011). The number of data points within the TCP and modern record (n) is shown for each record.

A comparison of the two modern reconstructions and the composite observed record show that the proxy reconstructions do not faithfully record all of the years with dryer conditions (Figure 2.6). Both the PDSI reconstruction and the speleothem reconstruction have reduced variability compared to the composite records, and both records are lagged behind the precipitation record (the PDSI record has a lag of 10 years, while the speleothem record has a lag of 7 years). None of the distinct troughs in the precipitation record are clearly observed in either of the reconstructions; however, the peak in precipitation around 1993 is also distinctly seen in the speleothem record 7 years later (around 2000), and the peak in 1887 can also be observed in the PDSI record 10 years later (around 1997). Overall, these two proxy reconstructions seem to represent the average precipitation conditions during the historical time period, and not distinct drought events. If the same relationship is true in the TCP reconstructions, a significant change in the average precipitation of the reconstructions could be evidence of drought.
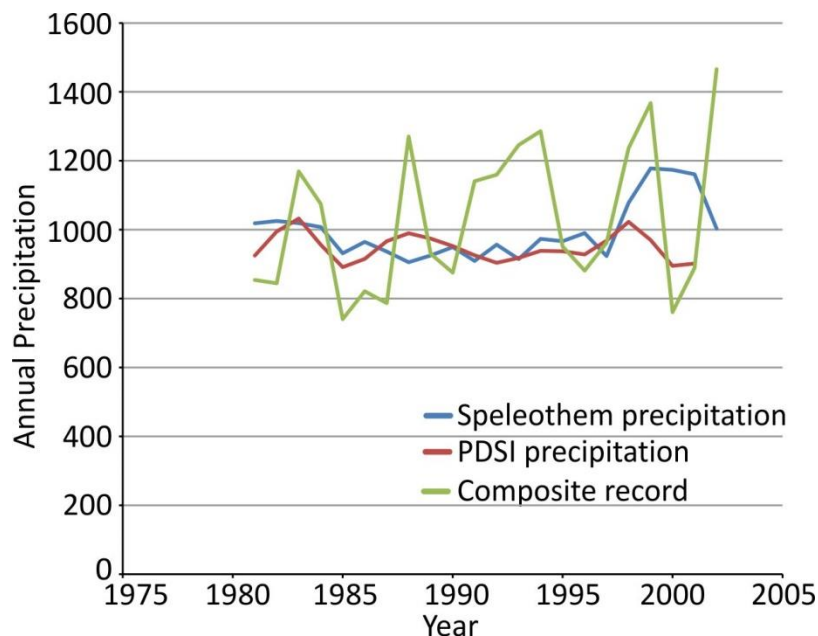
Figure 2.6   **Annual precipitation of the two modern precipitation reconstructions (the speleothem record and the PDSI record) compared to the composite observed record for the period 1981-2002.**

While the six reconstructions have similar average annual values to the observed precipitation record, one of the reconstructions showed the opposite relationship between precipitation and the proxy record than expected (Figure 2.7). The *P.*

coronatus record (Hodell et al., 2005a) produced an equation with a positive slope, while the other δ^{18}O-type proxies produced equations with negative slopes (Table 2.3). This positive slope indicates that precipitation increases with higher δ^{18}O values, which is opposite to the expected trend for δ^{18}O proxies. As mentioned earlier, the poor relationship between the proxy and precipitation could be a result of having a lower number of modern data points (11 data points compared to 99 modern data points in the PDSI record), resulting in a reconstruction that is not representative of the Yucatan climate.
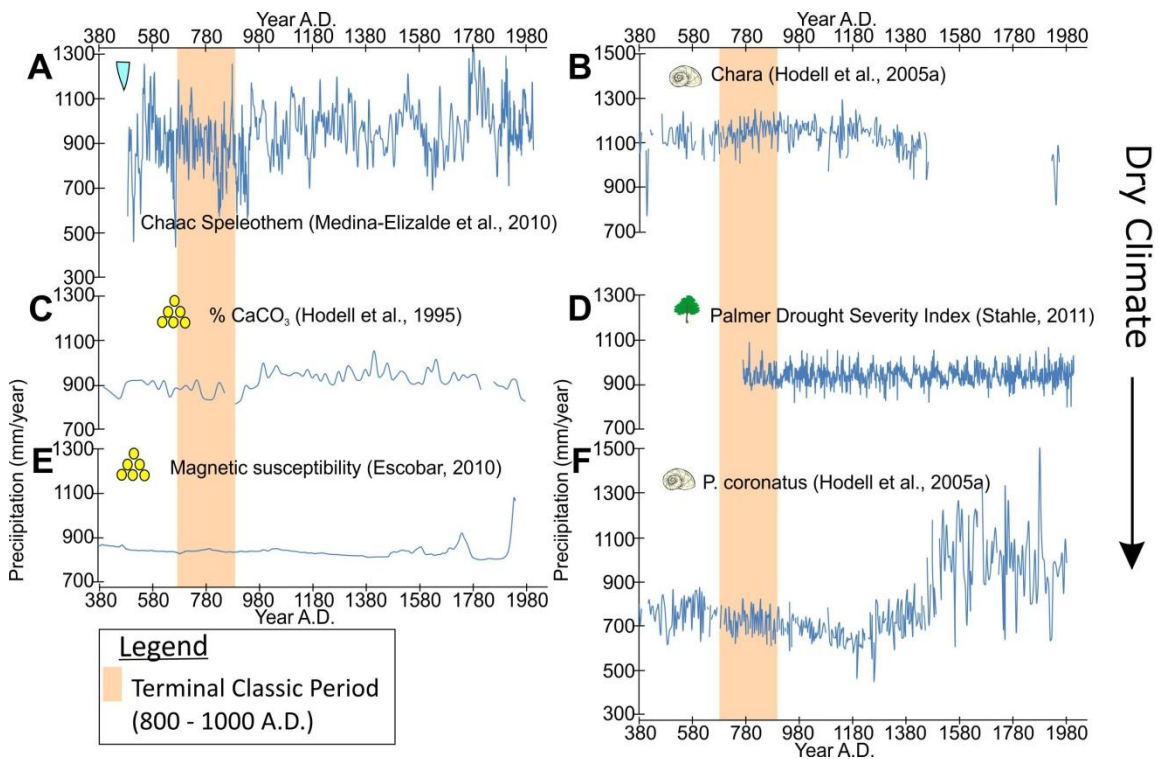
Figure 2.7   **Reconstructed precipitation records for the years 380 A.D. to present. The arrow on the right side indicates the tendency for dry climate and the peach shading highlights the TCP. Note that the P. coronatus record (Hodell et al., 2005) shows a precipitation trends opposite to that shown in Figure 2.4.**

2.3.3.   Assumptions and uncertainty

There are a number of sources of uncertainty in the proxy records. The first is the original age model used to establish the exact chronologies for each record. The age models generated for the records used in this study are based on radiocarbon

dates, the identification of marker beds, or layer counting. These age ties are used to create a time-depth relationship (Ohno et al., 1993), based on linear interpolation between each datum (Kohfeld and Harrison, 2000; Telford et al., 2004). Radiocarbon dating has inherent uncertainty (±25 to 112 years in the collected proxy records from the Yucatan Peninsula), and using a model to interpolate between these points carries this uncertainty into the age model as well (Breitenbach et al., 2012). Additionally, the calculation of radiocarbon years assumes that the ratio of $^{14}C/C$ ratio in the atmosphere has remained constant, although this ratio is known to have varied over the past 1000 years (Stuiver, 1980), causing a discrepancy between the radiocarbon age and calendar age time scales and increasing the uncertainty in the age dates. Secondly, radiocarbon dating is based on the assumption that the carbon being dated formed in equilibrium with the atmosphere; in the case of carbonates formed in lakes, this assumption is not necessarily true, which can lead to anomalous ages known as the "freshwater reservoir effect" (Broecker and Walton, 1959; Philippsen, 2013). Third, linear models assume that there is no change deposition rate (for lake sediments) between the radiocarbon dated points and that the sediment has been undisturbed. The effects of bioturbation would cause sediments of different ages to be mixed, which could lead to an incorrect depth-age relationship. Fourth, the growth rate of shells is assumed to be constant throughout time, and vital effects caused by the different formation processes of each fossil species are ignored (although some others attempt to use only one species and adult specimens to reduce vital effects (eg. Curtis et al., 1996). Finally, using statistical relationships between instrumental measurements and proxy data to reconstruct precipitation assumes that the relationship between observed precipitation and the proxy record does not change over time. If the relationship has changed, the proxy may not be useful for paleoclimate reconstructions as the modern relationship between precipitation and the proxy is not representative of the relationship in the past.

For all $\delta^{18}O$ records, the statistical relationships established between $\delta^{18}O$ and total annual precipitation also assume that the temperature and composition of the water in which the shell (or speleothem) formed has remained stable over time. All of the analyzed shell carbonate studies assumed that the samples were formed in closed-basin

lakes and aguadas[1], which are hydrologically disconnected from the groundwater (Curtis and Hodell, 1996; Curtis et al., 1998; Hodell et al., 1995; Hodell et al., 2005a). This assumption implies that no large sources of water with different $\delta^{18}O$ compositions or different temperatures are being added to the system, and that the main control on the $\delta^{18}O$ of the water is changes in the ratio of evaporation to precipitation (E/P). The temperature of these types of lakes then reflects the mean annual temperature of the atmosphere, which is thought to have been relatively stable over the Holocene (Curtis and Hodell, 1996). The speleothem study by Medina-Elizalde et al. (2010) similarly assumed a constant temperature, as the cave that the speleothem formed in has a stable mean annual air temperature of 26°C. However, the assumption that the temperature was stable introduces uncertainty into the oxygen isotope proxy records, as the temperature of formation does affect $\delta^{18}O$. Kim and O'Neil (1997) found the relationship between the fractionation factor (between calcite and water) and temperature to be:

$$1000 ln\alpha_{(calcite-water)} = 18.03(10^3 T^{-1}) - 32.42 \qquad (2.2)$$

Rearranging, the relationship between temperature and $\delta^{18}O$ of seawater is (Kohfeld, 1998):

$$\delta^{18}O_{calcite(PDB)} = \frac{T(°C)}{4.97} + (0.99973 * \delta^{18}O_{w(SMOW)} - 0.27) \qquad (2.3)$$

This equation suggests that for every degree decrease in temperature, there is a 0.2‰ increase in $\delta^{18}O$. Because dry periods are recorded in these proxy records as an enrichment in $\delta^{18}O$, the apparent periods of drying in the proxy record could also be partly attributed to cooler periods that occurred throughout the proxy record. Output from GCMs suggest that the temperature may have been up to 1.2°C cooler during the TCP (see Chapter 3), which would correspond to a 0.24‰ increase in $\delta^{18}O$. For the oxygen isotope proxy records with a low range in $\delta^{18}O$ (1-2‰), this may cause an apparent drying in the proxy record. For example, a 0.24‰ change in $\delta^{18}O$ in the

[1]aguada: a sinkhole lake that is sealed off from the aquifer by organic matter or a clay layer at the base of the lake (Flores-Nava, 1994).

speleothem record (Medina-Elizalde et al., 2010) would cause an apparent decrease in precipitation of 48 mm/year.

Thus, the nature of climate reconstructions has inherent uncertainty due to the low resolution of proxy data and uncertainty in dating techniques. Known uncertainty in the reconstructions raises the question of whether certain precipitation records are more reliable than others due to higher uncertainties associated with some proxies as well as differences in degree of uncertainty associated with the age model from each record. Some records can be identified has have higher-quality age models based on the total number of dated samples bracketing the TCP or their use of more-reliable, high resolution methods of dating. For instance, the speleothem (Medina-Elizalde et al., 2010) and PDSI (Stahle et al., 2011) records have 29 and 99 dates respectively, compared to the *Pyrgophorus sp.*, *Physocypria sp.*, and *Cyprinotus sp.* (Hodell et al., 1995) records, the *Pyrgophorus coronatus* and *Cytheridella ilosvayi* (Curtis and Hodell, 1996) records, and the *D. stevensoni* (Hodell et al., 2005a) record, which only have 2 modern dates to constrain them. More confidence should be placed in the reconstructions with more age ties to constrain the age model; this logic is already used by paleo-databases to rank the reliability of age models (Farrera et al., 1999; Kohfeld et al., 2013; Pickett et al., 2004; Street-Perrott et al., 1989). Furthermore, the PDSI record (Stahle et al., 2011) also would have more reliable age dates as tree rings can be counted annually. However, as noted earlier, the PDSI record (Stahle et al., 2011) is not located directly on the Yucatan Peninsula, and therefore may not have recorded the Terminal Classic droughts associated with the Yucatan Peninsula.

Better precipitation reconstructions also likely come from records that had more data points in the modern portion of the record, as the linear relationships used to reconstruct total annual precipitation were based on these points only. By this measure, the most accurate reconstructions would be from the speleothem record (Medina-Elizalde et al., 2010), the sediment density record (Hodell et al., 2005b), and the PDSI record (Stahle, 2011). However, the sediment density record had to be eliminated because the 7-fold change in density between modern and TCP time periods suggests that processes other than precipitation were controlling this proxy. Thus, the speleothem and PDSI records will be given more weight in further analysis (Chapter 3).

2.4. Conclusions

The qualitative comparison of available proxy data from the Yucatan Peninsula confirms that 10 of 17 proxy records have qualitative evidence of the Terminal Classic droughts. The records with the most conclusive evidence of drought during the TCP are:

- speleothem $\delta^{18}O$ (Medina-Elizalde et al., 2010)
- Chara $\delta^{18}O$ (Hodell et al., 2005a)
- Pyrgophorus coronatus $\delta^{18}O$ (Curtis and Hodell, 1996)
- % $CaCO_3$ and %S (Hodell et al., 1995)
- sediment density (Hodell et al., 2005b)

While the timing of these events is not coherent between these records, such as dry periods occurring after the TCP, there is enough uncertainty in the radiocarbon age dates, and subsequently the age models (up to 112 years) that could place the dry events within the TCP. Records that show periods of drought occurring near the TCP are:

- Pyrgophorus sp. $\delta^{18}O$ (Hodell et al., 1995)
- Cytheridella ilosvayi $\delta^{18}O$ and Cochliopina sp. $\delta^{18}O$ (Curtis et al., 1998)
- Cytheridella ilosvayi $\delta^{18}O$ (Curtis and Hodell, 1996)

The seventeen proxy records were also used to reconstruct precipitation for the Yucatan Peninsula based on the approach used by Medina-Elizalde et al. (2010). Precipitation reconstructions were eliminated if: (a) they had less than five modern data points (1900 to present); or (b) they did not produce a reasonable representation of the modern-day climate, which was indicated by negative precipitation values or annual precipitation values over 2000 mm/year. Six of 17 reconstructions met these criteria.

Two of the records (the speleothem record and the PDSI record) were used to reconstruct both modern and TCP precipitation. From these two records, decreases in precipitation of up to 200 mm/year can be seen during the TCP (speleothem record, Medina-Elizalde et al., 2010: see Figure 2.7).

Uncertainty in the precipitation reconstructions is brought in from uncertainty in the age model of each proxy record. However, a failure to produce a reasonable precipitation reconstruction (based on the elimination criteria) is not necessarily the result of a poor age model, but a lack of data from the modern portion of the observed precipitation record. Creating a linear relationship between the proxy record and the precipitation record that represents the climate depends on having modern proxy data measurements, and the confidence in a reconstruction increases with more modern data points.

This analysis showed that the most confidence can be placed in the PDSI record (Stahle, 2011) and the speleothem record (Medina-Elizalde et al., 2010). However, other records produced similar mean annual precipitation values which should not be discounted. The majority of the reconstructed precipitation records produced a mean annual precipitation that was within the range of the observed mean annual precipitation on the Yucatan Peninsula today. However, only two records had median annual precipitation values that were less than composite observed record during the TCP. Those two proxy records provide evidence supporting the theory of TCP droughts, but the remaining records suggest that climate conditions during the TCP were similar to today's climate. Overall, these results do not provide conclusive evidence of TCP droughts.

Chapter 3.   Approach for producing a daily climate time series for the Terminal Classic Period

3.1. Introduction

As discussed in Chapter 1, one goal of this study is to generate daily paleoclimate data that can be used for recharge modeling in the Yucatan study region. The original intent was to use the paleoclimate data to infer the climate of the Yucatan during the Terminal Classic Period (TCP). However, all of the proxy records discussed in Chapter 2 gave annual estimates of precipitation, and in numerous cases the resolution of the proxy records was lower than annual for much of the record. A second dataset was also examined as a possible representation of the paleoclimate. The PaleoR dataset is the product of a project that aims to create a global paleoclimate reanalysis dataset based on proxy data (Goodwin et al., 2013; Goodwin et al., 2014). However, this dataset was not used because the earliest time period of the dataset (1000-1020 AD) was not constrained by any proxy data on the Yucatan Peninsula, and it was thought that this would not produce an accurate representation of the paleoclimate for this study. Due to the limitations of the proxy datasets, an alternative approach was needed.

General Circulation Models (GCMs) are numerical models that simulate global climate, including parameters such as precipitation, temperature, solar radiation, and humidity. Although daily output is available from these GCMs, using this output directly for climate studies does not account for any uncertainty or bias that may be found in the models. Moreover, these models are too coarse to reproduce the climate at a local or regional scale, and require downscaling to project local climates (discussed in Chapter 1).

The downscaling approach used in this study is a stochastic weather generator in combination with shift factors derived from the GCMs. For future climate change studies, monthly (or seasonal) shift factors for key climate parameters, such as temperature, precipitation and humidity, are derived from GCM output from a baseline model (for example 1981-2010) and a future scenario (such as 2040-2069 to represent the 2050s for a particular future emissions scenario). The same GCM is used for both model runs.

The weather generator used in this study is the Long Ashton Research Station Weather Generator (LARS-WG) (Racsko et al., 1991). LARS-WG uses precipitation, minimum and maximum temperature, and solar radiation to generate a time series that is different than that of the input data, but that has the same statistical distribution (Semenov and Barrow, 2002). Unlike earlier stochastic weather generators, LARS-WG is based on the length of wet and dry days to incorporate variability into the model. This means that the other parameters, such as temperature and precipitation, are dependent on the series of wet and dry days as opposed to the other way around (Racsko et al., 1991). The model calculates the statistical characteristics of each climate variable (temperature, precipitation, solar radiation, and wet and dry series) in a climate record, and uses these statistics to generate a new baseline climate time series representative of the observational record. This baseline climate time series can then be perturbed using shift factors, creating a climate time series that represents a different time period (Section 3.2.3). While using the length of wet and dry series was the motivation for using LARS-WG, this study was unable to use them to calculate shift factors due to reduced variability in the model output (see Section 3.3.1, Appendix B).

In this study, a novel backward shift factor approach is employed using output from a baseline model (1979-2005) and a paleoclimate model (850-1000 AD) to generate backward shift factors for the TCP (Table 3.1). These shift factors were applied using two approaches: (1) application of shift factors using the stochastic weather generator, and (2) application of shift factors directly to observed data in order to reconstruct a daily time series of the climate during the TCP. The implications of using both methods are discussed in this chapter, as well as the limitations of using a stochastic weather generator.

Table 3.1   Climate records and definitions used to create reconstructions of the TCP climate.

Terminology	Definition
Composite observed climate record	The annual climate record from Medina Elizalde (2016), which is a combined record of three climate stations on the Yucatan Peninsula at Merida Airport, Merida Observatory and Progreso (1900-2002).
Daily observed data	The daily climate record from Merida Airport weather station (1995-2010).
Historical experiment	Daily climate data extracted from the CCSM4 model Historical experiment to represent the historical period (1979-2005).
Past1000 experiment	Daily climate data extracted from the CCSM4 model past1000 experiment to represent the TCP (850-1000 AD).
Historical period	The time period from 1979-2005.
Stochastic data (historical)	The 30-year daily stochastic climate series generated by LARS-WG using the daily observed climate data.
Stochastic reconstruction	The 30-year daily stochastic climate series representative of the Terminal Classic Period (TCP). Generated by LARS-WG by perturbing the baseline climate series with shift factors.
Direct shift factor reconstruction	The reconstruction of the TCP created by applying shift factors directly to the observed record from Merida Airport.
Climate normals	Climate variables averaged over a 30-year time period (represent the monthly average climate conditions).

3.2. Climate data

3.2.1.   Observed data

Two observed datasets were collected to represent the historical period. One was a composite record of annual precipitation (1900-2002), comprised of data from climate stations at Progreso, Merida Observatory, and Merida airport (Medina-Elizalde, personal communication, 2016- see Figure 3.3). This composite observed record was used in Chapter 2 to create statistical relationships between precipitation and proxy

records and for comparison to reconstructed precipitation records. The second record is a daily observed climate record (1995-2010) from Merida Airport, including minimum and maximum temperature and precipitation. Annual climate data were calculated from the daily observed record for comparison to proxy and model data. The composite observed record has a lower median value than that of the daily observed record (950 mm/year as opposed to 1200 mm/year), and the composite record has much lower variability than the daily record (Figure 3.1). The daily observed record ranges from 400 mm/year to 4700 mm/year, while the composite observed record ranges only from 750 mm/year to 1500 mm/year. In Chapter 2, the composite observed record was considered to be the best representation of the Yucatan climate as it incorporated much more of the variability in annual precipitation than the precipitation reconstructions did; however, compared to the daily observed record, it lacks the degree of variability. The larger variability in the daily observed record indicates this record incorporates more of the extreme precipitation events seen on the Yucatan Peninsula, and that these events may have been lost in the creation of the composite observed record. For this reason, the daily observed record was chosen as the most representative of the Yucatan climate for generating shift factors. This record was used to generate a 30-year stochastic weather series in LARS-WG (the stochastic data) which has the same statistical characteristics as the daily observed record (Figure 3.1). Due to the way climate series are generated in LARS-WG, the median value of annual precipitation in the stochastic data is different from the daily observed record (almost 2000 mm/year compared to 1200 mm/year). LARS-WG smooths the observed data and fits it to a normal distribution in an attempt to eliminate the influence of random events (Semenov and Barrow, 2002). The calculated average of the stochastic data is 2090 mm/year, which is only slightly higher than the calculated average of the daily observed record (1872 mm/year), indicating that LARS-WG was able to reproduce the average annual precipitation of the observed data quite well. Smoothing the data also results in reduced variability in the stochastic data with a range in annual precipitation of 900 mm/year to 2900 mm/year (excluding two outliers at 3800 and 4200 mm/year).
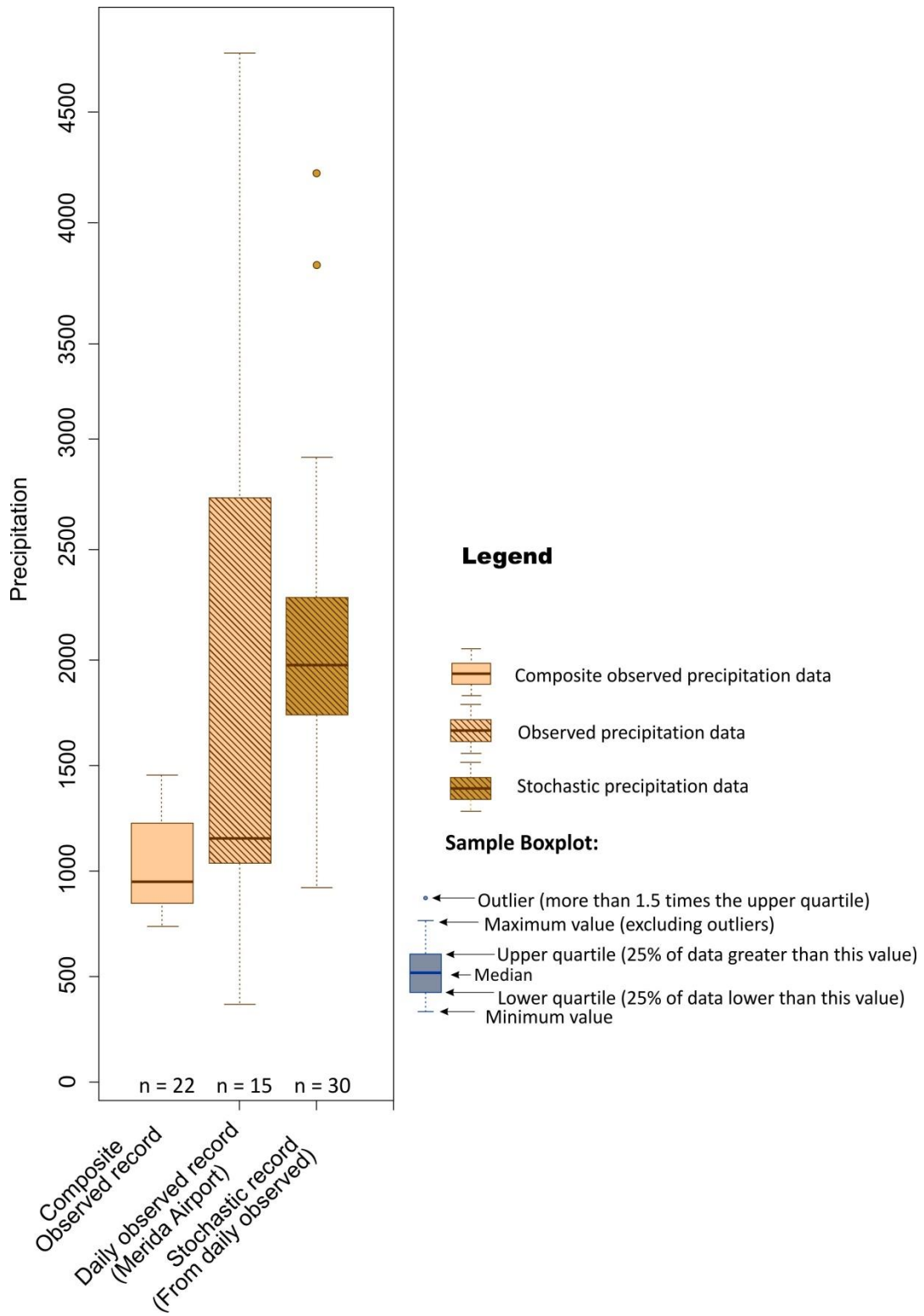
Figure 3.1 Comparison of precipitation for the composite observed record (1981-2002), the daily observed record (1995-2010), and the stochastic data for the historical period (1979-2010).

While the smoothing of the LARS-WG precipitation data is unavoidable, it does significantly alter the distribution of the annual precipitation. The distribution of the observed precipitation record is skewed to the right, while the stochastic precipitation has a normal distribution (Figure 3.2). The tail to the right of the annual observed record indicates that there are some years with high annual precipitation which cause the mean to be higher than the median. Since LARS-WG uses the mean precipitation for generating the precipitation, the resulting stochastic precipitation has a higher mean as well. This ultimately changes the median of the stochastic data because LARS-WG generates records with a normal distribution (where the mean value is the same as the median). The consequence of raising the median value of annual precipitation gives the stochastic series more years with higher precipitation than the observed data; 50% of years in the stochastic data have an annual precipitation greater than approximately 2000 mm/year, while in the observed record 50% of the data have an annual precipitation greater than approximately 1000 mm/year. This effect is likely to have implications for recharge modeling, as some studies have shown that the timing and amount of rainfall that falls in heavy rainfall events are important factors for the amount of recharge that can occur (e.g. Milehame et al., 2008; Thomas et al., 2016; Trenberth et al., 2003). The effect of different rainfall distributions will be further analyzed in Chapter 4.
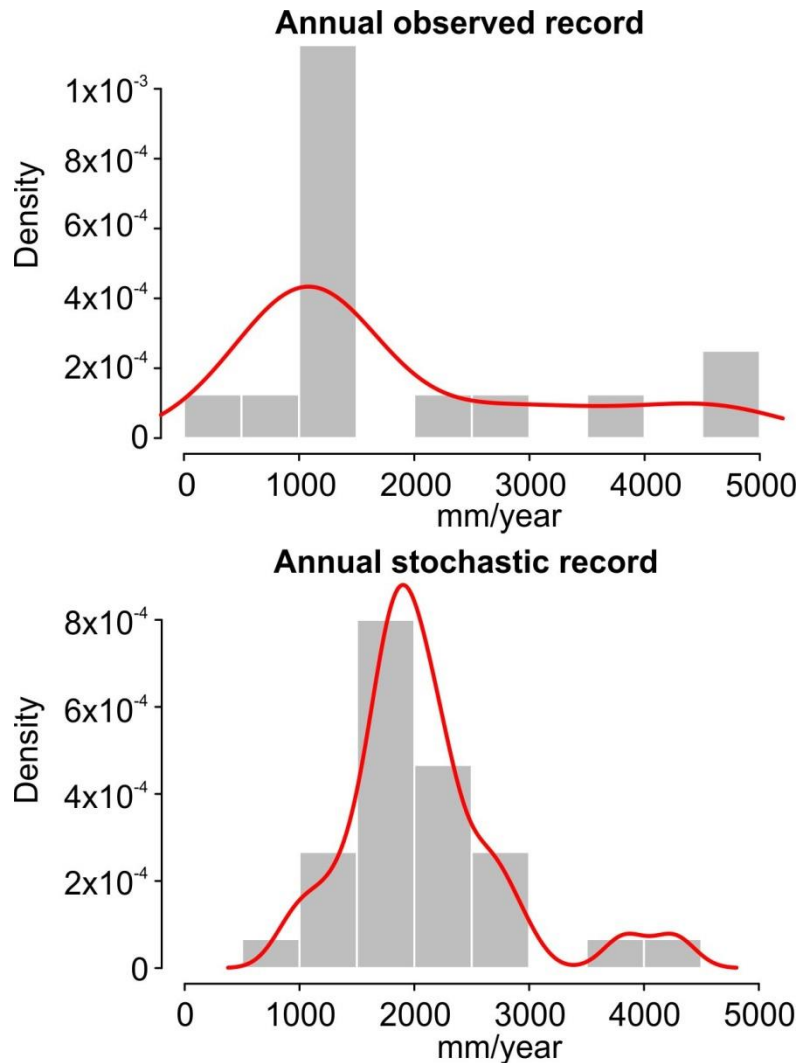
Figure 3.2   **Histogram (gray) and density plots (red) of the annual observed precipitation and annual stochastic precipitation. The density indicates the probability of an annual precipitation that falls within each bin.**

3.2.2. Model data

For this study, the Community Climate System Model Version 4 (CCSM4) model was used for both historical and the paleoclimate simulations (Table 3.2). The CCSM4 GCM is a coupled model with components for the atmosphere, land, ocean, and sea ice. It has been used to run many climate experiments, including those for the preindustrial control period, the recent past, future climate projections, and the paleoclimate (Gent et al., 2011). The CCSM4 is just one of the models being used for CMIP5, and was

chosen for this study due to the availability of model data for both the historical and paleoclimate periods. The model has a 1° resolution, with grid sizes of 1.25°X 0.9° (Gent et al., 2011). The CCSM4 model, while an improvement on previous versions, still has a number of biases and tends to overestimate precipitation (Gent et al., 2011). However in this approach, by calculating shift factors between two experiment runs in the same model, the majority of these biases are assumed to be eliminated.

Table 3.2   List of experiments and the institution that provided model output for this study.

Model experiment	Modeling Group
Historical experiment- CCSM4 model	National Center for Atmospheric Research (NCAR)
AMIP experiment- CCSM4 model	National Center for Atmospheric Research (NCAR)
past1000 experiment- CCSM4 model	National Center for Atmospheric Research (NCAR)

Data from the ESGF portal is in netCDF form, which is a common file format for climate data consisting of gridded climate data over a period of time. NetCDF files can be manipulated using NetCDF operators (NCOs), which are command-line utilities used to process netCDF files (Zender, 1995). As these files are very large, NCOs were used to extract data from all grid cells over the Yucatan Peninsula (Latitude 16-22, Longitude 268-273) and average the data from these cells, resulting in a single time series to represent the Yucatan Peninsula (Figure 3.3).
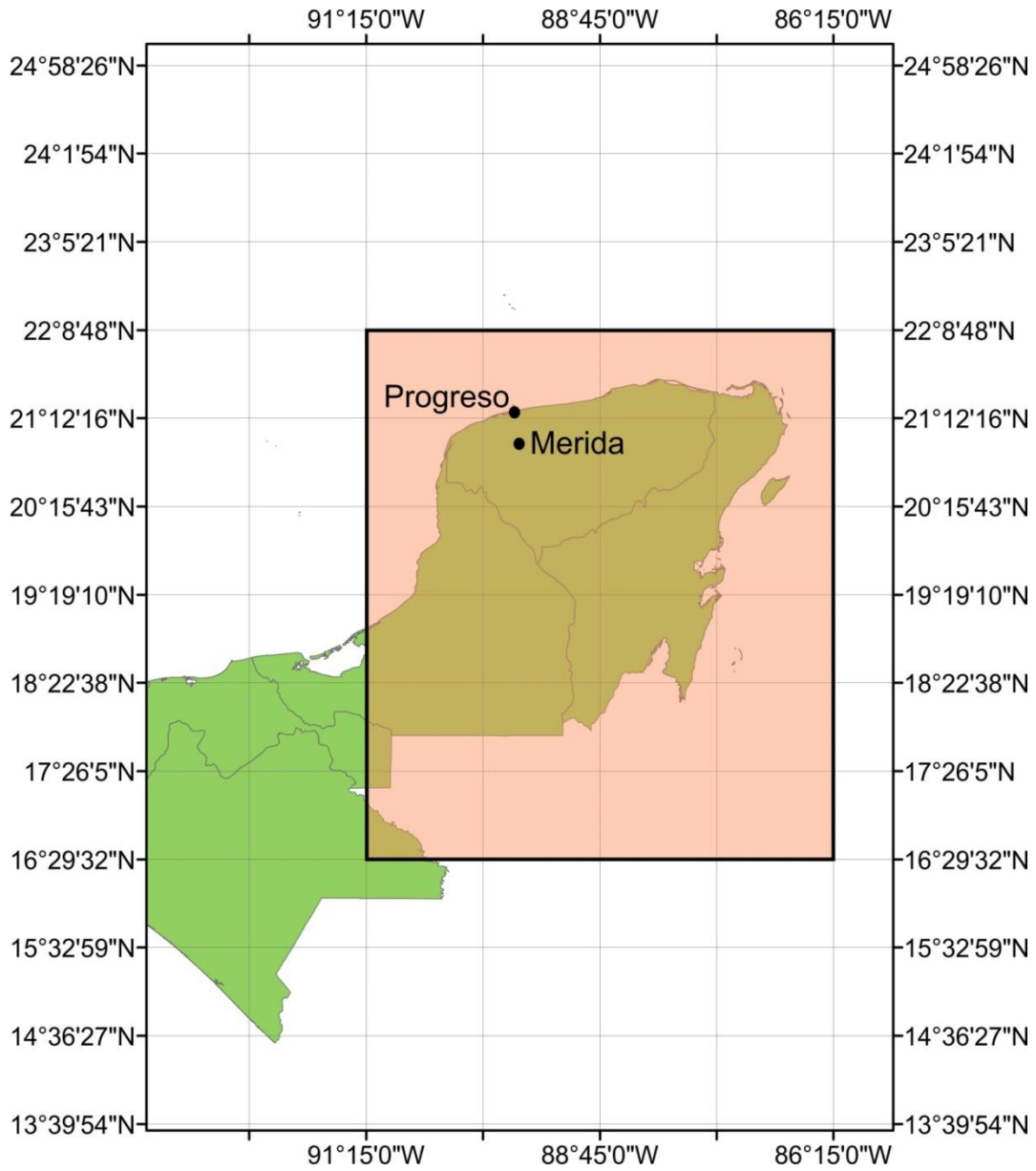
Figure 3.3   The 1.25° x 0.9° grid of the CCSM4 model over the Yucatan Peninsula, Mexico. The peach shaded area indicates the grid cells that were extracted from the GCM output and averaged to create a climate time series for the Yucatan. The daily observed climate record was collected from Merida Airport station, and the data for the composite observed record is a combination of climate stations at Progreso, Merida Airport, and Merida Observatory.

An example NCO code for averaging maximum daily temperature (tasmax) over the Yucatan Peninsula is as follows:

```
>ncwa –a lat,lon –d lat,16.,22. –d lon,268.,273. –v tasmax inputfile.nc outputfile.nc

>ncks –v tasmax –s '%f\n' outputfile.nc>outputfile.csv
```

In this NetCDF extraction code, inputfile.nc is the gridded maximum temperature data globally, and outputfile.nc is the averaged maximum temperature data for the Yucatan. This output file is then converted to a .csv file for further analysis of the data. The resulting file is a time series of daily maximum temperature of the Yucatan Peninsula for the entire record stored in the original netCDF file. The length of the record depends on which experiment the data are from. It should be noted that in the GCM output, the latitudes and longitudes are based on the grid size, and so are not whole numbers. In this code, a period is placed after the latitude and longitude values to tell the program to extract cells beginning with those numbers, regardless of what numbers come after the decimal place. For example, lat,16.,22. extracts data from the cells between latitudes 16.02 and 21.68 degrees north, because cell boundaries exist at those points.

Data from two CCSM4 model experiments were extracted as potential candidates to represent the historical period: the historical experiment and the Atmospheric Model Intercomparison Project (AMIP) experiment. While both of these experiments are run for a similar time period (1850-2005 for historical and 1979-2008 for AMIP), the input parameters and purpose of the experiments vary. The historical experiments use conditions that are based on observations, and include (Taylor et al., 2009):

- atmospheric composition due to anthropogenic and volcanic inputs
- solar forcings
- emissions of short-lived species and aerosols (both natural and anthropogenic)
- land use changes

The AMIP experiment is an atmosphere-only model with the same conditions as the historical experiment, but with observed sea surface temperatures (SSTs) and sea ice extents imposed on the model. Some of the main purposes of the historical experiment are to compare model performance to the observed climate and to provide

54

initial conditions for future climate scenarios, while the main purposes of the AMIP model are to evaluate how the model performs when it is uncoupled and to provide a less computationally demanding option for running high-resolution climate models (Taylor et al., 2009).

The past1000 (or Last Millennium) experiment was downloaded to represent the paleoclimate. This experiment spans the time period 850-1850 AD, although only the time from 850-1000 AD is used in this study for the TCP. Forcings on this experiment include solar and orbital variations, volcanic aerosols, and land use changes, which are similar to the forcings used for the Historical experiments (Bothe et al., 2013; Taylor et al., 2009). Confidence in the past1000 model was tested in Bothe et al. (2013) by comparing temperature output to reconstructions of global temperature (Mann et al., 2009), central Europe average temperatures (Dobrovolny et al., 2010), and southwest North American temperatures (Wahl and Smerdon, 2012). That study concluded that, overall, the past1000 model lacked consistency with the reconstructed temperature datasets, although there were some time periods and regions (tropical Pacific, subtropical North Pacific and South Atlantic) that fit the data better. This lack of consistency in the model may have been due to the uncertainty in the reconstructions themselves, which are also just interpretations of the past climate. As the results of the consistency tests were similar to previous ensembles, the uncertainty in the past1000 model was considered to be within an appropriate range (Bothe et al., 2013).

Using the NCO code above, daily data for Minimum Near-Surface Air Temperature (tasmin), Maximum Near-Surface Air Temperature (tasmax), Near-Surface Air Temperature (tas), and Precipitation (pr) were extracted for all available ensemble members of each experiment. The ensemble members of each experiment were averaged according to the standard practices for model output (Taylor, 2013). Daily solar radiation data are only required from one ensemble member according to the standard practices (Taylor, 2013).

The daily model data were amalgamated to obtain annual data, for a comparison to proxy data (which has annual resolution) and for comparison to the composite observed climate record (Medina-Elizalde, personal communication, 2015). Daily model

data were also compared to the daily observed climate record for Merida airport (The Weather Company, 2016).

Choice of model experiment to represent the historical period

The precipitation output of the CCSM4 model for both the AMIP experiment and the historical experiment were compared with the goal of choosing one experiment to represent the historical period for generating shift factors. A comparison of the average annual precipitation over the Yucatan Peninsula shows that neither experiment has a median value similar to the composite observed record or the daily observed record (Figure 3.4). The median value of annual precipitation for the AMIP experiment is higher than that of the composite observed record (around 1350 mm/year compared to 950 mm/year), and the historical experiment has a slightly lower median (~890 mm/year). GCMs are known to have uncertainty for smaller regions, so this result is not unexpected for the Yucatan Peninsula (Gent et al., 2011).   Given that both models are unsatisfactory, the historical experiment was chosen to represent the historical time period for calculating shift factors because it used the same forcings as the past1000 experiment (e.g., volcanic aerosols, solar variations, and land use changes). Therefore, the bias in both datasets should be the same, and for generating shift factors the two models are consistent.
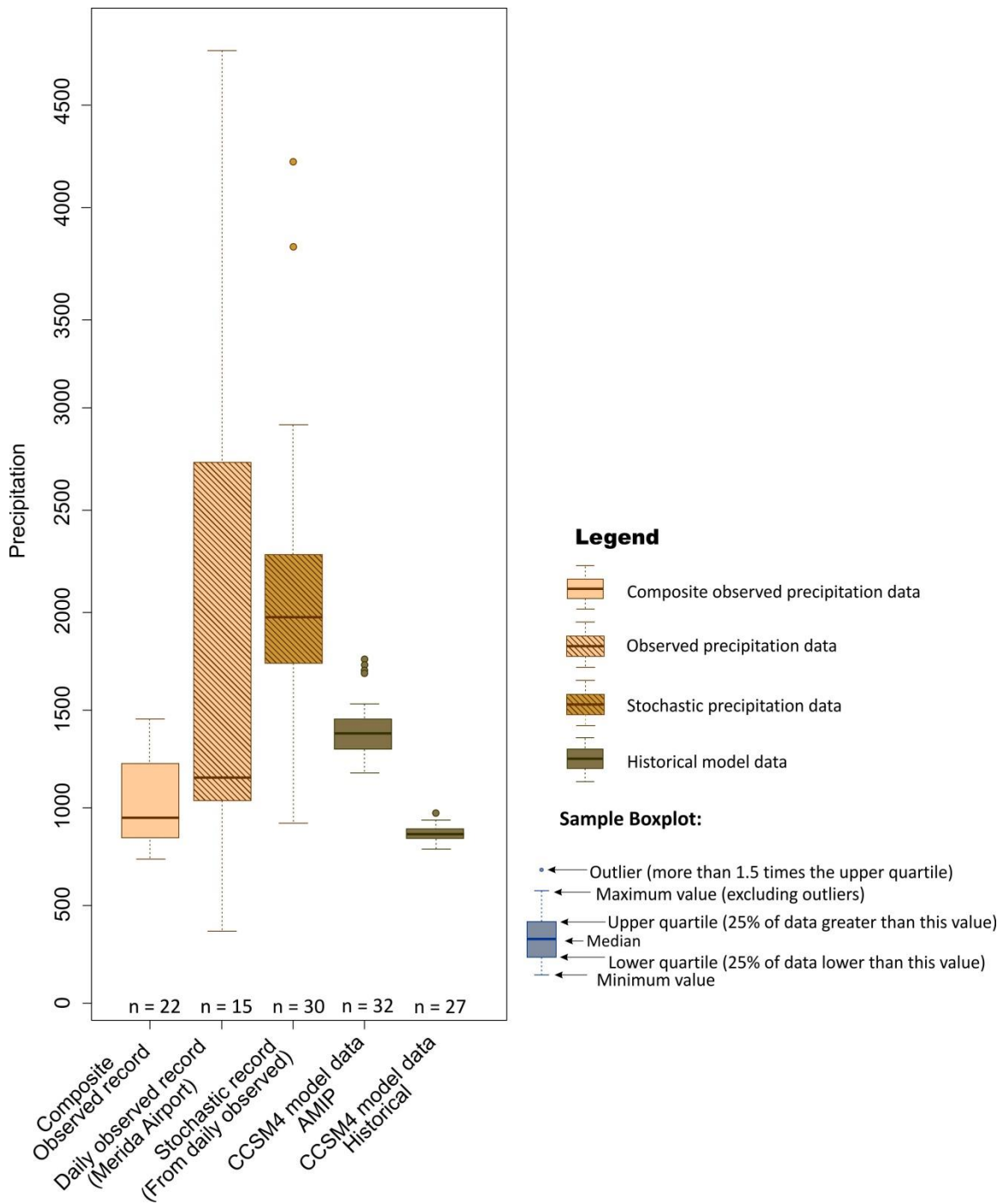
Figure 3.4   Comparison of annual precipitation extracted from the AMIP experiment and the historical experiment to the composite annual precipitation record from the Yucatan Peninsula (1979-2010) daily observed precipitation record (1995-2010), and stochastic record.

The daily observed record and the composite observed record both have much greater variability in annual precipitation than both of the model datasets, with the daily observed data having the greatest variability. The range of the observed data is nearly 800 mm/year, while the AMIP experiment has a range of only 300 mm/year (with some outliers) and the historical experiment has a range of less than 200 mm/year. Possible reasons for the reduced precipitation variability in the model data include: 1) the inability of the CCSM4 model to reproduce precipitation at a local scale, which is an effect of its grid size (Gent et al., 2011; Hewitson et al., 2014); and 2) the consequence of the averaging technique used to extract model data, as the local scale variations in precipitation may be larger than the variation of the entire Yucatan Peninsula on average. However, the averaging technique was justified because extracting data for one grid cell may also not have been representative of the local climate, as GCMs generally do not reproduce the local climate very well. Using an inaccurate representation of the local climate may have created shift factors that did not follow the seasonal climate patterns observed on the Yucatan Peninsula, as the GCMs failed to recreate the seasonality seen in the daily observed data (see next section).

Comparison of the daily observed climate (at Merida) and the stochastic data to the historical model climate

Daily temperature and precipitation output from the CCSM4 historical model was compared to the daily climate record from Merida. This comparison again shows that the variability of the model data is much less than the variability of the observed record (Figure 3.5). The daily observed precipitation record has periods of very little or no rain, while the model daily precipitation has a small amount of rain every day. This difference between the two datasets was also noticed while calculating shift factors, as LARS-WG was unable to detect any wet and dry series for the CCSM4 historical model (see Section 3.3.1). Similarly, LARS-WG calculated very long wet series for the past1000 experiment, which has a similar seasonal precipitation pattern to the historical experiment. This has implications for the generated TCP climate, as the shift factors may not be representative of the actual change in the length of wet and dry series. The ability to include wet and dry series was one of the main reasons LARS-GW was chosen for this study. This poor representation of shift factors for wet and dry series led to the decision to use the same length of wet and dry series as the daily observed dataset in

58

the generated TCP climate. Daily temperature in the CCSM4 model also has a reduced variability compared to the daily observed temperature, with a range of approximately 22-28°C compared to 14-35°C in the observed record. However, the seasonal pattern of temperature mimics the daily observed temperature very well, and on average the two temperature datasets appear to be very similar (Figure 3.5).
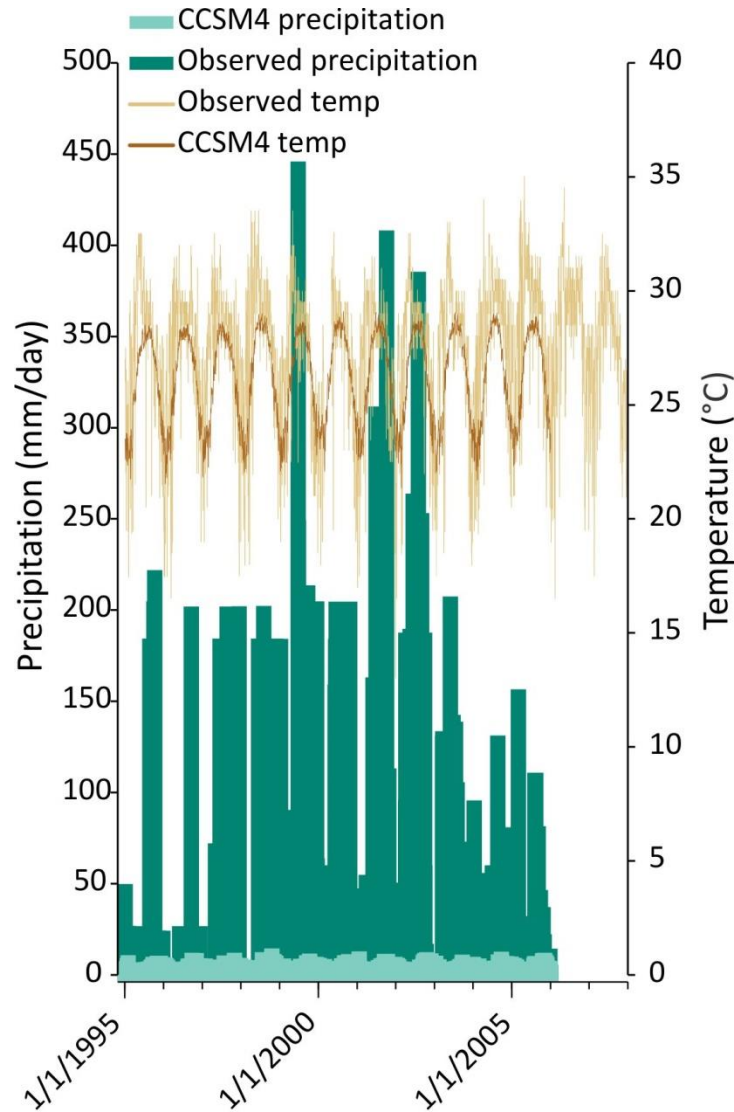
Figure 3.5   Daily temperature and precipitation records from the CCSM4 historical experiment and the observed daily record from Merida (1995-2010).

The greatly reduced variability in precipitation model output raised the question if the averaging technique used to extract model output for the Yucatan Peninsula could

have resulted in a smoothing of the data and reduced variability. The precipitation output of one grid cell centered over Merida ((latitude 20.20° to 21.30°, longitude 270° to 271.3°) was compared to the precipitation average of the Yucatan Peninsula and the observed record from Merida Airport to determine how well one grid cell was able to capture the observed precipitation variability (Figure 3.6). The single-cell model output has slightly higher variability than the cell-averaged model output, but still has much lower variability than the daily observed record. The low variability of both model datasets indicates that the reduced variability compared to the observed record is a result of the CCSM4 model's inability to accurately capture the local-scale climate, and not of the method used to extract model output.
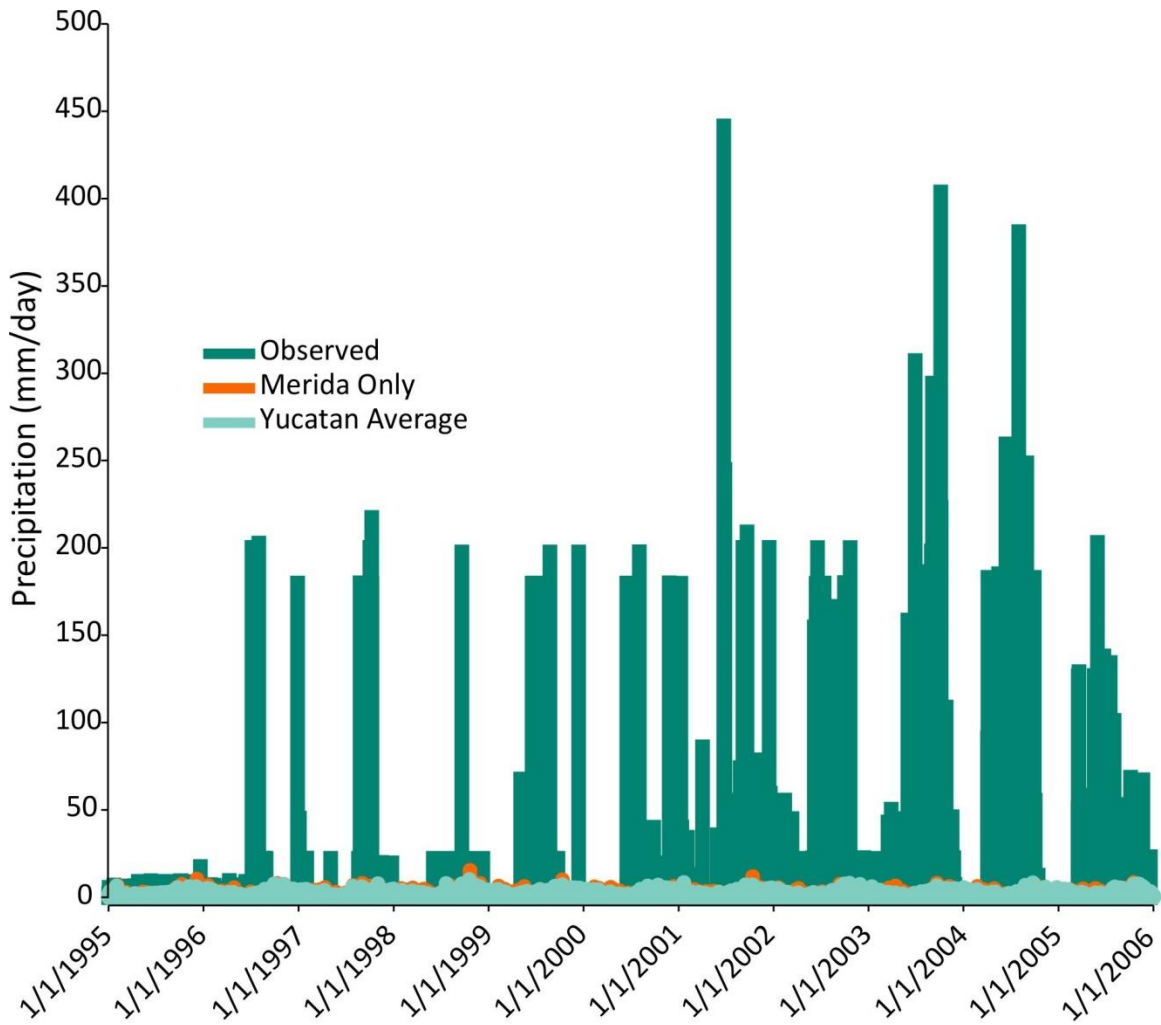
Figure 3.6   **The variability in precipitation output from one grid cell of the CCSM4 historical experiment (Merida Only) compared to the average of precipitation output for the entire Yucatan Peninsula (Yucatan Average), and the daily observed precipitation record from Merida Airport (Observed).**

The lack of variability in precipitation and temperature the model is also seen in the climate normals calculated for the model and daily observed data (1995-2010). Temperature in the model follows the same seasonal pattern as the observed, but throughout the year, model calculated minimum temperatures are overestimated by up to 3°C and maximum temperatures are underestimated by as much as 5°C, indicating overall reduced variability. This also results in average temperatures in the model being underestimated (Figure 3.7). The climate normals for the two datasets (observed and historical) also show that the seasonality of precipitation on the Yucatan Peninsula is not

captured by the model (Figure 3.7). In the observed data, the wet season falls between May and October, but in the model data this season occurs much later, from August to February. This inability of the model to capture seasonal rainfall and climate variability confirms that a shift factor approach is necessary to adequately reconstruct the TCP climate.
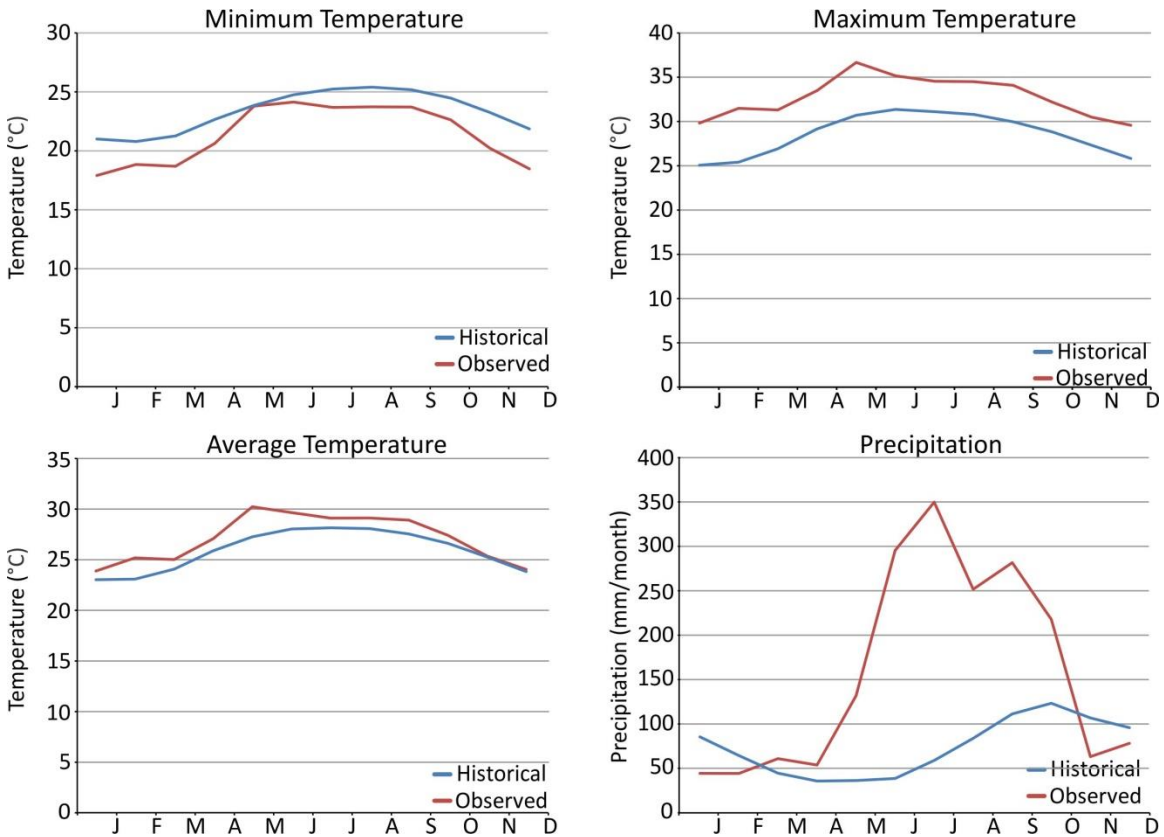
Figure 3.7 **Monthly climate normals for the historical experiment model output (1979-2005) and the daily observed climate data (1995-2010).**

3.2.3. Comparison of proxy data reconstructions to model data

Precipitation from the historical model was compared to two precipitation reconstructions based on proxy records with data from the historical period: the speleothem record (Medina-Elizalde et al., 2010) and the PDSI record (Stahle et al., 2011). The median annual precipitations of both of these reconstructions are very close to the median annual precipitation of the composite observed record, but slightly lower than that of the daily observed record (Figure 3.8). This indicates that the reconstructed precipitations for these proxies are not unreasonable based on the observed climate of

the Yucatan, as the higher median of the daily precipitation record may be due to the greater variability seen in the daily record. However, both of the reconstructions have less variability than the composite observed precipitation, which in turn has less variability than the daily observed record. This is likely an effect of the low resolution of the proxy data as well as the linear regression technique used to calculate precipitation, which has the effect of creating a more subdued climate signal (see Chapter 2).

The median annual precipitation of the historical experiment is slightly lower in comparison to both the proxy reconstructions and the composite observed record. However, the range in precipitation of the reconstructions is less than that of the model data, suggesting the model is slightly better than the proxy records at reproducing the variability in precipitation experienced on the Yucatan Peninsula, but not as good as the daily observed data as discussed previously.
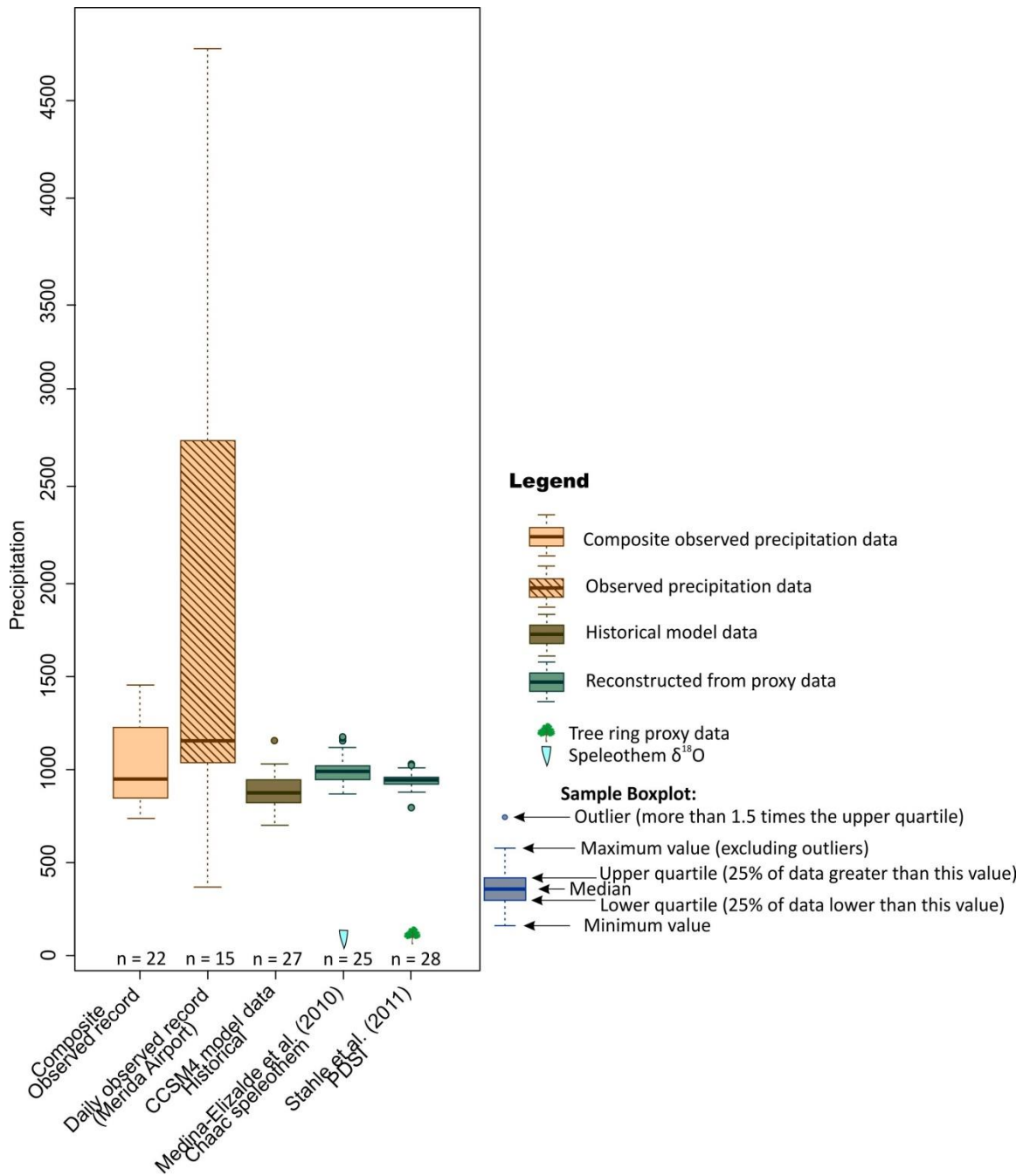
Figure 3.8   **Comparison of the composite observed and modeled annual precipitation for the historical period (1981-2010) to precipitation calculated by two proxy datasets which had modern data: Speleothem $\delta^{18}O$ (Medina-Elizalde et al., 2010) and PDSI reconstructed from tree rings (Stahle et al., 2011).**

       The precipitation output of the past1000 model was then compared to the all of the reconstructed precipitation records which were not eliminated from analysis (see

Chapter 2). As discussed in Chapter 2, the most confidence is placed in the speleothem record (Medina-Elizalde et al., 2010), and the PDSI record (Stahle et al., 2011). The past1000 model output is consistent with these two records, having the same median annual precipitation as the PDSI record and a slightly higher median than the speleothem record (Figure 3.9). The range of the past1000 model output is also similar to these reconstructions, with a range of approximately 700-1200mm/year. This range is again less than that of the observed record for the time period 1995-2010 on the Yucatan Peninsula, which ranged from 400 mm/year to over 4500 mm/year (see Figure 3.4,Figure 3.9), indicating that the model does not reproduce the annual variability experience at the Yucatan Peninsula. Other reconstructions for the Yucatan Peninsula have median annual precipitations that plot both higher and lower than the model output, which further indicates that these proxies may not be as reliable. Although they have reduced variability, the consistency of the median values of the best proxy reconstructions with the past1000 model output indicates that the model reproduces the average paleoclimate reasonably well, and may be used to create shift factors.
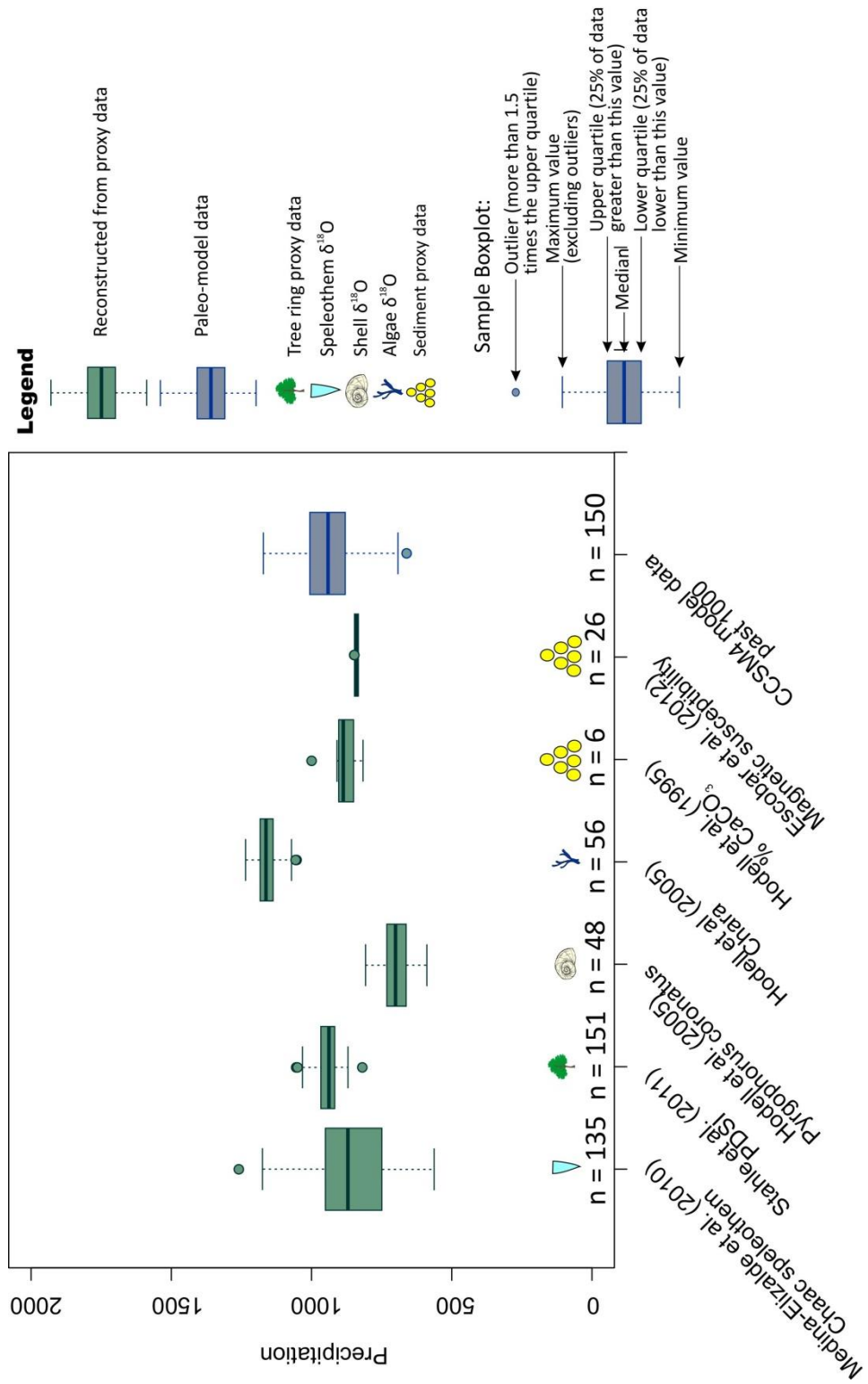
Figure 3.9   **Comparison of reconstructed precipitation records to the past1000 model output (850-1000 AD) for the Yucatan Peninsula.**

3.3. Methodology

3.3.1. Creating shift factors from model data in LARS-WG

Shift factors were created in LARS-WG between the historical and past1000 experiments from the CCSM4 model according to the procedure outlined in Semenov and Barrow (2002). Using output from two different time periods of the same GCM should reduce any bias that is present in the model. Also, due to the coarse grid size, the GCM output may not be representative of the climate for a small region such as the Yucatan Peninsula. However, applying shift factors (created from the GCM output) to observed climate (downscaling) will ensure that the generated climate for the TCP will be more representative of the local climate.

In practice, there are two approaches for applying shift factors:
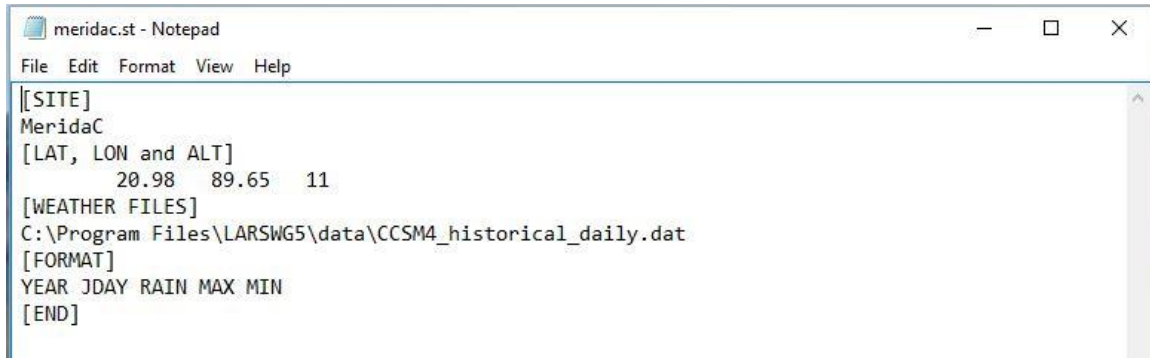
1) Apply shift factors to a stochastic weather series that is based on the observed climate (see Section 3.3.2);

2) Apply shift factors directly to the observed climate (see Section 3.3.3).

Both of these methods are explored in this thesis given that the median annual precipitation was poorly reproduced in the stochastic data.

LARS-WG requires (at a minimum) precipitation data, but ideally uses precipitation in combination with minimum temperature, maximum temperature, and solar radiation (or sunshine hours). For the shift factors, daily GCM output for all of the variables of interest are required. In this study, solar radiation was not used to calculate shift factors, because the shift factors will be applied to an observed climate time series for which no solar radiation data were available. Thus, it is assumed that solar radiation has remained the same through time for this region.

Daily minimum and maximum temperature and precipitation for the historical (1979-2005) and past1000 (850-1000) experiments were organized into a data file for input into LARS-WG. The format of the data file is specified in a site file, which tells the program where to look for the file, the location of the site, and which variables are

present in the file. The site file for the historical data is given as an example (Figure 3.10). The same site location in LARS-WG was used for both the historical and past1000 experiment climate series (latitude 20.98°N, longitude 89.65°W, altitude 11m).

Figure 3.10   LARS-WG site file for the historical period at Merida. The file indicates the location of the data file containing daily precipitation (RAIN), maximum temperature (MAX) and minimum temperature (MIN) data.

Each of the time periods was then used to perform a site analysis in LARS-WG. The site analysis generates two files for each time series: the statistical characteristics of the input data (.stx file) and the parameter information that LARS-WG will use to generate a new climate time series (.wgx file). Shift factors for the relative change in wet and dry series are calculated from the .wgx file; the relative change in mean temperature standard deviation and absolute change in minimum and maximum temperature are calculated from the daily GCM data; and the relative changes in mean precipitation are calculated from the .stx file.

To calculate the relative change in the length of wet and dry series, the average length of a series (which is found for each month in the .wgx file) in the past time period is divided by the average length of the series in the historical time period. This is done for each month, giving relative changes for each month. However, LARS-WG did not detect any wet or dry series in the historical model data for the Yucatan Peninsula, so no shift factors could be used for the length of wet and dry series. This is represented as a shift factor of 1, meaning the observed climate wet and dry series will be multiplied by 1 (Table 3.3). This gives the generated climate the same length of wet and dry series as the observed climate. One of the main advantages of LARS-WG in comparison to other

weather generators, and a key reason it was chosen for this study, is that it can account for changes in wet and dry series. These parameters are important for incorporating changes in the timing and length of droughts (Racsko et al., 1991; Semenov and Barrow, 2002). So, it is unfortunate that this feature of LARS-WG could not be taken advantage of.

The relative change in mean temperature standard deviation and the absolute change in minimum and maximum temperature were calculated from the daily GCM data. The average daily temperature was obtained from the daily minimum and maximum temperatures, and all the data from each time period were pooled together. The standard deviation of the daily mean temperatures and the average of the minimum and maximum temperatures for each month were calculated. For example, the historical model data spans 27 years, which is 9855 days. Of those days, 837 days are in January, and the average minimum and maximum temperature of a January day was calculated to be 20.26°C and 24.31°C, respectively, with a standard deviation of 0.71°C. The daily average and standard deviation of all of the months were calculated for both the historical and the past1000 time series. The relative change in standard deviation for each month is found by dividing the standard deviation of the past time period by the standard deviation of the historical time period. The absolute change in minimum or maximum temperature is found by subtracting the mean monthly temperature of the historical period from the mean monthly temperature of the past time period. Although the shift factors are for each month, the absolute changes in temperature were calculated from daily data, and so are added (or subtracted) to each day in that month when LARS-WG generates the new time series.

The relative change in monthly rainfall is similarly calculated by dividing the average monthly rainfall of the past time period by the average monthly rainfall of the historical period. The mean precipitation amounts for each month are found in the .stx file.

Table 3.3 **Shift factors calculated using daily GCM data from the historical and past1000 experiments. Relative shift factors were calculated for precipitation, length in wet and dry series, and mean temperature standard deviation (SD), while the change in minimum and maximum temperatures were calculated as absolute shift factors. Note that a shift factor of 1 for the wet and dry series indicates that there is no change in the length of wet and dry series.**

	Rain	Wet series	Dry series	Minimum temp	Maximum temp	SD
January	1.066987	1	1	-0.72872	-0.78985	2.072345
February	1.058302	1	1	-0.67426	-0.68978	1.916223
March	1.117915	1	1	-0.63428	-0.75227	1.533429
April	1.126559	1	1	-0.98791	-1.06642	1.761901
May	1.123325	1	1	-1.09391	-1.21946	1.684766
June	1.18635	1	1	-1.06714	-1.14133	1.939456
July	1.13387	1	1	-1.09992	-1.10018	1.670346
August	1.09464	1	1	-0.99757	-1.03505	1.435609
September	1.027414	1	1	-0.84559	-0.84732	1.397803
October	1.038478	1	1	-0.74618	-0.73264	1.507098
November	1.067094	1	1	-0.75205	-0.76483	1.853645
December	1.083132	1	1	-0.61506	-0.65191	1.941538

3.3.2. Application of shift factors to a stochastic weather series to reconstruct the TCP climate

As mentioned above, two approaches were used to generate a daily climate time series for the TCP. First, the calculated shift factors were used to generate a stochastic daily time series for the TCP. To do this, the shift factors were used to create a scenario file for LARS-WG, which tells the program how to perturb a baseline dataset. The observed daily data from Merida underwent site analysis to produce the parameter information used by LARS-WG to generate a new time series. In the generator, the default scenario is a baseline scenario, which simply generates weather data without applying shift factors. To incorporate the shift factors, the scenario file with the calculated shift factors is selected while running the weather generator, producing a 30-year time series that is representative of the shifted climate, here the TCP (the stochastic reconstruction). This reconstructed time series is further discussed in Section 3.4.1.

3.3.3. Direct application of shift factors to observed data to reconstruct the TCP climate

In the second approach, the shift factors were applied to the daily observed temperature and precipitation data for Merida Airport. This was done by creating daily shift factors for precipitation, minimum and maximum temperature, and average temperature. The shift factor for the standard deviation in temperature was not be applied in this method, as no observed record of this parameter was available. The calculated shift factor for each month were applied mid-month (the 15th of every month), and shift factors for the days in between were linearly interpolated between these values. These daily shift factors were applied to the daily observed value of each climate parameter, creating a 15 year long reconstruction representative of the TCP (the direct shift factor reconstruction). This time series is also discussed in Section 3.4.1.

3.4. Results and discussion

3.4.1. The reconstructed precipitation for the Terminal Classic Period

The stochastic reconstruction

The climate generated by LARS-WG is a 30 year record that is representative of the TCP. It was generated by applying the shift factors determined from the historical and past1000 models to the stochastic daily climate series generated directly from the observed climate at Merida Airport. The representative TCP time series is daily, but in order to compare its precipitation to the reconstructions from the proxy records, it was summarized at an annual scale.

The median annual precipitation of the stochastic TCP reconstruction is the closest to the median of the stochastic precipitation (of the historical period), although it is slightly higher (2250 mm/year), and the calculated average annual precipitation of the stochastic TCP climate is 2340 mm/year, which is higher than the average annual precipitation of the stochastic climate (2090 mm/year), indicating the TCP precipitation has more years with higher rainfall (Figure 3.11). The stochastic TCP precipitation also

has a large range, similar to the historical stochastic climate and the daily observed climate (a range of 1000 mm/year to 4400 mm/year). Similarly to the historical stochastic precipitation, the stochastic reconstructed precipitation has a normal distribution due to the smoothing effect of generating a climate time series in LARS-WG.

The median annual precipitation of the stochastic reconstructed climate is also higher than the most reliable reconstructions of the TCP (900 mm/year for the speleothem record from Medina-Elizalde et al., 2010; and 1050 mm/year for the PDSI record from Stahle et al., 2011). This indicates that the average annual precipitation for the TCP does not show evidence of drought, while the proxy record does. However, unlike the proxy data, the stochastic reconstruction has the advantage of having a higher resolution (daily), so the seasonal distribution of precipitation can be examined for evidence of drought instead of relying on the average annual precipitation. The daily record also incorporates much more variability and extreme events, which could play a role in the seasonal water balance (Section 3.4.2).

The direct shift factor reconstruction

The direct shift factor reconstruction has a precipitation distribution that is much more similar to the daily observed record (Figure 3.11). The median values of the two time series are similar, with the direct shift factor reconstruction having a low median value (1300 mm/year), which is slightly higher than the median annual precipitation of the daily record (1200 mm/year). This reconstruction also has a higher median value than the proxy records for the TCP, similar to the stochastic reconstruction. As these are based on the daily observed record for Merida, which itself has a higher median annual precipitation than the proxy records, this is not unexpected. The average of the direct shift factor reconstruction is higher than the average of the daily observed record (2060 mm/year and 1873 mm/year, respectively), indicating more annual precipitation during the TCP. A higher range in extreme precipitation values is seen in the direct shift factor reconstruction, with some annual precipitation values exceeding 5000 mm/year, which indicates greater variability in annual precipitation during the TCP. The similar distribution of the direct shift factor reconstruction and the daily observed record suggests that this method was more accurate for reconstructing precipitation of the TCP;

however, the seasonal distribution of precipitation will also be an important factor in choosing between the methods. The seasonal climates are analyzed in the next section.
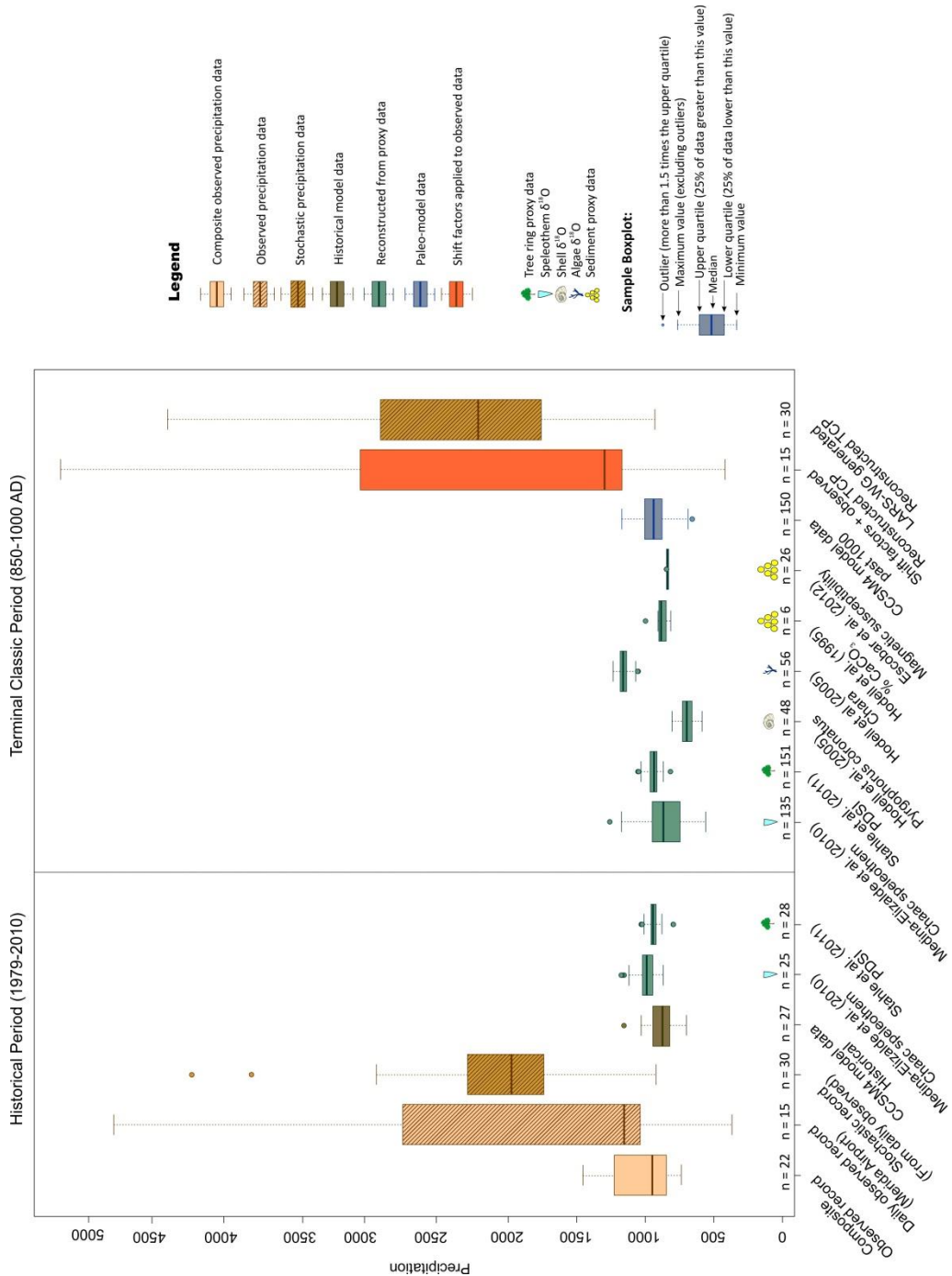
Figure 3.11   Average annual precipitation for all precipitation reconstructions (Chapter 2), CCSM4 model output from the historical and past1000 experiments, observed and composite observed precipitation, and the reconstructed TCP precipitation.

3.4.2. Comparison of the reconstructed climate records to the observed and stochastic records

A comparison of the climate normals of the two reconstructed TCP climates with the climate normals of the stochastic data and the daily observed record show that the variability and seasonality of the direct shift factor reconstruction most closely resembles that of the observed record (Figure 3.12). Seasonal precipitation of the direct shift factor reconstruction show that overall there is more precipitation that occurs during the wet months (May-October) compared to the daily observed record, and that there is little to no increase in precipitation seen during the dry months. This seasonal pattern fits well with the shift factors calculated for precipitation, which were larger during the wet season. The stochastic reconstruction shows a similar seasonal pattern, but with a larger increase in precipitation occurring during the wet months, in particular June. Compared to the historical stochastic dataset, the stochastic reconstruction shows a decrease in precipitation during the dry months.

The direct shift factor reconstruction has very similar monthly temperatures to the stochastic reconstruction, indicating that either method of applying shift factors is likely adequate for reconstructing temperatures. Both of these reconstructions indicate overall reduced temperatures during the TCP, being lower than the stochastic data and the observed data in most months.
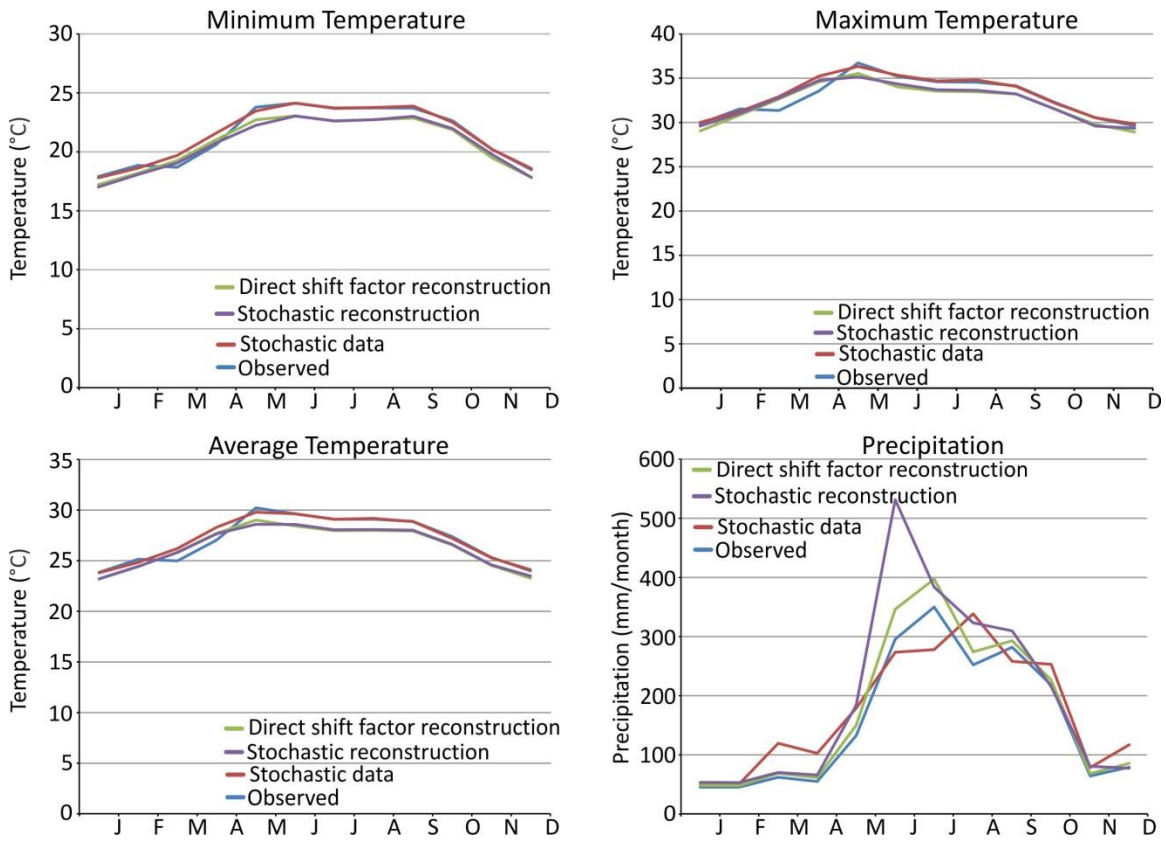
Figure 3.12   Monthly climate normals for the observed climate record (1995-2010), the stochastic climate record (1979-2010), the direct shift factor reconstruction (15 years representative of the TCP), and the stochastic reconstruction (30 years representative of the TCP).

The seasonal distribution of both precipitation reconstructions follows the expected seasonal pattern of a wet season from May to October and a dry season by November to April, unlike the CCSM4 model data which was used to calculate the shift factors. This is a good indication that both of the reconstructed TCP climates have captured the seasonal pattern and variability of rainfall that occurs on the Yucatan Peninsula today, which was expected because shift factors were not used for the length of the wet and dry series. However, making this assumption that seasonal rainfall pattern and variability was the same during the TCP as it is today is a significant limitation of this study and points to the need for the models to better capture rainfall variability. For this study, assuming the variability during the TCP was the same as the observed data is reasonable, rather than ignoring variability completely.

The observed record, historical stochastic record, stochastic reconstruction and direct shift factor reconstruction will be used to model recharge on the Yucatan Peninsula (Chapter 4). Groundwater recharge on the Yucatan Peninsula is thought to be closely linked to precipitation, as the carbonate rocks of the Peninsula are highly permeable (Perry et al., 2003). Therefore, a comparison of the precipitation normals for a historical baseline dataset and a reconstructed precipitation dataset can give an indication of any changes in groundwater recharge that may be simulated by the recharge model. Due to the more accurate annual distribution of the direct shift factor reconstruction, this reconstruction will be used at the "baseline" dataset, although the stochastic reconstruction will also be considered for recharge modeling (Chapter 4). The change in climate normals between the direct shift factor reconstruction and the daily observed record indicate that the TCP climate has more precipitation for all months, with the increases in precipitation being the greatest during the wet season (May to October) (Table 3.4). The greatest increase in precipitation occurs in June (50.72 mm/month), near the beginning of the wet season.

Table 3.4   Change in precipitation climate normals between the daily observed climate (1995- 2010) and the direct shift factor reconstruction of the TCP climate.

	Precipitation (mm/month)
January	3.07
February	2.75
March	6.79
April	6.56
May	17.68
June	50.72
July	47.56
August	22.31
September	10.90
October	8.30
November	4.01
December	6.31

These changes in precipitation indicate that the Yucatan Peninsula experienced greater annual precipitation during the TCP, and that even more precipitation occurred

during the wet season than the present climate. Although this shifted climate shows no evidence of droughts, shift factors were not able to be applied for the length of wet and dry series, which play a key role in the variability of precipitation. More days with no precipitation, especially during the dry season, could lead to droughts during the TCP. However, without these shift factors, the direct shift factor reconstruction has the same variability as the observed climate, which was a major limitation of this study. This assumption means that the reconstructed climate underestimates precipitation variability and extreme values (of both high and low precipitation), so the possibility of droughts should not be excluded.

3.5. Conclusions

This goal of this portion of the study was to create a daily climate time series representative of the TCP using a shift factor approach. While daily climate data for this time period are available from the past1000 experiment of the CCSM4 model, comparison of the model data and observed data from the Yucatan Peninsula showed that there is bias in both of the model datasets (historical and past1000). In addition, the CCSM4 model is not able to capture the seasonal distribution or variability in climate experienced on the Yucatan Peninsula today, especially for precipitation. For this reason, using the daily model output alone would likely not produce an accurate representation of the climate during the TCP. However, the two model datasets were used to create backward shift factors from output from the historical and past1000 experiments, which were applied using two shift factor techniques. In the first technique, shift factors were applied to a stochastic dataset representative of the historical climate data using LARS-WG. However, using LARS-WG to apply shift factors created a stochastic precipitation reconstruction that had a different distribution than the observed data, leading to the addition of the second shift factor technique. This second method applied shift factors directly to the observed data, and produced a reconstruction which much better reproduced the skewed distribution of annual precipitation observed on the Yucatan Peninsula. Applying shift factors had multiple purposes:

- To eliminate bias (especially for precipitation) found in the CCSM4 model.

77

- To incorporate the variability (in temperature and precipitation) seen in the observed data but that was lacking in the CCSM4 model output.

- To downscale the data to a local scale, as the CCSM4 model grid is too coarse to fully capture local scale processes.

LARS-WG was chosen for this study for its ability to include changes in the length of wet and dry series and for generating years of climate data from simple climate parameters. Unfortunately, the lack of variability in the model data meant that LARS-WG was unable to detect wet and dry series, so shift factors for these climate parameters were not able to be used in this study. In addition, when generating a weather series, LARS-WG smoothed the data to create a normal distribution. This created problems in the stochastic precipitation data, as the median value of precipitation in the stochastic datasets was much higher than that of the observed data from the Yucatan Peninsula.

Using two techniques to apply shift factors showed that the choice of technique is more important for precipitation than temperature on the Yucatan Peninsula. Due to the skewed distribution of annual rainfall on the Yucatan Peninsula, the direct shift factor approach is better suited for reconstructing precipitation, as it produced a reconstruction with a similar distribution as the observed data. The direct shift factor reconstruction did not show any evidence for drought during the TCP: in fact, it showed an increase in annual precipitation. However, this dataset did show that the majority of this rainfall occurred during the wet season. Because changes in variability were not able to be included in this study, it is important to remember that the reconstructions may underestimate climate variability, and that more precipitation extremes (of high and low rainfall) may have occurred during the TCP, and that these may have contributed to droughts. The impact of these different reconstructions on groundwater recharge will be assessed in Chapter 4.

Chapter 4.   Recharge modeling

4.1. Overview

The historical average annual stochastically-generated precipitation (see Chapter 3) had a normal distribution with a much lower median precipitation rather than a skewed distribution as represented in the observed data, which was found to be a manifestation of using LARS-WG. For this reason, two approaches (a direct shift factor approach and a stochastic approach) were used to reconstruct the TCP climate.

In this chapter, four precipitation time series are used in a recharge model to create four scenarios to analyze the effect of different rainfall distributions on the recharge model:

- observed climate for the historical period
- stochastic climate for the historical period
- reconstructed climate for the TPC generated by applying shift factors directly to the observed precipitation data
- reconstructed climate for the TCP generated by applying shift factors within a stochastic weather generator.

4.2. MIKE SHE modeling software

MIKE SHE is an integrated surface and groundwater modeling tool created by DHI Software as one of the MIKE Zero modeling tools (DHI, 2007a). While this program can simulate both subsurface and surface flow, MIKE SHE is used in this project to simulate the unsaturated zone (UZ) to estimate the amount of water entering the groundwater system (groundwater recharge). Groundwater recharge is calculated for both the historical time period (1979-2005) and the Terminal Classic Period (850-1000 AD). The model is not meant to be a calibrated, accurate representation of recharge,

but rather a conceptual or interpretive model to examine how recharge may have changed between the two time periods.

There are a number of options in MIKE SHE for calculating vertical unsaturated flow. The most computationally intensive method uses Richards' equation, which is a modification of Darcy's Law for flow through unsaturated porous media:

$$\frac{d\theta}{dt} = \frac{d}{dz}\left[K(\theta)\left(\frac{d\psi}{dz} + 1\right)\right]$$ (4.1)

where θ is the moisture content, t is time, z is elevation, $K(\theta)$ is the unsaturated hydraulic conductivity, and Ψ is the matric potential (negative pressure head or soil tension). The solution of Richards' equation takes soil moisture and capillarity into account, both of which change as water infiltrates, making the equation non-linear. Another option in MIKE SHE for solving unsaturated flow is a formulation based on gravity only, which is a simplification of Richards' equation. The gravity flow method ignores capillary forces and thus the matric potential term, and assumes that all of the vertical unsaturated flow is due to gravity. This approximation is less computationally-intensive, and is found to be accurate enough to calculate the time-varying recharge to groundwater, but may not be able to capture all of the detailed dynamics of the unsaturated zone (DHI, 2007b). The third option, the Two-Layer Water Balance Method, is a less complex method for solving vertical unsaturated flow based on a simplified evapotranspiration (ET). This method assumes the unsaturated zone consists of only two layers with average unsaturated conditions, and provides an estimate of groundwater recharge and actual evapotranspiration (AET). However, this method is not accurate in dry areas where the water table is deep (DHI, 2007b).

MIKE SHE also has an option to include macropore (or bypass) flow. For an area such as the Yucatan Peninsula which is composed of karstic limestone, high permeability zones (such as fractures, solution cavities) allow rapid infiltration (Back and Hanshaw, 1980). This means that the incorporation (or exclusion) of macropores may play a large role in the amount of water that infiltrates through the soil and reaches the groundwater.

The models for this project used the gravity flow method with no macropore flow to simulate groundwater recharge on the Yucatan Peninsula. The effects of using macropore flow were analyzed in a sensitivity analysis (Appendix C).

4.3. Model domain

A watershed scale was selected as the most appropriate size for modeling recharge on the Yucatan Peninsula. Data for watersheds on the Yucatan Peninsula were obtained from The GeoGratis Data Portal (Natural Resources Canada, 2010). The model domain is the northernmost watershed on the Yucatan Peninsula (Figure 4.1). The domain was simplified to exclude small islands and peninsulas that would be too small for the grid size used in the model. As this model is a regional model, a relatively coarse grid size of 1985 m was used. This grid size is larger than the cell size of the topography digital elevation model (DEM) (1000 m), as using a grid size smaller than the resolution of the input data would increase computational time unnecessarily.

Figure 4.1   The model domain for the Yucatan Peninsula (outlined in black). The coastline of the Yucatan Peninsula was simplified for input into MIKE SHE.

4.4. Boundary conditions

The upper and lower boundaries of the model are defined by the ground surface and the water table, respectively.   The ground surface was the DEM, which was obtained from the United Nations Environment Programme (UNEP) Environmental Data Explorer (UNEP, 2006). Elevations on the Yucatan Peninsula range from 0 to 195 masl, with the lowest elevations occurring along the coast and higher elevations towards the south of the model (Figure 4.2).
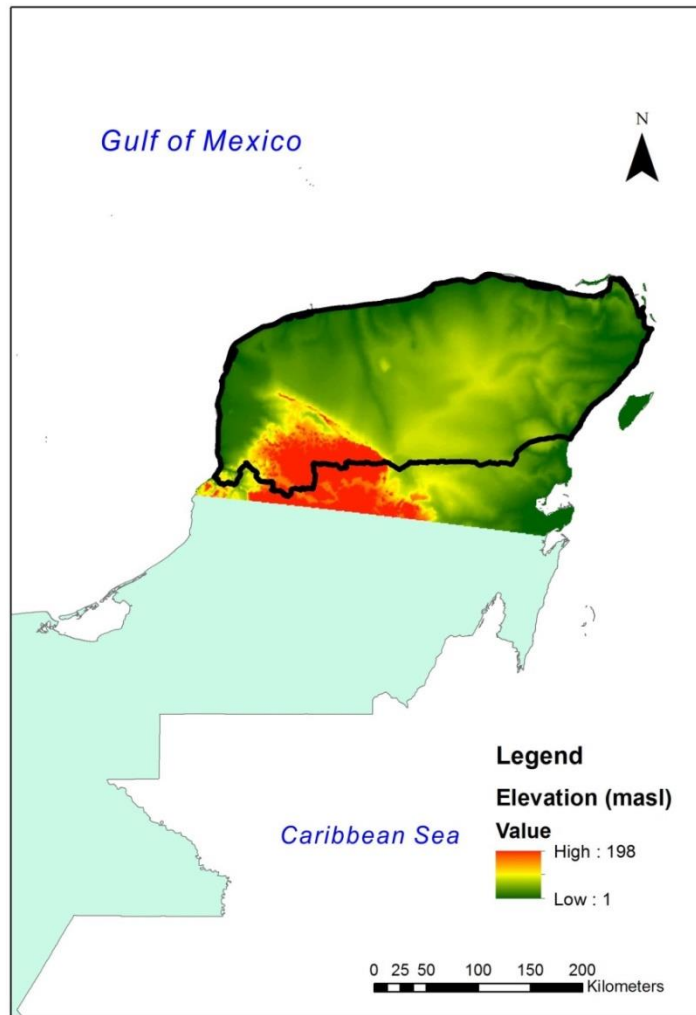
Figure 4.2   Elevations on the Yucatan Peninsula within the model domain. Elevations range from 1 masl at the coast up to 198 masl in the hilly region in the southwest of the model domain.

The water table represents the lower boundary of the model, as only the unsaturated zone is being modeled. In MIKE SHE, if the saturated zone is not simulated, the water table is set by the user and is represented as a pressure head boundary based on the specified groundwater elevation (DHI, 2007b). This sets the water table as a fixed boundary, so that the water level does not change during the simulation. However, changes in groundwater recharge can still be calculated by analyzing the water balance for the unsaturated zone. Detailed groundwater elevations for the Yucatan Peninsula were not available, so groundwater elevations for the entire watershed were calculated by creating a linear relationship between nine known

groundwater elevation points and the ground surface elevation at those points, resulting in a linear equation that could be used to calculate the groundwater elevation for the entire model domain (Figure 4.3) (Wassenar et al., 2009). The resulting groundwater elevations mimic the topography, with higher groundwater elevations in the southwest of the model and groundwater elevations close to 0 masl along the coast (Figure 4.4). This representation for water table depth is a limitation of the model, but was necessary due to limited spatial data.

The chart shows groundwater elevation plotted against ground surface elevation with the trendline equation $y = 0.7643x + 1.4776$ and $R^2 = 0.718$.
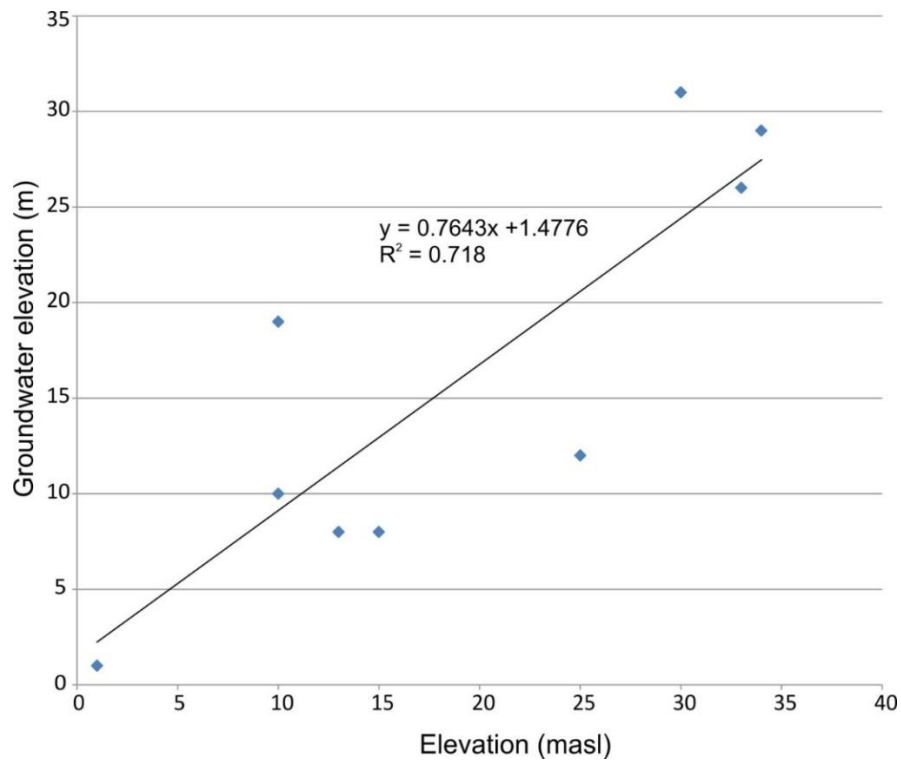
Figure 4.3   **Groundwater elevation plotted against ground surface elevation for nine points on the Yucatan Peninsula. Groundwater elevation data from Wassenaar et al. (2009).**
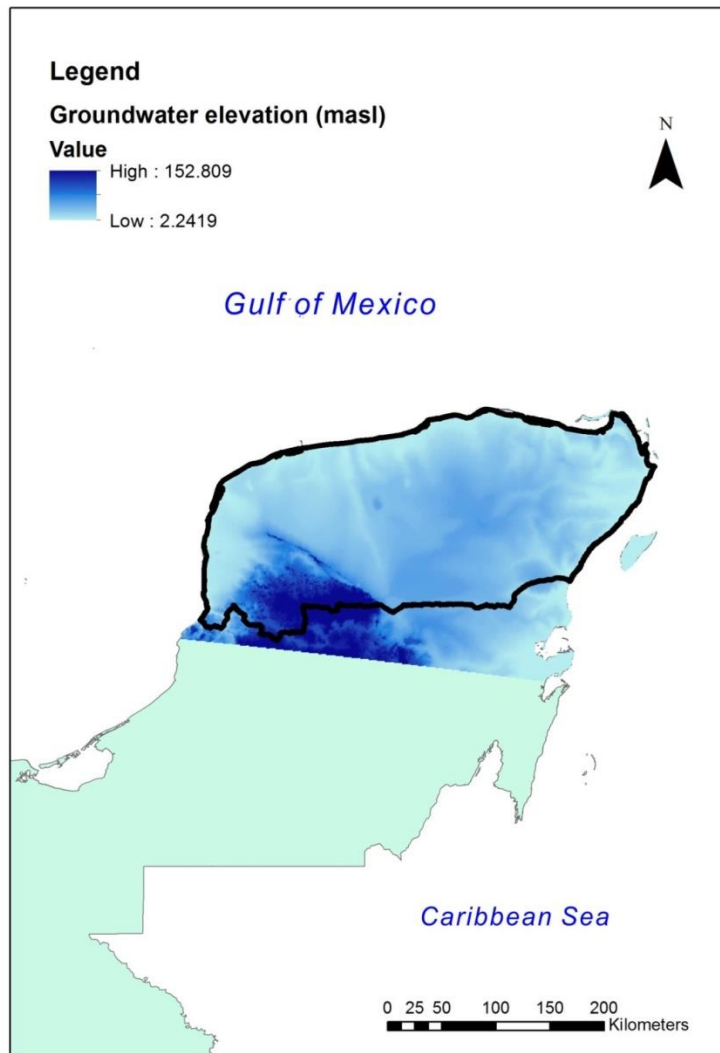
Figure 4.4   Interpolated groundwater elevations within the model domain on the Yucatan Peninsula. Groundwater elevations are approximated to closely mimic topography, and represent generalized regional groundwater flow towards to coast.

The edges of the model are considered to be no-flow boundaries. Modeling of the unsaturated zone assumes that flow is vertical, so that no water in the soil zone is lost or gained through horizontal flow (DHI, 2007b). However, the water balance tool in MIKE SHE calculates surface and subsurface drainage in and out of the model. This give a sense of how much water is entering or leaving the system horizontally without actually simulating horizontal flow. Overland flow (OL), which occurs on the ground surface, treats the edges of the model as specified heads based on the water depths at

the edges of the model. The edges of the model act as a source of water if the specified heads are higher than the water depth inside the model, and water will leave the model if the specified heads are lower than those on the inside of the model (DHI, 2007b).

Precipitation is a specified flux boundary applied over the entire upper surface of the model, generating infiltration the upper boundary of the model (DHI, 2007b). A uniform climate was chosen to represent the entire watershed, although there is a known north-south precipitation gradient on the Yucatan Peninsula (Bautista et al., 2011), which may mean that precipitation is underestimated in the south of the model. However, the assumption of uniform precipitation is thought to be appropriate for the conceptual nature of the model, as its purpose is to understand the regional changes in recharge between two different time periods.

4.5. Initial parameters and settings

Simulation specifications

The initial MIKE SHE model was set up to simulate the time period from January 1st, 1979 to December 31st, 2005 (the historical period). It includes unsaturated flow (using gravity flow), evapotranspiration (ET), and overland flow (OL). Rivers and lakes were not simulated, as a detailed river network was not available and the amount of surface water on the Yucatan Peninsula is low (Perry, et al., 2003).

When only unsaturated flow is simulated, the initial moisture content of the model is 0 (dry). Accordingly, the model must first "spin up" to a state of dynamic equilibrium in its moisture content. Once this equilibrium is obtained, the recharge can be examined. The water balance output shows that the model reached equilibrium within one year, so for this study the entire length of the model will be used for calculating the water balance components.

The maximum recommended time step for unsaturated flow (using either Richards' equation or gravity flow) is 2 hours, so this value was used as the maximum time step (DHI, 2007b). All other time steps, for overland flow and unsaturated zone parameters, were left as the default values (Table 4.1).

Table 4.1   Initial parameters used for time step control, OL computational control and UZ computational control. Default values were used for all parameters except for the Max allowed UZ time step, which was changed to 2 hours.

Time step parameters:	
Initial time step	6 hours
Max allowed OL time step	0.5 hours
Max allowed UZ time step	2 hours
Increment rate of reduced time step length	0.05
Max precipitation depth per time step	10 mm
Max infiltration amount per time step	10 mm
Input precipitation rate requiring its own time step	0.1 mm/hour
OL computational control parameters:	
Maximum number of iterations	200
Maximum head change per iteration	0.0001 m
Maximum residual error	0.0001 m/day
Under-relaxation factor	0.9
Threshold water depth for overland flow	0.0001 m
Threshold gradient for applying low-gradient flow reduction	0.0001
UZ computational control parameters:	
Max profile water balance error	0.001 m

Soils and vegetation

The most common soil type on the Yucatan Peninsula is Rendzic Leptosols (Dijkshoorn et al., 2005) (Figure 4.5). According to the FAO (1988), these soils are found overlying calcareous material and are less than 75 cm thick. Soil properties in MIKE SHE for a Rendzic Leptosol were estimated based on the properties found in Estrada-Medina et al. (2013a), who found that Yucatan Leptosols contains 49-72% sand, 11-22% clay, 14-31% silt, and are well-drained (

Table 4.2). Using the United States Department of Agriculture (USDA) soil textural classification, Leptosols are classified as a sandy loam (National Cooperative Soil Survey, 2016).
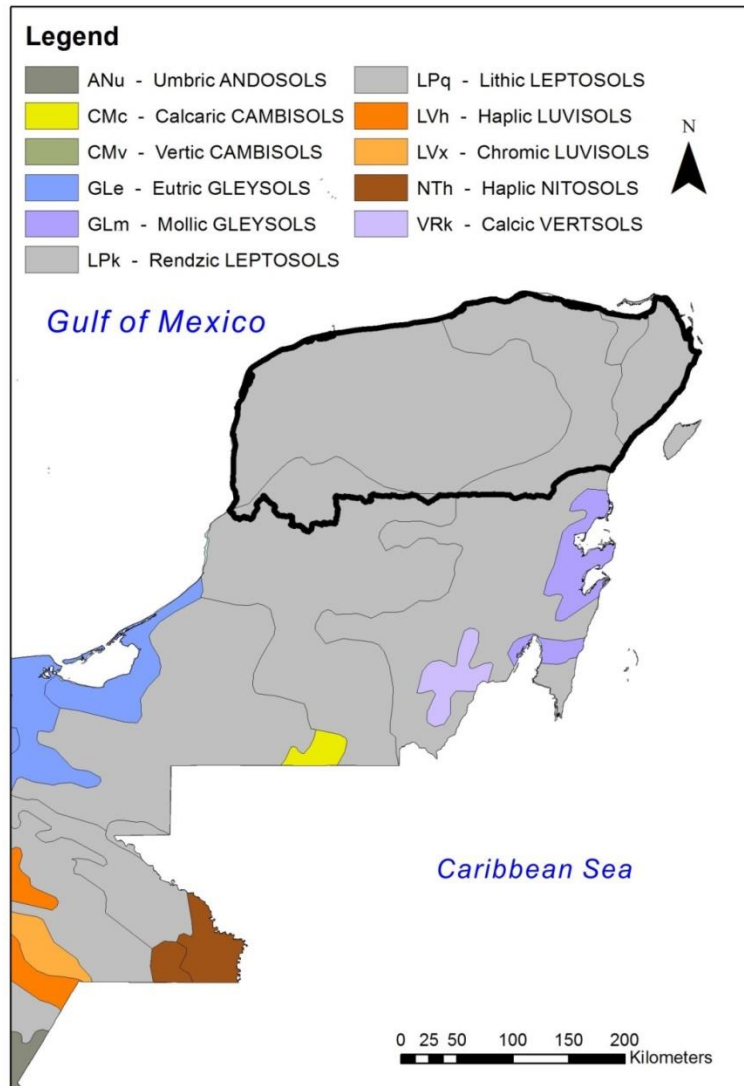
Figure 4.5   Soil map of the Yucatan Peninsula. Leptosols, the most common soil type on Yucatan Peninsula, are shown in light grey.

Table 4.2   Soil properties for a Rendzic Leptosol (or sandy loam). Default values were used where information about Yucatan soils was not available. Field capacity, specific yield, and wilting point are calculated by MIKE SHE based on the soil moisture retention curve of the soil.

Property	Value	Reference
Saturated moisture content (θ_s)	0.41	Leij et al., 1996
Field capacity (θ_{fc})	Calculated by MIKE SHE	
Specific Yield ($\theta_s - \theta_{fc}$)	Calculated by MIKE SHE	
Wilting point (θ_{wp})	Calculated by MIKE SHE	
Residual moisture content (θ_r)	0.065	Leij et al., 1996
Pressure head at field capacity (ρF_{fc})	2*	
Pressure head at wilting point (ρF_w)	4.2*	
Green and Ampt suction at wetting front	-1 m*	
Alpha (α)	0.075 cm^{-1}	Leij et al., 1996
n	1.89	Leij et al., 1996
Manning's m	0.470899*	
Saturated hydraulic conductivity (K_s)	1.23 x 10^{-5} m/s	Leij et al., 1996
Shape factor (l)	0.5*	
Bulk density (ρ_b)	1440 kg/m^3	Linsley et al., 1982 in Environmental Science Division, 2016

* indicates the default value in MIKE SHE was used

Beneath the thin soil, much of the unsaturated zone is composed of calcareous materials. Estrada-Medina et al. (2013a) observed three main rock types for a quarry on the Yucatan Peninsula: laja (hard surface rock), sascab (soft, high-porosity limestone), and coquina (fossiliferous rock with high porosity). This stratigraphy was incorporated into the MIKE SHE model by creating a soil profile with 4 layers, and assigning different properties to the soil and rock types where available (Table 4.3). Unfortunately, the only property with published values for the three limestone types was bulk density; all other properties are identical for all of the limestone types. Both the soil moisture retention curve and the hydraulic conductivity function were estimated using the van Genuchten method. The effect of assigning porosity to the carbonate layers is explored in Appendix C on macropore flow.

The hydraulic conductivity of limestones in the model was 1.2 m/s. This values was chosen because it is a mid-range value from a number of studies from the Yucatan Peninsula and the Caribbean, which ranged from 1 x 10^{-6} m/s to 6 m/s for limestones at the 100s of kilometers scale (Charvet, 2009; Gonzalez-Herrera et al., 2002; Holding, 2014; Marin 1990; Mendez Ramos 1991; Moore et al., 1992; Reeve and Perry, 1990; Roulier et al., 2006). Since macropore flow was not used in this simulation, a higher hydraulic conductivity was desirable to reproduce the effects of fractures, solution cavities and small sinkholes in the karstic limestone of the Yucatan Peninsula. A lower hydraulic conductivity could be used for the limestone if macropore flow was simulated, because the hydraulic conductivity would be representative of the limestone matrix only (DHI, 2007b). However, the final hydraulic conductivity did not appear to have a large effect on the model. The sensitivity of the model to changes in hydraulic conductivity is further analyzed in Appendix C.

Table 4.3   Properties of the limestone bedrock beneath the thin Leptosol soil. Limestone is treated as a soil in the model because it is part of the unsaturated zone. Default values were used for parameters where information about limestone was not available. Field capacity, specific yield, and wilting point are calculated by MIKE SHE based on the soil moisture retention curve of the soil.

Property	Value	Reference
Saturated moisture content (θ_s)	0.11	Roulier et al., 2006
Field capacity (θ_{fc})	Calculated by MIKE SHE	
Specific Yield (θ_s - θ_{fc})	Calculated by MIKE SHE	
Wilting point (θ_{wp})	Calculated by MIKE SHE	
Residual moisture content (θ_r)	0.01*	
Pressure head at field capacity (pF_{fc})	2*	
Pressure head at wilting point (pF_w)	4.2*	
Green and Ampt suction at wetting front	-1 m*	
Alpha (α)	0.0365 cm^{-1}	Roulier et al., 2006
n	1.83	Roulier et al., 2006
Manning's m	0.453552*	
Bulk density (ρ_b)	1800 kg/m^3 (laja) 1450 kg/m^3 (sascab) 2000 kg/m^3 (coquina)	Estrada-Medina et al., 2013a
Saturated hydraulic conductivity (K_s)	1.2 m/s	(Charvet, 2009; Gonzalez-Herrera et al., 2002; Holding, 2014; Marin 1990; Mendez Ramos 1991; Moore et al., 1992; Reeve and Perry, 1990; Roulier et al., 2006
Shape factor (l)	0.5*	

* indicates the default value in MIKE SHE was used

In MIKE SHE, when only the unsaturated zone is being simulated, the unsaturated zone must extend down to the water table. At the highest elevations in the model, the water table is located nearly 60 m below the ground surface, so the soil zone must extend to that depth to avoid errors during model runs (DHI, 2007b). The depth of each layer was based on the stratigraphy observed in Estrada-Medina et al. (2013a), as well as meeting the requirement of a 60 m deep unsaturated zone (Table 4.4). The unsaturated zone was discretized according to modeling protocol (DHI, 2007b) (Table 4.5).

Table 4.4   Depth range for each layer in the soil profile.

Soil/rock type	Depth below ground surface (m)
Rendzic Leptosol	0-0.25
Laja	0.25-2.5
Sascab	2.5-5
Coquina	5-60

Table 4.5   Vertical discretization used for soil layers. According to modeling protocol, the discretization can decrease with depth, as the majority of the unsaturated zone processes occur near the surface (DHI, 2007b).

Depth (m)	Cell height	Number of cells
0-1	0.2	5
1-5	0.5	8
5-60	1	55

The majority of vegetation on the Yucatan Peninsula is tropical dry to tropical moist forest, with some areas of savannah and crops (Dunning et al., 1998; Leyden et al., 1998; Rico-Gray and Garcia-Franco, 1991). The Leaf Area Index (LAI) in MIKE SHE was assigned based on values for tropical deciduous and tropical evergreen forests from the Global Synthesis of LAI data (Scurlock et al., 2001) (Table 4.6). Three vegetation zones were assigned to the model using a shapefile of the forest types for the Yucatan Peninsula (Figure 4.6) (UNEP, 2006). Minimum and maximum LAI values were chosen for both tropical deciduous and tropical evergreen forests, and a time series was created for each where the maximum LAI occurs in the middle of the wet season (August), and then decreases to the minimum LAI value during the dry season (November-April). In addition to the LAI, ET parameters for the entire model can also be specified in the vegetation dialogue in MIKE SHE. The interception capacity (C_{int}) determines how much water is intercepted by vegetation; C2 is related to how much evaporation always occurs in the soil; C1 gives the LAI where actual ET and potential ET are equal; and C3 is dependent on the soil type, and is related to the effect of soil moisture on transpiration. Typical values for these parameters are 0.05 mm, 0.15, 0.3, and 10 mm, respectively (DHI, 2007b; Kristensen and Jensen, 1975). These values are the defaults in MIKE SHE, and were used for all vegetation types in both the historical and TCP recharge models. A fifth ET parameter, called the Aroot parameter, describes how the root

system of the plants is distributed. The default value in MIKE SHE is 1, which indicates that at a depth of 1 m, 60% of the roots are located in the upper 20 cm of soil (DHI, 2007b). This value was also used in both recharge models, as information about these parameters for the Yucatan Peninsula was not available.
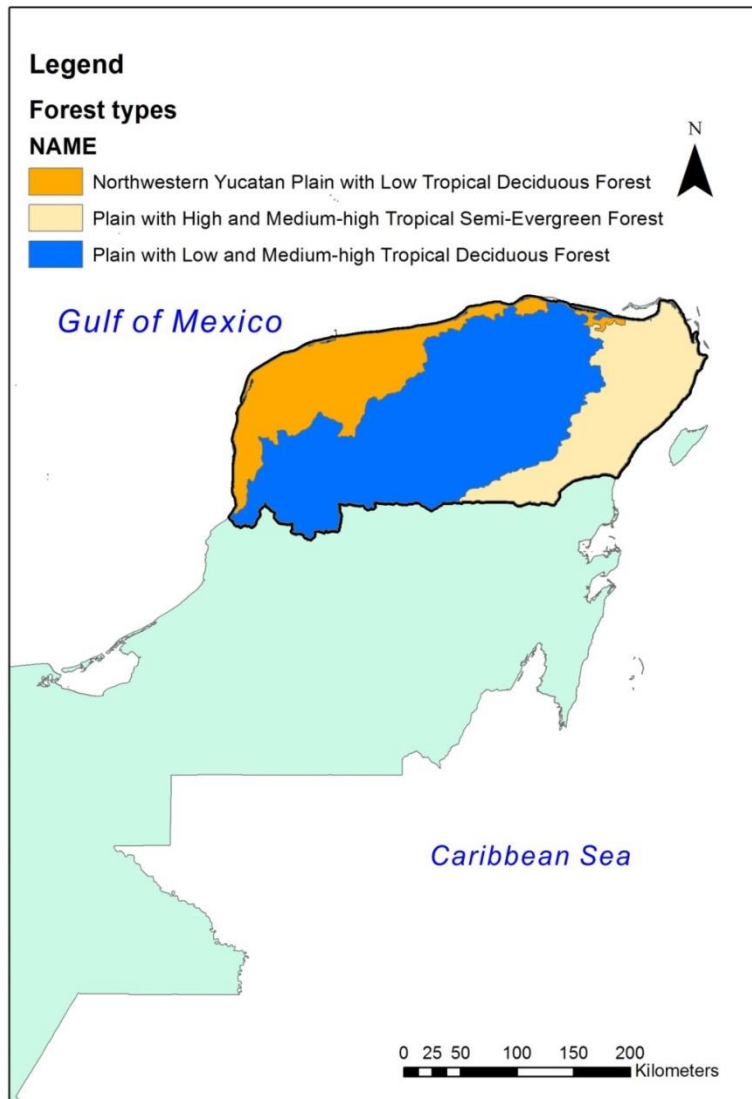
Figure 4.6 **Types of forests on the Yucatan Peninsula. For the purpose of the model, both types of deciduous forests were assigned the same LAI values.**

Table 4.6   **Range of LAI for tropical deciduous and tropical evergreen forests from the Global Synthesis of LAI data (Scurlock et al., 2001). LAI for a tropical semi-evergreen forest was estimated by taking the average of the tropical evergreen and tropical deciduous forests LAIs.**

Biome	Number of observations	Mean	Standard Deviation	Minimum	Maximum
Tropical deciduous	18	3.92	2.53	0.6	8.9
Tropical evergreen	61	4.90	1.95	1.48	12.3

The depth that plants can extract water from in the model is limited by the rooting depth. Estrada-Medina et al. (2013b) showed that soils on the Yucatan Peninsula are shallow (0.1-0.3 m in depth), and that although some soils may exist in the fractures found in the karst limestone, the majority of tree species in dry tropical forests are more likely to receive most of their water supply from the near-surface soil. For this reason, a shallow rooting depth of 0.3 m was assigned for all vegetation types.

The amount of vegetation is also related to the overland flow properties. In MIKE SHE, overland flow is modeled using a finite difference method. Manning m ranges from 10 $m^{1/3}$/s for thickly vegetated channels to 100 $m^{1/3}$/s for smooth or bare channels (DHI, 2007b). The Yucatan Peninsula is largely composed of tropical forest which is likely thickly vegetated, so Manning's m was left at the default value of 10 $m^{1/3}$/s. Overland flow also relies on the detention storage (the depth of water that must pond on the surface for overland flow to occur) and the initial water depth (the depth of water on the surface). The default values for both of the parameters are 0 mm. Due to the rapid infiltration into the karst bedrock, there is little to no surface water on the Yucatan Peninsula so these values were thought to be representative of overland flow in the study site and left at 0 mm (Perry et al., 2003).

Climate

Precipitation is input into MIKE SHE as a daily time series file. Two simulations were carried out for the historical period. The first simulation used the daily stochastic precipitation record (generated based on the observed, see Chapter 3). This time series includes wide variations in precipitation, from 0 to 400 mm/day (Figure 4.7).
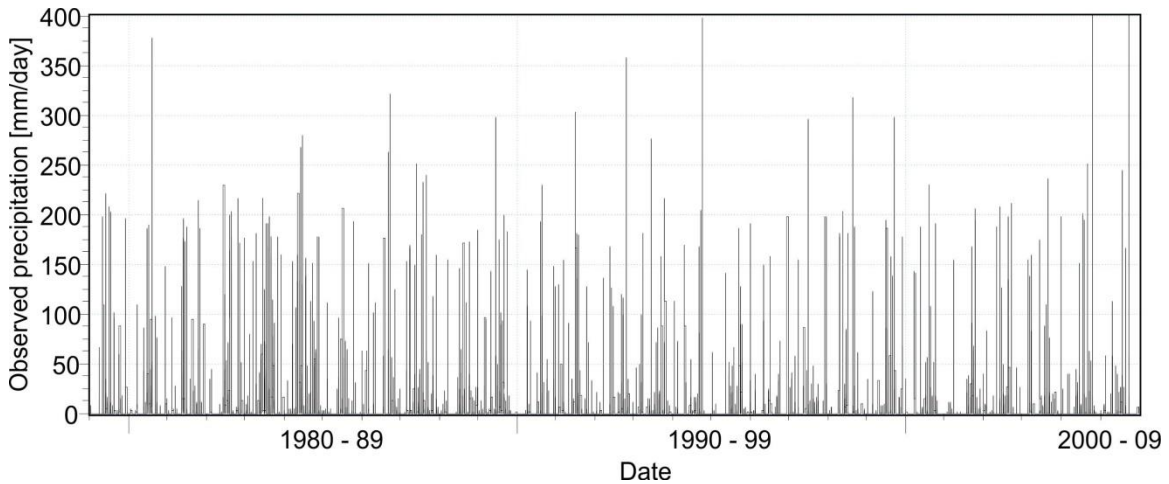
Figure 4.7   Baseline precipitation (1979-2005) used in the initial model run.

The second historical simulation used the daily observed precipitation record (1995-2010). The observed precipitation record also varies from 0 to 400 mm/day, but has fewer days with higher rainfall amounts (Figure 4.8). The effects of precipitation distribution using different precipitation datasets for the historical model and TCP reconstructions are analyzed in Section 4.6.
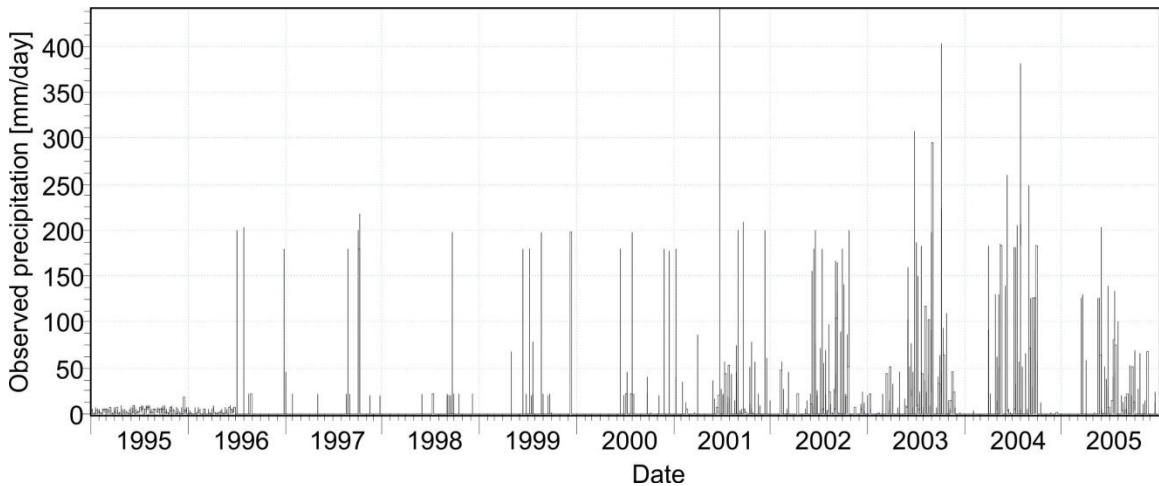
Figure 4.8   Observed precipitation (1995-2005) used in the historical observed model run.

Temperature was also reconstructed using both shift factor methods in Chapter 3; however, MIKE SHE does not require temperature as an input unless snowmelt is included in the simulation. Snowmelt was not simulated in the recharge models as snow

95

does not occur on the Yucatan Peninsula, so the reconstructed temperature records were not used for this portion of the study.

The initial reference ET was calculated using AWSET, a program which calculates potential ET using either the Penman, FAO modified Penman, or Penman-Monteith method (Hess, 1999). These formulas use minimum and maximum temperature, solar radiation, humidity, and wind speed to estimate the potential evapotranspiration (PET). A uniform distribution was used for the reference ET. In MIKE SHE, the reference evapotranspiration is the amount of ET that occurs from the surface if there were an unlimited amount of water (DHI, 2007b). MIKE SHE uses this value as a guideline for calculating actual ET, but it is not necessarily the same as the amount of ET that actually occurs in the model. The daily ET time series calculated from AWSET ranges from 0 to 60 mm/day, with the majority of days within 20-50 mm/day (Figure 4.9).
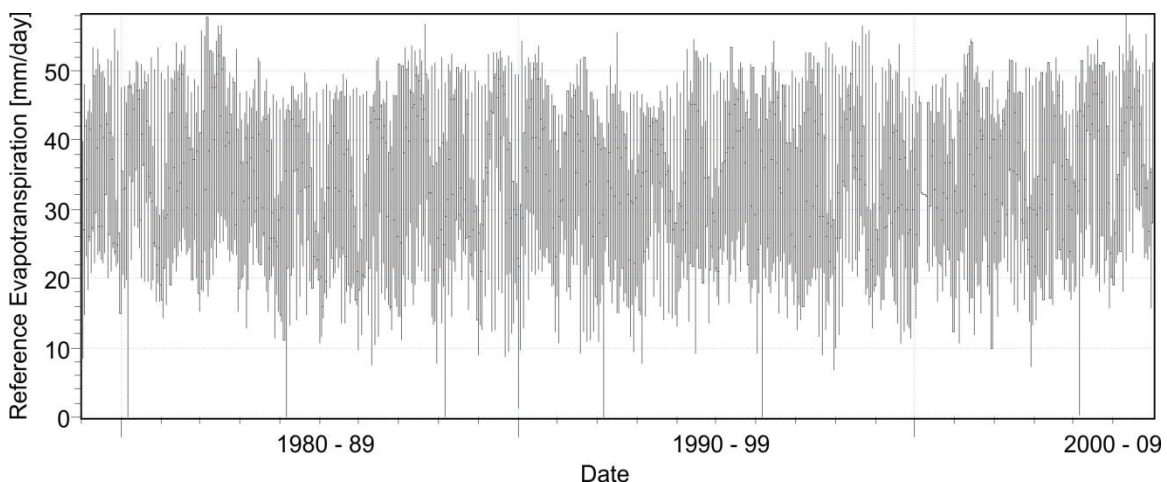
Figure 4.9   Reference evapotranspiration (1979-2005) used in the initial model run (calculated by AWSET).

The initial run using ET calculated using the Penman-Monteith method (in AWSET) caused large amount of evapotranspiration to occur in the model and resulted in a negative recharge rate. This led to the decision to find an alternative reference ET dataset. The new reference ET for the model was created by calculating the average daily ET from a set of spatially varying monthly ET data (Trabucco and Zomer, 2009). The result is a spatially variable ET dataset (Figure 4.10), which was used for every time step in the MIKE SHE model. While in reality ET is not the same for every day of the

year, the purpose of using this dataset was to reduce ET values to be more representative of the Yucatan Peninsula. MIKE SHE simply uses this dataset as a reference point for calculating ET in the model. This did lower ET in the model, and resulted in positive recharge values.
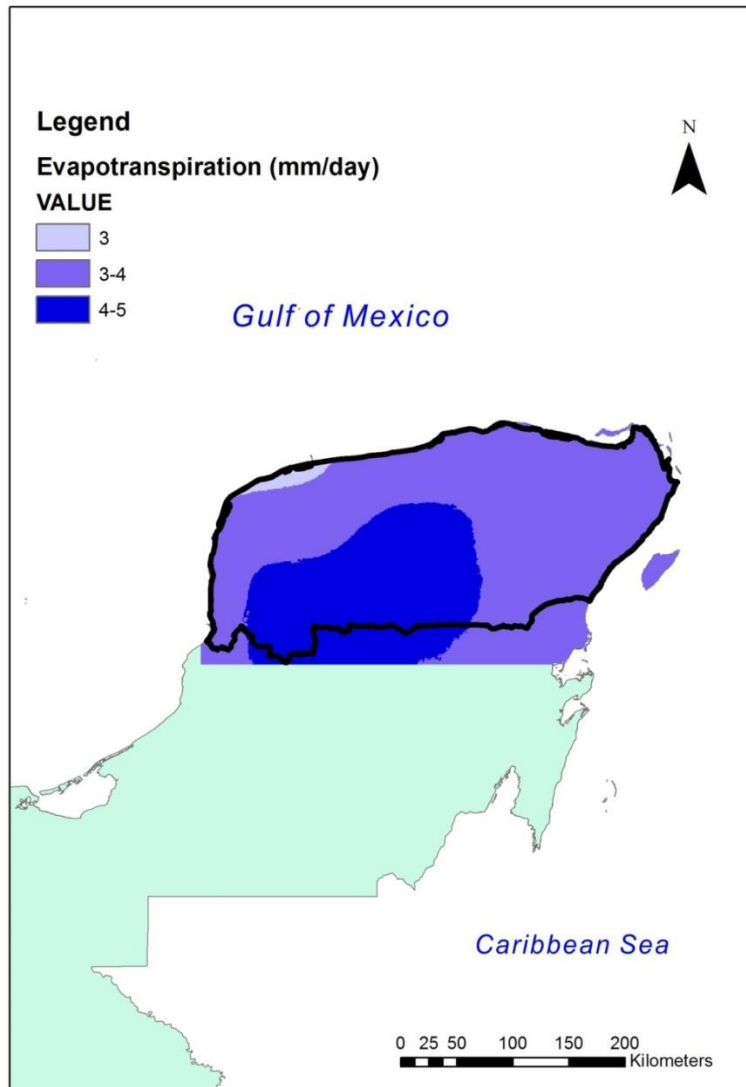
Figure 4.10   Average daily PET over the Yucatan Peninsula. The spatially variable PET dataset was created a subset of Global PET data (Trabucco and Zomer, 2009).

4.5.1.   Differences in the TCP model

The model for the TCP period has many similar parameters to the historical model. This is based on the assumption that the physical characteristics of the peninsula - such as the soils, geology, topography, and average groundwater elevations - have not changed in the past 1000 years. It is unlikely that these parameters would have changed significantly in this time period, as many of them are based on the carbonates that make up the Yucatan Peninsula, which were deposited long before the Mayans inhabited the region in the Tertiary (Gondwe et al., 2010).

One change that was made to the TCP model was the Leaf Area Index, which is an important factor in the water balance as it affects how much water is able to infiltrate into the soil. The Maya are known to have had a noticeable impact on the surrounding environment, due to their large population and agricultural practices. These practices lead to less forest cover during the TCP (Leyden et al., 1998). In addition, stresses on the environment (such as drought) can also lead to decreased plant growth, and therefore a lower LAI (Scurlock et al., 2001). For these reasons, the LAI in the TCP model was reduced by 25% year round (and for both vegetation types) to simulate decreased forest cover during the TCP. As this LAI is an estimation, and has the potential to largely affect recharge in the model, a sensitivity analysis of LAI was carried out and is included in Appendix C.

The other difference in the TCP model is precipitation. Two TCP scenarios were run using precipitation from the direct shift factor reconstruction and the stochastic reconstruction created in Chapter 3. Changes between the historical model scenarios and the TCP model scenarios are analyzed in Chapter 5.

4.6. Simulation results

Effect of different precipitation distributions (historical and reconstructed TCP scenarios)

The historical model scenarios show that the amount of recharge is only slightly affected by using a normal distribution of annual rainfall. The models were run for

slightly different simulation periods (the observed scenario from 1995-2005, the stochastic scenario from 1979-2005), so the total amount of precipitation and recharge in the models is not directly comparable. Comparing the percent of annual rainfall that is allocated to each water balance component indicates how changes in precipitation distribution affect the model, as no other parameters were changed between the two models.

In the observed precipitation scenario, which has more precipitation extremes (high and low values) and a lower median value for annual precipitation, total recharge is 60% of the total precipitation (Table 4.7). The total recharge in the stochastic precipitation scenario is 58% of precipitation. The distribution of the other water balance components in each of the scenarios shows that in the stochastic precipitation scenario, the lower recharge is mostly offset by more evapotranspiration (30% in the stochastic scenario compared to 28% in the observed scenario).

The recharge values for both models fall within the range of published recharge rates for the Yucatan Peninsula (30-70% calculated by Beddows, 2004). However, other publications agree on a much lower recharge rate of 14-17% (Gondwe et al., 2010; Lesser, 1976 *in* Back and Hanshaw, 1980). These recharge rates were determined using a variety of methods. In Gondwe et al. (2010), recharge was estimated by subtracting actual evapotranspiration (AET) from the total amount of precipitation, which gave an annual average recharge of 17%. AET was estimated using satellite imagery and satellite data as inputs into the Penman-Monteith equation. Lesser (1976) estimated potential ET based on solar radiation and average air temperature, and this ET estimate was used by Back and Hanshaw (1980) to calculate recharge using a water balance approach of inputs and outputs from the hydrogeological system, which gave an annual recharge estimate of 14%. Beddows (2004) also used a similar water balance approach, but instead of using theoretical values for water balance components, the author used field measurements of discharge along the Caribbean coast of the Yucatan Peninsula to estimate annual recharge. Beddows (2004) showed that the discharge along the coast was much higher than would be expected if recharge was only 14% of precipitation (as estimated be Lesser, 1976), and argued that recharge could be between 30-70%. This large range in estimated recharge rates suggests that recharge

99

may vary largely spatially on the Yucatan Peninsula, and that the model may overestimate recharge compared to other published values for the Yucatan Peninsula.

In the stochastic precipitation data, the normal distribution and higher median precipitation mean that this record has more years with higher rainfall than the observed data. Higher precipitation rates can lead to reduced recharge as the infiltration capacity of the soil is reached, and this appears to be the case in the stochastic simulation. As the infiltration capacity is reached, precipitated water is unable to infiltrate through the soil and recharge the groundwater, and so it is lost to runoff or evapotranspiration. The effect of precipitation extremes maybe not have been accounted for in other recharge estimates which estimated evapotranspiration based on average temperature and solar radiation, which were in the range of 14-17% (Back and Hanshaw, 1980; Gondwe et al., 2010). However, the method used by Beddows (2004) likely took precipitation extremes into account, as discharge at the coast (from the groundwater) would have directly reflected the amount of precipitation that occurred on the Yucatan Peninsula. The recharge estimates from this study more closely reflect those of Beddows (2004), with the average annual estimates ranging from 56-64%.

Table 4.7   **Average annual water balance components for the historical scenarios**

	Observed historical precipitation scenario		Stochastic historical precipitation scenario	
	Average annual amount (mm)	Percent of precipitation (%)	Average annual amount (mm)	Percent of precipitation (%)
Precipitation	2426.80	100.00	2161.19	100.00
Evapotranspiration	683.70	28.17	651.70	30.15
Overland boundary flow/runoff	279.00 (out)	11.50 (out)	238.11 (out)	11.02 (out)
Saturated zone boundary flow	1458.40 (out), -0.10 (in)	60.10 (out), 0.00 (in)	1265.07 (out), -0.04 (in)	58.54 (out), 0.00 (in)
Overland storage change	1.10	0.05	0.30	0.01
Unsaturated zone storage change	-1.50	-0.06	-0.56	-0.03
Recharge	1458.30	60.09	1265.07	58.54
Error	-6.1	-0.25	-6.59	-0.31

The water balance components also have different monthly averages, although this is partially an effect of using different precipitation datasets, as the recharge model strongly depends on precipitation. The observed data and the stochastic data have a similar seasonal precipitation pattern, although the observed precipitation shows greater precipitation during the wet season and less during the dry season, which could be an effect of the stochastic data having a normal distribution (Figure 4.11). This same pattern is seen in seasonal recharge, which depends largely on precipitation due to rapid infiltration on the Yucatan Peninsula. The observed and stochastic datasets show a similar amount of ET during the wet season, but the observed data have less ET during the dry season by up to 15 mm/month (in March). As mentioned above, overall higher ET in the stochastic data is likely due to the larger amount of years with overall higher precipitation in the stochastic dataset. The stochastic data have greater monthly runoff than the observed data during the dry season, but less runoff during the wet season, which is a direct reflection of the monthly precipitation distributions.
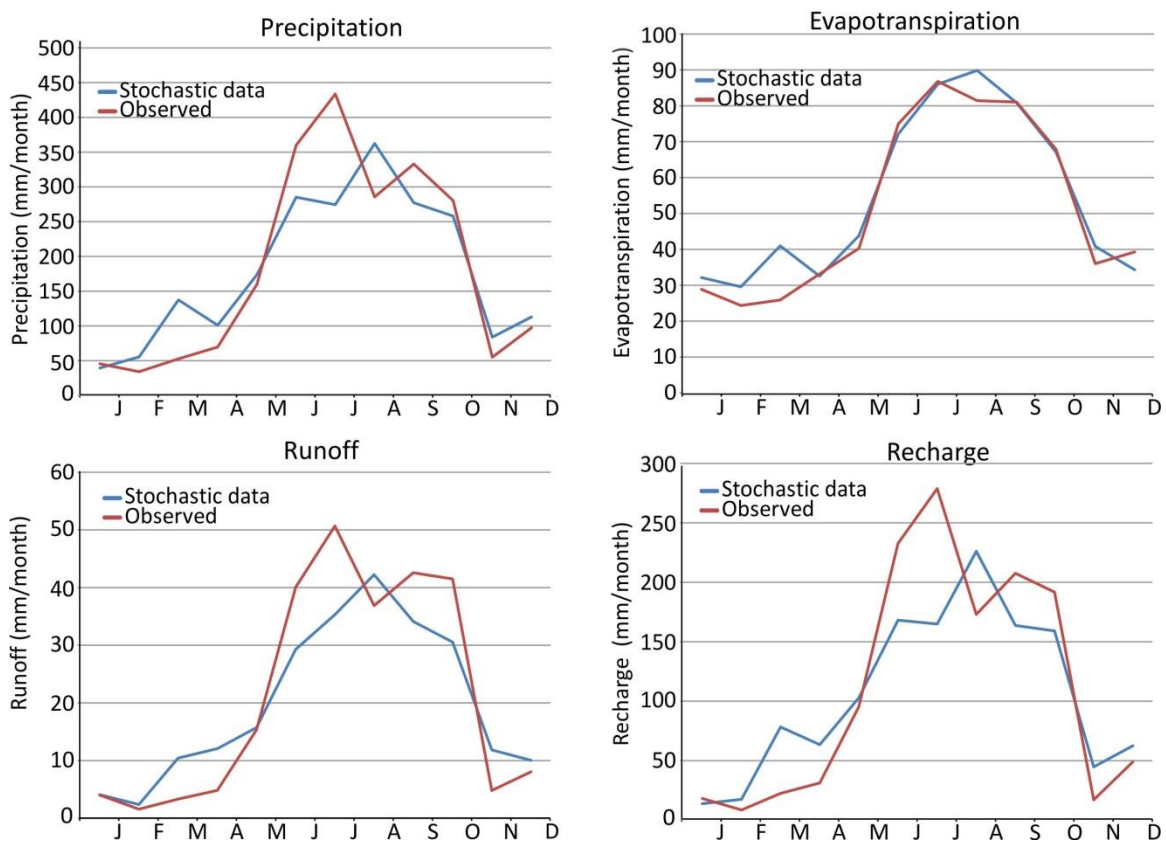
Figure 4.11   Average monthly water balance components for both historical model simulations (observed and stochastic precipitation).

The two TCP scenarios (stochastic reconstruction and directly shifted reconstruction) do not show large differences in water balance components (Table 4.8). The percent of recharge is nearly identical for both scenarios (61.83% for the directly shifted reconstruction and 61.77% for the stochastic scenario).

Table 4.8   Average annual water balance components for the TCP recharge scenarios.

	Directly shifted reconstruction		Stochastic reconstruction	
	Average annual amount (mm)	Percent of precipitation (%)	Average annual amount (mm)	Percent of precipitation (%)
Precipitation	2672.00	100.00	2340.77	100.00
Evapotranspiration	698.00	26.12	616.07	26.32
Overland boundary flow/runoff	316.20 (out)	11.83 (out)	273.50 (out)	11.68 (out)
Saturated zone boundary flow	1652.00 (out), -0.10 (in)	61.83 (out), 0.00 (in)	1445.76 (out), -0.03 (in)	61.77 (out), 0.00 (in)
Overland storage change	1.20	0.01	0.23	0.01
Unsaturated zone storage change	-1.30	-0.05	-0.33	-0.01
Recharge	1652.00	61.83	1445.76	61.76
Error	-5.90	-0.22	-5.53	-0.24

The similarity between the two TCP scenarios is also seen in the average monthly water balance components for these models (Figure 4.12). The seasonal distribution of precipitation is slightly different between the two, with peak precipitation occurring a month later (July) in the directly shifted reconstruction than the stochastic reconstruction (June). Monthly recharge and runoff follow the precipitation pattern very closely for both datasets, so this causes peak runoff and recharge to occur in different months as well. Peak evapotranspiration occurs in July in both scenarios, but the stochastic reconstruction scenario has higher ET by almost 10 mm/month. This higher ET could be due to higher precipitation, making more water available for evapotranspiration.
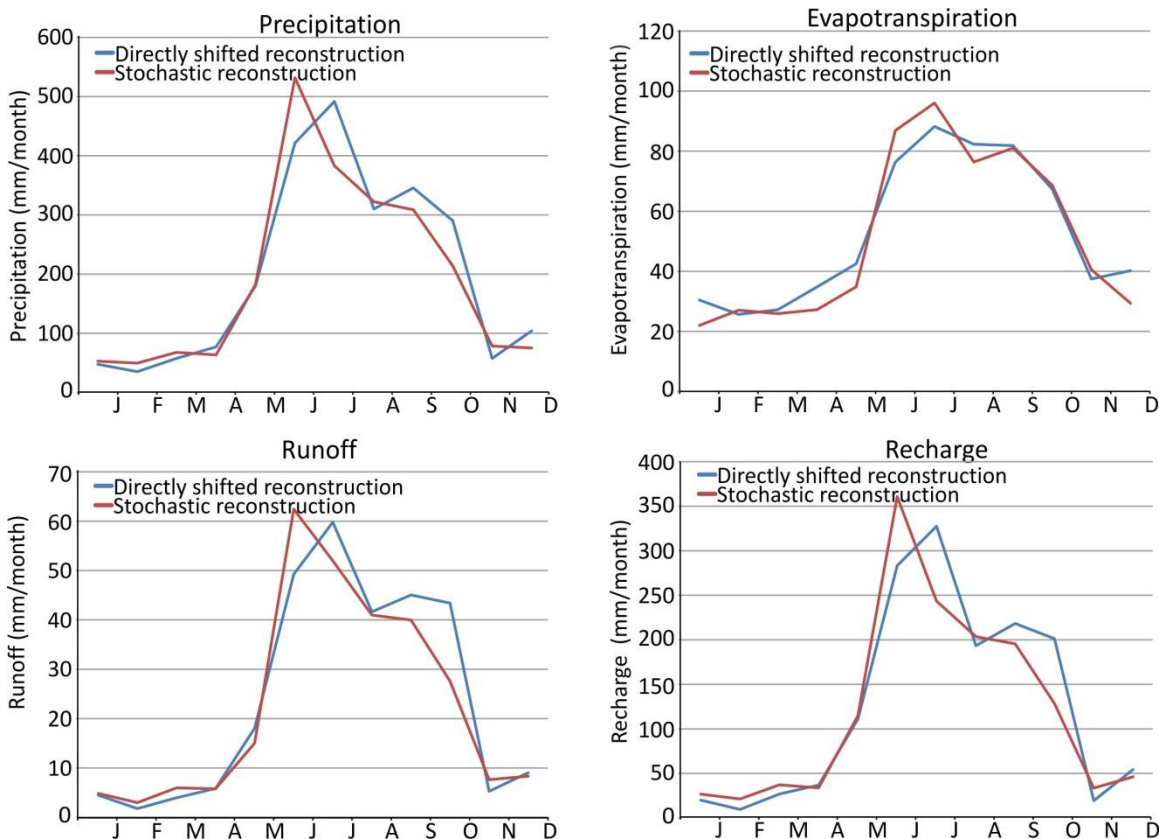
Figure 4.12   Average monthly water balance components for TCP scenarios (directly shifted and stochastic precipitation reconstructions).

It is interesting that water balance components for the two TCP simulations are so similar, because they have different distributions much like the stochastic and observed historical data. However, the differences in the historical model components are also small (differences up to 2%), so it could be that precipitation distribution does not really have a large effect on the model. In the TCP scenarios, the stochastic reconstruction has a normal distribution, while the directly shifted reconstruction has a skewed distribution with a low median value (see Chapter 3). The stochastic simulation does have a slightly lower percent of recharge (0.14%), which could be indicative of reduced recharge due to the soil reaching its infiltration capacity (much like the historical stochastic data). However, it is not a large enough difference to conclude that precipitation distribution has a significant effect on the recharge model for this time period. Regardless, the direct shift factor reconstruction is still more appropriate for the Yucatan Peninsula as it does not normalize climate time series. This approach will be used for comparison of recharge between the historical and TCP time periods.

Changes between the historical time period and the TCP

The observed precipitation scenario and the directly shifted reconstruction were chosen to compare recharge between the historical and TCP time periods. Given that the two TCP scenarios had very similar water balance components (see above), this choice is unlikely to have a significant effect on the results of this comparison. The historical and the TCP models used the same parameters for geology and soils, but different precipitation records and different LAI values. However, Appendix C shows that LAI did not have a large effect on the model.

The TCP scenario has a slightly higher average annual recharge than the historical scenario (a difference of 1.74%) (Table 4.9). It also has slightly lower average annual ET (26% compared to 28%) and slightly higher runoff (a difference of 0.33%). These water balance components suggest that the historical and TCP time periods were quite similar on average; however, the seasonal distributions of these components show there are differences between the two time periods.

Table 4.9   Average annual water balance components of the observed precipitation scenario and the directly shifted reconstruction.

	Observed precipitation scenario		Directly shifted reconstruction	
	Average annual amount (mm)	Percent of precipitation (%)	Average annual amount (mm)	Percent of precipitation (%)
Precipitation	2426.80	100.00	2672.00	100.00
Evapotranspiration	683.70	28.17	698.00	26.12
Overland boundary flow/runoff	279.00 (out)	11.50 (out)	316.20 (out)	11.83 (out)
Saturated zone boundary flow	1458.40 (out), -0.10 (in)	60.10 (out), 0.00 (in)	1652.00 (out), -0.10 (in)	61.83 (out), 0.00 (in)
Overland storage change	1.10	0.05	1.20	0.01
Unsaturated zone storage change	-1.50	-0.06	-1.30	-0.05
Recharge	1458.30	60.09	1652.00	61.83
Error	-6.1	-0.25	-5.90	-0.22

The seasonal water balance components show that the majority of the differences in recharge occur during the wet season (Figure 4.13). While the TCP scenario has up to a 50 mm/month higher recharge during the wet season, the monthly changes are close to 0 during the dry season. This is a reflection of the shift factors for precipitation, which were higher during the wet season (see Chapter 3). More runoff also occurs during the TCP dry season, which is likely related to the higher precipitation amounts seen in the TCP model. While these models do not show evidence of seasonal drought, the shift factors used in this study were unable to incorporate variability (see Chapter 3), so it is possible that the changes between the two time periods seen in this study are underestimated. As more precipitation occurs during the wet season (without much of a change in average annual rainfall), the Yucatan Peninsula could be susceptible to dry season droughts. It is likely that the droughts that affected the Mayans during the TCP occurred during the dry season, but without incorporating changes in variability into this study, the reconstructions were unable to reproduce this. These results are also in accordance with those found in Chapter 3, which suggested that more annual rainfall occurred during the TCP. As recharge is closely linked the rainfall for the Yucatan Peninsula, a higher annual recharge during the TCP was expected.
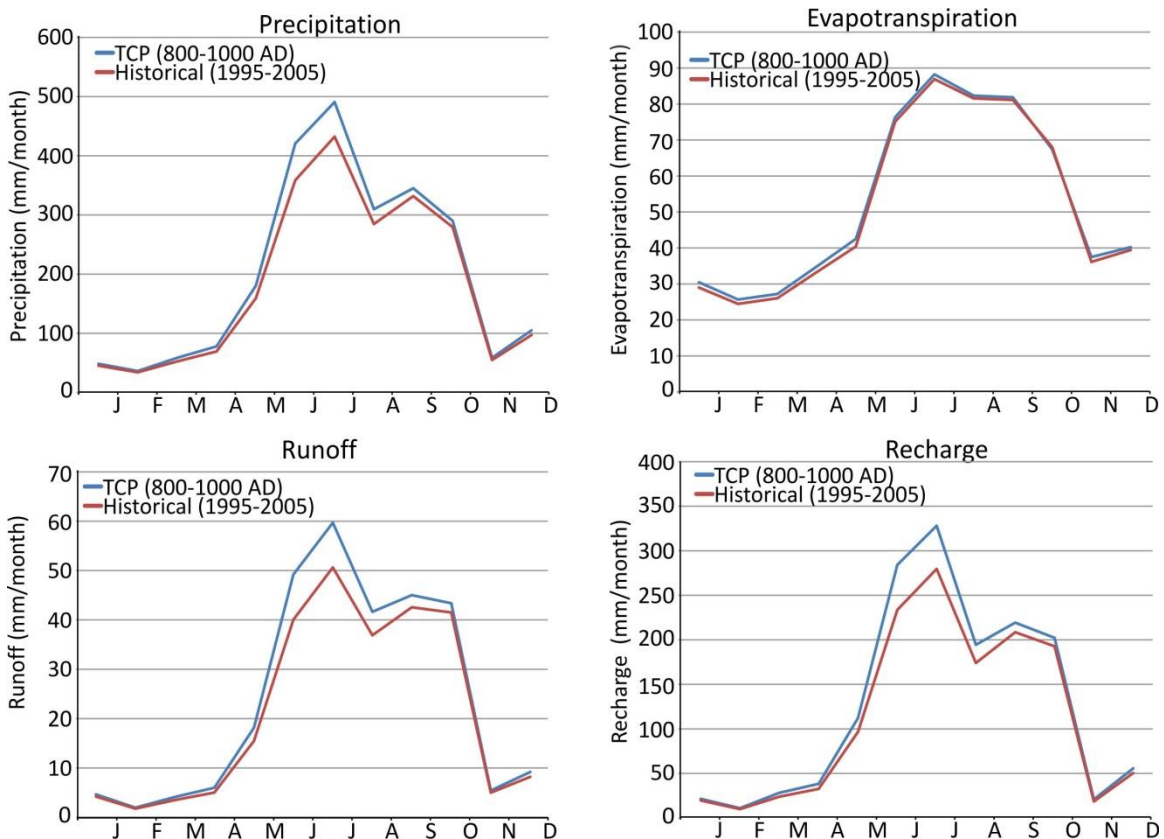
Figure 4.13   Seasonal water balance components for the directly shifted reconstruction (TCP) and the observed record (Historical).

4.7. Sources of uncertainty

One of the most challenging aspects of creating the recharge model for the Yucatan Peninsula was the availability of detailed data. This problem introduced uncertainty in the model, by limiting the spatial detail and requiring numerous parameters to be estimated based on published values. An important assumption made in this model is that precipitation is uniform across the entire study area although the north coast of the Yucatan Peninsula is noticeably drier than the south (Bautista et al., 2011). A uniform precipitation was considered to be reasonable for this model as the purpose is to estimate regional changes in recharge. However, this does introduce uncertainty as rapid infiltration on the Yucatan Peninsula means recharge is closely linked to changes in precipitation. If numerous daily precipitation records had been available, a spatially variable time series could have been created to reduce uncertainty.

Estimated values were used for numerous parameters, with some with the potential to have a larger effect on recharge than others. Leaf Area Index and hydraulic conductivity in particular could play a large role in how much water is able to pass though the soil zone. LAI is typically very difficult to measure, and detailed datasets for LAI were not available for the Yucatan Peninsula. While the chosen estimates are based on the vegetation zones found on the Yucatan, the LAI of areas that are less vegetated (such as cities and beaches) are not taken into consideration. Additionally, the LAI values used are averages of the vegetation types found in each type of forest on the Yucatan, but in reality LAI is likely much more variable spatially than indicated by the model. Hydraulic conductivity was similarly difficult to estimate, as the unsaturated zone on the Yucatan Peninsula is mainly composed of karstic limestones. Karst features cause the hydraulic conductivity to vary largely, as small-scale fractures have much higher hydraulic conductivities than the surrounding limestone (Bauer-Gottwein et al., 2011). However, estimates of the larger-scale conductivity were used in the final model. Using large-scale estimates of the conductivity should reduce uncertainty in regional recharge, but the calculated recharge at a local scale is likely not accurate throughout the model.

4.8. Conclusions

Groundwater recharge on the Yucatan Peninsula was calculated for four simulations of the Yucatan Peninsula climate (observed, historical stochastic data, directly shifted reconstruction, and the stochastic reconstruction) by modeling unsaturated flow in MIKE SHE. This model was created using published data on the Yucatan Peninsula for soil and rock characteristics, leaf area index, topography, and climate. While no calibration data were available for the study region, the annual error in the initial model run is low (0.31% of precipitation) and the water balance components are closely related to precipitation, which shows that the model simulates the high permeability limestones reasonably well.

The TCP model varies slightly from the historical model, but was based on the assumption that the geology and physiology of the Yucatan Peninsula have not changed significantly in the past 1000 years. The TCP model has a lower LAI to simulate

vegetation conditions that would have existed during the TCP due to stresses on the environment from the large Mayan population. It can be assumed that using the same properties for the geology and soils of the Yucatan Peninsula will reduced any biases in the model when analyzing the difference in recharge between the historical and TCP time periods.

The four precipitation simulations were analyzed to determine the effect of different rainfall distributions on the recharge model. The stochastic data, which has a higher median than the observed data and a normal distribution, was shown to have slightly lower recharge than the observed data, even though it has more years with higher precipitation compared to the observed data. The lower recharge could be evidence of the model reaching its infiltration capacity during higher rainfall events, preventing increases recharge and causing more water to be lost to runoff and evapotranspiration. The two TCP scenarios did not show any significant differences in the water balance components, despite having different distributions (similarly to the two historical scenarios), suggesting that precipitation distribution does not have a large effect on the model. Although the two scenarios appeared equally viable for estimating recharge, the direct shift factor reconstruction and the observed data were the only two scenarios with the correct annual distribution of rainfall for the Yucatan Peninsula.

Model output from these two scenarios was then used to analyze the change in recharge between the historical and TCP time periods. While overall the TCP scenario (the directly shifted reconstruction) had more average annual recharge, the seasonal distributions of recharge showed that the most of this difference in recharge occurred during the wet season on the Yucatan Peninsula. It is difficult to fully analyze the possibility of droughts without incorporating variability into the climate reconstructions, but this seasonal distribution of recharge suggests that the Yucatan Peninsula could have been susceptible to dry season droughts.

Chapter 5.   Limitations, conclusions, and recommendations

Throughout this study, a number of problems were encountered that limited the methods used and the results of the study. While a main goal of this study was to develop a methodology for producing a daily paleoclimate time series, it became apparent that with the resources and data available there are still many assumptions that must be made to do this, and that reconstructing the paleoclimate is not a simple task. This chapter outlines the problems and limitations of this study, the final conclusions based on the data available, and recommendations for future work in this area.

5.1. Limitations of the study

5.1.1.   Reconstructing precipitation from proxy data

Numerous previous studies have attempted to reconstruct the climate on the Yucatan Peninsula for the TCP to look for evidence of drought during this period (Curtis and Hodell, 1996; Curtis et al., 1998; Hodell et al., 1995; Hodell et al., 2005a; Hodell et al., 2005b; Medina-Elizalde et al., 2010; Stahle et al., 2011). Most of these studies used a qualitative approach to reconstructing the climate, equating variations in the proxy record to changes in the moisture conditions of the Yucatan Peninsula. Medina-Elizalde et al. (2010) used a linear relationship between the modern portion of the proxy record and observed precipitation to estimate annual precipitation during the TCP; this method was used in this study to reconstruct precipitation from six proxy records which were determined to have adequate data for the modern portion of the record (see Chapter 2).

As discussed in Chapter 2, the linear regression reconstruction technique had some limitations. This technique assumed that the entire proxy record signal was due to precipitation (and not temperature), which, although temperature on the Yucatan

Peninsula is fairly constant, could give false results if this assumption is invalid. In addition, the need for data in the modern portion of the proxy record lead to the elimination of 11 proxy records during precipitation reconstructions which may have been useful for the study. Uncertainty in the age dating techniques and age models also introduced further uncertainty into these reconstructions.

One of the main failings of this approach was the loss in variability in the precipitation reconstructions. Proxy records already have low resolution, and for this study, all the proxy records available had annual or lower resolution, which resulted in precipitation reconstructions with only annual resolution. While some evidence of drought was observed in the reconstructed precipitation at an annual time scale, calculated shift factors and recharge modeling (Chapters 3 and 4) suggest that the Yucatan Peninsula may have experienced seasonal droughts in the dry months, even if the average annual precipitation was higher during the TCP than it is today. This seasonal distribution of rainfall may not be recorded in annual proxy records, which may explain why some proxy records seemed to record drought at different times, or not at all. In addition to this, because the reconstruction technique reduced the variability of the precipitation reconstructions and eliminated extreme values, they may not be an adequate indicator of the full range of precipitation amounts that could be expected on the Yucatan Peninsula.

5.1.2. Using GCM data for shift factors

Model output from two experiments of the CCSM4 model (the historical and past1000 experiments) were used to calculate shift factors. Some downfalls of the CCSM4 model were already known, such as the model's tendency to overestimate precipitation (Gent et al., 2011). However, the biases of the model were eliminated by calculating shift factors between two experiments of the same model.

GCMs are also too coarse to accurately reproduce the climate at a local scale, which creates the need for downscaling. In general, GCMs also do not simulate climate cycles such as ENSO very well, and while improvements have been made on this front in the CCSM4, the model is still is not perfect (Gent et al., 2011). However, preliminary

work on the effects of ENSO, PDO, and MJO on precipitation and temperature on the Yucatan Peninsula showed that there is not necessarily a strong correlation between these climate variables and the climate indices on the Yucatan Peninsula (Appendix D). Moreover, the poor representation of the local climate became apparent in the lack of variability in the model data for the Yucatan Peninsula, and the inability of the model data to reproduce the seasonal pattern of precipitation seen in the observed climate data (Chapter 3). Additionally, the median values of annual precipitation of the model data were much lower than the median annual precipitation of the observed data, which is likely an effect of the reduced precipitation variability in the models. These problems were observed in both the historical and the past1000 model data.

Despite these issues, GCM output was still the best option for calculating backwards shift factors, as monthly (or even seasonal) shift factors were not possible from the proxy reconstructions. Calculating the shift factors between the two time periods in the same model at least reduced model bias, and then changes between the models seem to follow the correct seasonal pattern (with greater precipitation changes occurring in the wet season and not halfway through the wet season, which is when the models showed the greatest monthly precipitation), suggesting that the regional-scale changes between the models are somewhat realistic. Unfortunately, the reduced variability in the model output lead to more problems in using a stochastic weather generator for downscaling, as discussed below.

5.1.3. Using a stochastic weather generator

Stochastic weather generators are commonly used for applying monthly or seasonal shift factors to a baseline stochastic weather series in order to generate a different stochastic weather series that is "shifted" from the baseline. This shift factor approach has been used in the forward sense to project the future climate in previous groundwater studies (Allen et al., 2004; Allen et al., 2010; Jyrkama and Sykes, 2007; Scibek and Allen, 2006). However, in this study this shift factor approach was not appropriate due to two problems encountered while using LARS-WG.

First, using a stochastic weather generator assumes that the "shifted" climate is statistically the same as the baseline climate, apart from the parameters that are forced to shift. For this study, LARS-WG was selected specifically because it can apply shifts to a wider range of climate parameters, particularly wet and dry series length, which would be important for detecting changes in drought occurrence. The problem encountered was not with the stochastic weather generator itself, but rather the model output. LARS-WG was unable to detect the length of wet and dry series in the model output, because the variability in the model output was so low that there were no wet or dry series; the model had a small amount of precipitation occurring every day, as opposed to having some days with no precipitation and some days with very high precipitation as is seen in the observed data (see Chapter 3). Unfortunately, this meant that shift factors for the length of wet or dry series could not be calculated because these climate parameters did not exist in the model output. Without changes in the length of wet and dry series, it must be assumed that climate variability was the same during the TCP as it is today, which may not be true. These assumptions severely limit the usefulness of the reconstructed daily climate time series for the TCP, as climate variability plays an important role in determining the timing and severity of precipitation extremes such as storms and droughts. Not incorporating climate variability means that the shift factors potentially underestimate the expected changes, as more extreme precipitation values could have occurred during the TCP climate.

The second failing of LARS-WG was that it generated a climate which is not representative of the observed climate on the Yucatan Peninsula. A large portion of precipitation on the Yucatan Peninsula occurs in extreme storm events, such that up to 75% of the annual precipitation occurs in these events during the wet season (Gondwe et al., 2010). This means that while there are days with very high precipitation, many days also have very low or no precipitation. Similarly, while there are a few years with very high precipitation in the observed record, many years have a much lower annual precipitation; 840 to 1500 mm/year on average (Gondwe et al., 2010). The result is a skewed annual precipitation distribution, where the median annual precipitation is lower than the average annual precipitation. However, when LARS-WG generates weather data, it smooths the data and creates a normal distribution (Semenov and Barrow, 2002), which raises the median annual precipitation to equal to the average annual

precipitation. This normal distribution was generated for both the stochastic historical data and the stochastic reconstruction. As a result, this common approach for applying shift factors was not applicable for the Yucatan Peninsula, as the precipitation distribution had the potential to affect the amount of recharge that occurred in the models. To better capture the actual precipitation distribution (and assuming that this skewed distribution would have been the same during the TCP), a direct shift factor approach was used to reconstruct the paleoclimate. While this approach was successful in this regard, the direct shift factor approach lacked the ability to incorporate changes in variability as no shift factors for the length of wet and dry series were calculated.

5.1.4.   The recharge model

The purpose of the recharge model was to analyze regional changes in the recharge conditions for the TCP. Although this did not require detailed geological data, a major limitation of the model was that the soil and rock parameters had to be estimated based on previously published values for the study area and similar rock types. While the sensitivity analysis showed that the hydraulic conductivity (K) values of the soil and limestone did not have a large effect on the model, a number of other soil properties (such as field capacity and residual moisture content, and shape factor) were less well constrained and had to be left at default values in the model.

Another limitation of the model was using a uniform precipitation to represent the Yucatan Peninsula climate. Although there is a known precipitation gradient (Bautista et al., 2011), climate data from multiple climate stations were not available for the historical or TCP time periods, which meant that the spatial distribution of precipitation could not be included in the model. As recharge is closely linked to groundwater recharge on the Yucatan Peninsula, this limitation meant that spatial recharge also could not be analyzed. Because spatial recharge was not modeled, spatial changes in geological properties, such as the calcrete aquitard fount near the coasts (see Chapter 1), were not included in the model.

5.2. Conclusions

5.2.1. Precipitation reconstructions and proxy data

A qualitative analysis of the available proxy data for the Yucatan Peninsula showed that some proxy records had more evidence of TCP droughts than others. Variations in the timing and amplitude of the drought signals in the proxy records could be due to uncertainty in the age models and age dating techniques, the inability of low resolution proxy data to record seasonal droughts, or differing responses of each proxy record to drought. Five records appeared to have more conclusive evidence of droughts during the TCP:

- speleothem $\delta^{18}O$ (Medina-Elizalde et al., 2010)
- Chara $\delta^{18}O$ (Hodell et al., 2005a)
- Pyrgophorus coronatus $\delta^{18}O$ (Curtis and Hodell, 1996)
- % $CaCO_3$ and %S (Hodell et al., 1995)
- sediment density (Hodell et al., 2005b)

Of the seventeen proxy records analyzed, six were found to be appropriate for reconstruction based on the number of data points in the modern record and their ability to produce reasonable precipitation values for the Yucatan Peninsula (positive values and less than 2000 mm/year). However, the linear regression technique used to reconstruct precipitation relied on the relationship between the modern proxy record and observed precipitation data. Therefore, the reconstructions with the most data points in the modern portion of the proxy record were determined to be the most reliable (the speleothem record by Medina-Elizalde et al., 2010 and the PDSI record by Stahle, 2011). These reconstructions had median values of precipitation similar to those of the model data: the speleothem reconstruction had a median value of 900 mm/year and the PDSI reconstruction had a median value of 950 mm/year, while the model data had median values of 950 mm/year and 1000 mm/year for the historical model and past1000 model data, respectively. However, the proxy records and model data had a lower range in annual precipitation compared to the daily observed precipitation record, suggesting that the model data and reconstructions did not capture the true variability in rainfall on the Yucatan Peninsula.

The two records used to reconstruct modern precipitation (the speleothem record and the PDSI record) showed that the historical climate had a higher median annual precipitation than the TCP, although this change was more noticeable in the speleothem record. The PDSI record may show less evidence of drought than the speleothem record because it was not located directly on the Yucatan Peninsula, and the intensity of the TCP droughts may have varied spatially. However, the lack of evidence of drought in the other precipitation reconstructions could suggest that droughts on the Yucatan Peninsula may not have been as extensive as previously thought, and that the TCP was not significantly drier than the current climate.

5.2.2.   Generating and applying shift factors

The historical and past1000 experiments of the CCSM4 model were both found to have reduced variability compared to the daily observed record, and neither reflected the seasonal pattern of precipitation on the Yucatan Peninsula. However, the GCM model was still used to generate shift factors, as the daily output available from GCMs provided a more useful option than the reconstructions from proxy data. Calculating the shift factors between the two model experiments has the benefit of eliminating bias from the CCSM4 model.

The shift factors calculated by LARS-WG indicated that temperatures during the TCP were up to 2°C cooler than the current climate, and that more precipitation occurred during the TCP. However, during the TCP more rain fell during the wet season, while dry season precipitation was similar to the current climate. Notwithstanding, changes in the length of wet and dry series were not able to be included in the shift factors, so the shift factors may underestimate the change between the current and TCP climates.

Unfortunately, the common method of applying shift factors to a stochastic weather series (generated using LARS-WG) was found to not be applicable for this study. While the observed annual precipitation on the Yucatan Peninsula has a skewed distribution, LARS-WG generated a weather series with a normal distribution, which overestimates the number of higher precipitation events on the Yucatan Peninsula. As higher precipitation events have the potential to limit recharge, this method could not be

115

used to create a daily climate time series for use in the recharge model. Instead, an alternative method was used which directly applied shift factors to observed data. This created a daily climate time series for the TCP that had the same precipitation distribution as the observed data, albeit shifted at a monthly time scale. This precipitation time series is thought to be more representative of the climate conditions that would have occurred during the TCP. For this reason, the daily observed data and the directly shifted reconstruction were chosen to represent the historical and TCP periods for the comparison of recharge on the Yucatan Peninsula; however, all four precipitation datasets (stochastic historical, observed historical, stochastic reconstruction, and directly shifted reconstruction) were used in the recharge model to analyze the effects of differing precipitation distributions on recharge.

5.2.3.   Recharge modeling

Four model simulations were run in MIKE SHE to estimate regional recharge on the Yucatan Peninsula. MIKE SHE has the capability to integrate both groundwater and surface water; however, to calculate recharge, only the unsaturated zone was modeled. A sensitivity analysis (Appendix C) showed that the recharge model was only slightly affected by changes to the hydraulic conductivity of the limestone (up to a 4% difference in annual recharge for the low-K scenario). The effects of changing the leaf area index (LAI) were found to be negligible (no significant change in the annual or seasonal water budgets), while the effects of simulating macropores in the model had the potential to increase annual recharge by up to 6%. However, using a large-scale estimation for the K of fractured limestone was thought to be more representative of the regional hydraulic conductivity for the Yucatan Peninsula, as detailed information about the location, size, and extents of fractures and dissolution features was not available.

A comparison of differing precipitation distributions showed that using a precipitation dataset with a normal distribution in the model had a small effect on the amount of annual recharge. This effect was more pronounced in the two historical precipitation models, which showed that the observed precipitation scenario calculated 1.55% higher annual recharge than the stochastic precipitation scenario. This indicates that although the stochastic precipitation scenario had a higher average annual

116

precipitation (more years with higher rainfall), it calculated less recharge annually. This indicates that at higher precipitation rates, soils in the model may reach their infiltration capacity and limit groundwater recharge. This further justified the use of the observed precipitation and the directly shifted precipitation scenarios for the comparison of recharge in the TCP and current climates.

Changes between the water balance of the historical (observed) and TCP (directly shifted reconstruction) scenarios indicated that on average, 1.74% more recharge occurred annually during the TCP. This slight increase in recharge was balance by a slightly lower annual evaporation during the TCP (26.12% compared to 28.17% in the historical model) and slightly higher runoff (11.83% compared to 11.50% in the historical model). The seasonal water balance components showed that during the TCP, more recharge occurred during the wet season (May-October), which is a direct reflection of the precipitation shift factors calculated by the GCMs, which were higher during the wet season. As mentioned previously, a limitation of this study was that changes in variability were not incorporated in the shift factors. Therefore, the results of the recharge models (which used the reconstructed precipitation time series) also do not include changes in variability. This means that the TCP climate may have had more extreme values which are not represented in the water balance. If less monthly precipitation occurred in the dry season during the TCP, the Yucatan Peninsula may have been susceptible to dry season droughts; however, without the incorporation of changes in variability, the results are not able to show this.

The results of recharge modeling disagree with the results of the modern proxy reconstructions, which suggested less annual rainfall during the TCP. The shift factor approach to reconstructing the paleoclimate, while it had numerous limitations, did not find any conclusive evidence of droughts during the TCP, and in fact suggested that more precipitation occurred on the Yucatan at this time. This disagreement between methods points to the need for more in depth studies of the paleoclimate on the Yucatan Peninsula. While the accepted paradigm is that droughts were a contributing factor to the Mayan's collapse, this study showed that the occurrence of these droughts is still uncertain.

117

5.3. Recommendations for future work

Paleoclimate-driven groundwater studies are becoming increasingly important as the need to understand the full range of potential effects from climate change arises. Unfortunately, paleoclimate data are nowhere near as detailed as they need to be for groundwater modeling, so reconstruction techniques must be used, despite a number of assumptions and problems being associated with them. Aside from suggesting more detailed paleoclimate data, recommendations for future work in this area include:

- **Choose a study area with high quality observed climate data**. Observed data for the Yucatan Peninsula were not easily accessible, and there were many gaps in the data. The original daily observed record spanned 1979-2005, but had to be shortened to 1995-2005 because the beginning years of the data had many missing data points. Additionally, multiple climate stations for the Yucatan Peninsula would have been useful for recharge modeling, as a spatially varying precipitation record could have been created.

- **Place a priority on finding proxy records that record seasonal changes in the moisture balance**. Some proxy records may have less than annual resolution, although these are likely rare. However, a proxy record that is sensitive only to moisture changes in a certain season could be useful for creating seasonal shift factors, or for studying precipitation extremes during that season (for example, droughts in the dry season).

- **Improve GCMs for seasonal precipitation patterns and precipitation extremes**. Work to improve GCMs is already in progress, but a number of problems in this study were related to relying on GCMs for shift factors, particularly the inability of LARS-WG to determine shift factors for the length of wet and dry days. Improvements of GCMs will lead to more confidence in shift factors and model output.

- **Conduct an analysis of the seasonal distribution of precipitation before choosing a weather generator (or shift factor technique)**. The Yucatan Peninsula was somewhat unique in that it had a skewed precipitation distribution; this is likely not the case for all study areas. A stochastic weather generator could be used if a study area with a more normal precipitation distribution was used, or alternative shift factor approaches could be developed for climates with a skewed precipitation distribution. The direct shift factor approach was more representative of the Yucatan Peninsula in this study, but lacked the ability to incorporate changes in variability into the reconstructed climate.

- **Develop alternative "backwards" shift factor approaches**. This study used a shift factor approach which is already used in future climate projections and attempted to use it in the reverse sense. While GCMs are a useful tool, they cannot reproduce the actual climate that occurred in the past (for example, a paleoclimate model simulates the climate conditions that existed

around the TCP, but will not simulate the exact TCP droughts that are found in proxy records). Therefore, developing a way to use proxy records as a way to calculate shift factors would give a more realistic reconstruction of the paleoclimate.

References

Allen, D.M., Mackie, D.C., and Wei, M. 2004. Groundwater and climate change: a sensitivity analysis for the Grand Forks aquifer, southern British Columbia, Canada. Hydrogeology Journal, 12: 270-290.

Allen, D.M., Cannon, A.J., Toews, M.W., and Scibek, J. 2010. Variability in simulated recharge using different GCMs. Water Resources Research, 46: 1-18.

Back, B.B. and Hanshaw, W. 1980. Chemical mass-wasting of the northern Yucatan Peninsula by groundwater dissolution. Geology: 8, 222-224.

Bauer-Gottwein, P., Gondwe, B.R.N., Charvet, G., Marin, L.E., Rebolledo-Vieyra, M., and Merediz-Alonso, G. 2011. Review: The Yucatan Peninsula karst aquifer, Mexico. Hydrogeology Journal, 19: 507-524.

Bautista, F., Palacio-Aponte, G., Quintana, P., and Zinck, J.A. 2011. Spatial distribution and development of soils in tropical karst areas from the Peninsula of Yucatan, Mexico. Geomorphology, 135: 308-321.

Beddows, P.A., 2004. Groundwater hydrology of a coastal conduit carbonate aquifer: Caribbean coast of the Yucatán Peninsula, México. PhD thesis, School of Geographical Science, University of Bristol, UK.

Bothe, O., Jungclaus, J.H., and Zanchettin, D. 2013. Consistency of the multi-model CMIP5/PMIP3-past1000 ensemble. Climate of the Past, 9: 2471-2487.

Breitenbach, S.F.M., Rehfeld, K., Goswami, B., Baldini, J.U.L., Ridley, H.E., Kennett, D.J., Prufer, K.M., et al. 2012. COnstructing Proxy Records from Age models (COPRA). Clim. Past, 8: 1765-1779.

Broecker, W.S. and Walton, A. The geochemistry of C^{14} in fresh-water systems. Geochimica et Cosmochimica Acta, 16: 15-38.

Cabrera, J.L.B., Romero, E.A., Such, V.Z., Garcia, C.G., and Porrua, F.E. 2010. Significance tests for the relationship between "El Niño" phenomenon and precipitation in Mexico. Geofisica Internacional, 49(4): 245-261.

Carrillo-Bastos, A., Islebe, G.A., and Torrescano-Valle, N. 2013. 3800 years of quantitative precipitation reconstruction from the northwest Yucatan Peninsula. PLOS ONE, 8(12): 1-10.

Centre for Environmental Data Analysis. 2016. ESGF Portal at CEDA [online]. Available from https://esgf-index1.ceda.ac.uk/projects/esgf-ceda/ [cited April 4, 2016].

Charvet, G. 2009. Exploration, Modeling and management of groundwater resources in northern Quintana Roo, Mexico. Master's thesis, Department of Environmental Engineering, Technical University of Denmark. 123 pp.

Curtis, J.H., Hodell, D.A. and Brenner, M. 1996. Climate variability on the Yucatan Peninsula (Mexico) during the past 3500 years, and implications for Maya cultural evolution. Quaternary Research, 46: 37-47.

Curtis, J.H., Brenner, M., Hodell, D.A., Balser, R.A., Islebe, G.A., and Hooghiemstra, H. 1998. A multi-proxy study of Holocene environmental change in the Maya lowlands of Petén, Guatemala. Journal of Paleolimnology, 19: 139-159

Dahlin, B. 1983. Climate and prehistory on the Yucatan Peninsula. Climatic Change, 5: 245-263.

de Vries, J.J. and Simmers, I. 2002. Groundwater recharge: an overview of processes and challenges. Hydrogeology Journal, 10: 5-17.

DHI. 2007a. MIKE SHE User Manual, Volume 1: User guide [online]. Available from http://www.hydroasia.org/jahia/webdav/site/hydroasia/shared/data_hydroasia/manuals/DHI_water_resources_software/MIKE-SHE-Integrated_surface_water_and_ground_water_modeling/MIKE_SHE_UserGuide.pdf [cited May 2016].

DHI, 2007b. MIKE SHE User Manual, Volume 2: Reference guide [online]. Available from http://www.hydroasia.org/jahia/webdav/site/hydroasia/shared/Document_public/Project/Manuals/WRS/MIKE_SHE_ReferenceGuide.pdf [cited May 2016].

Dijkshoorn, J.A., Huting, J.R.M., and Tempel, P. 2005. Update of the 1:5 million Soil and Terrain Database for Latin America and the Caribbean (SOTERLAC; version 2.0). Report 2005/01, ISRIC - World Soil Information, Wageningen [online]. Available from http://www.isric.org/data/soil-and-terrain-database-latin-america-and-caribbean-ver-20-soterlac [cited May 2016].

Dobrovolny, P., Moberg, A., Brazdil, R., Pfister, C., Glaser, R., Wilson, R., van Engelen, A., et al. 2010. Monthly, seasonal and annual temperature reconstructions for Central Europe derived from documentary evidence and instrumental records since AD 1500. Climatic Change, 101: 69-107.

Dunning, N., Beach, T., Farrell, P., and Luzzadder-Beach, S. 1998. Prehispanic agrosystems and adaptive regions in the Maya Lowlands. Culture and Agriculture, 20: 87-101.

Environmental Science Division (EVS). 2016. Section 2: Soil density. Division of Argonne National Library, Argonne, IL [online]. Available from http://web.ead.anl.gov/resrad/datacoll/soildens.htm [cited May 2016].

Escobar, J. 2010. Late Pleistocene and Holocene climate change in the Maya Lowlands. PhD Thesis, University of Florida.

Estrada-Medina, H., Bautista, F., Jimenez-Osornio, J.J.M., Gonzalez-Iturbe, J.A., and Aguilar Cordero, W. 2013a. Maya and WRB soil classification in Yucatan, Mexico: difference and similarities. ISRN Soil Science, 2013: 1-10.

Estrada-Medina, H., Santiago, L.S., Graham, R.C., Allen, M.F., and Jimenez-Osornio, J.J. 2013b. Source water, phenology, and growth of two tropical dry forest tree species growing on shallow karst soils. Trees, 27:1297-1307.

FAO, 1988. FAO/UNESCO soil map of the world, revised legend, with corrections and updates. World Soil Resources Report 601, FAO, Rome. Reprinted with updates as Technical Paper 20, ISRIC, Wageningen, 1997.

Farrera, I., Harrison, S., Prentice, I.C., Ramstein, G., Joel, G., Bartlein, P., Raymonde, B., et al. 1999. Tropical paleoclimates at the Last Glacial Maximum: a new synthesis of terrestrial data I. Vegetation, lake levels and geochemistry. Climate Dynamics, 15(1): 823-856.

Fensterer, C., Scholz, S., Hoffman, D., Spotl, C., Pajon, J.M., and Mangini, A. 2012. Cuban stalagmite suggests relationship between Caribbean precipitation and the Atlantic Multidecadal Oscillation during the past 1.3 ka. The Holocene, 22(12): 1405-1412.

Flores-Nava, A. 1994. Some limnological data from five water bodies of Yucatan as a basis for aquaculture development. Anales del Instituto de Ciencias Del Mar y Limnologia, 1-2 (21). Available online at http://biblioweb.tic.unam.mx/cienciasdelmar/instituto/1994-1-2/articulo440.html

Folan, W.T., Gunn, J., Eaton, J.D., and Patch, R. 1983. Paleoclimatological patterning in Southern Mesoamerica. Journal of Field Archaeology, 10(4): 453-468.

Gent, P.R., Danabasoglu, G., Donner, L.J., Holland, M.M., Hunke, E.C., Jayne, S.R., Lawrence, D.M., et al. 2011. The Community Climate System Model Version 4. Journal of Climate, 24: 4973-4991.

Gondwe, B.R.N., Lerer, S., Stisen, S., Marin, L., Rebolledo-Vieyra, M., Merediz-Alonso, G., Bauer-Gottwein, P. 2010. Hydrogeology of the south-eastern Yucatan Peninsula: New insights from water level measurements, geochemistry, geophysics and remote sensing. Journal of Hydrology, 389: 1-17.

Gonzalez-Herrera, R., Pinto, I., and Gamboa-Vargas, J. 2002. Groundwater-flow modeling in the Yucatan karstic aquifer, Mexico. Hydrogeology Journal, 10: 539-552.

Goodwin, I.D., Browning, S., Lorrey, A.M., Mayewski, P.A., Phipps, S.J., Bertler, N.A.N., Edwards, R.P., et al. 2013. A reconstruction of extratropical Indo-Pacific sea-level pressure patterns during the Medieval Climate Anomaly. Climate Dynamics, 43: 1197-1219.

Goodwin, I.D., Browning, S.A., and Anderson, A.J. 2014. Climate windows for Polynesian voyaging to New Zealand and Easter Island. PNAS, 111(41): 14716-14721.

Goosse H., Barriat, P.Y., Lefebvre, W., Loutre, M.F., and Zunz, V. 2008. Introduction to climate dynamics and climate modeling [online textbook]. Available from http://www.climate.be/textbook [cited August 2014].

Gunn, J. and Adams, R.E.W. 1981. Climatic change, culture, and civilization in North America. World Archaeology, 13(1): 87-100.

Haug, G.H., Hughen, K.A., Sigman, D.M., Peterson, L.C., and Rohl, U. 2001. Southward migration of the Intertropical Convergence Zone through the Holocene. Science, 293: 1304-1308.

Haug, G.H., Gunther, G., Peterson, L.C., Sigman, D.M., Hughen, K.A., and Aeschlimann, B. 2003. Climate and the collapse of Mayan civilization. Science, 299: 1731-1735.

Heaton, T.H.E., Holmes, J.A., and Bridgwater, N.D. 1995. Carbon and oxygen isotope variations among lacustrine ostracods: implications for paleoclimatic studies. The Holocene, 5(4): 428-434.

Hess, T. 1999. AWSET Potential evaporation program for automatic weather stations, Version 3.0. Cranfield University, Silsoe, Bedford, UK.

Hewitson, B.A.C., Janetos, T.R., Carter, F., Giorgi, R.G., Jones, W.T., Kwon, L.O., Mearns, E.L.F., et al. 2014. Regional context, *In* Climate Change 2014: Impacts, adaption, and vulnerability. Part B: Regional aspects. Contribution of working group II to the fifth assessment report of the Intergovernmental Panel on Climate Change. *Edited by* Barros, V.R., Field, C.B., Dokken, D.J., Mastrandrea, M.D., Mach, K.J., Bilir, T.E., Chatterjee, M., et al. Cambridge University Press, Cambridge, United Kingdom and New York, NY, USA. pp. 1133-1197.

Hodell, D.A., Curtis, J.H., and Brenner, M. 1995. Possible role of climate in the collapse of the Classic Maya civilization. Nature, 375: 391-393.

Hodell, D.A., Brenner, M., and Curtis, J.H. 2005a. Terminal Classic drought in the northern Maya lowlands inferred from multiple sediment cores in Lake Chichancanab (Mexico). Quaternary Science Reviews, 24: 1413-1427.

Hodell, D.A., Brenner, M., and Curtis, J.H. 2005b. Terminal Classic drought in the northern Maya lowlands inferred from multiple sediment cores in Lake Chichancanab (Mexico). Quaternary Science Reviews, 24: 1413-1427.

Hodell, D.A., Turchyn, A.V., Wiseman, C.J., Escobar, J., Curtis, J.H., Brenner, M., Gilli, A., et al. 2012. Late glacial temperature and precipitation changes in the lowland Neotropics by tandem measurement of $\delta^{18}O$ in biogenic carbonate and gypsum hydration water. Geochimica et Cosmochimica Acta 77: 352-368.

Holding, S.T. 2014. Risk to water security on small islands: a numerical modeling approach. PhD thesis, Department of Earth Sciences, Simon Fraser University, 227 pp.

Huntington, E. 1917. Maya civilization and climate change, in Proceedings of the 19th Congress of Americanists. Yale University Press, New Haven. 14 pp.

Jarvis, N.J., 1994. The MACRO Model (Version 3.1): Technical description and sample simulations. Reports and Dissertations 19. Department of Soil Science, Swedish University of Agricultural Science, Uppsala, Sweden, p. 51.

Jyrkama, M.I. and Sykes, J.F. 2007. The impact of climate change on spatially varying groundwater recharge in the grand river watershed (Grand Forks). Journal of Hydrology, 338: 237-250.

Kim, S.T. and O'Neil, J.R. 1997. Equilibrium and nonequilibrium oxygen isotope effects in synthetic carbonates. Geochemica et Cosmochimica Acta, 61(16): 3461-3475.

Kohfeld, K.E. 1998. Geochemistry and ecology of polar planktonic foraminifera, and application to paleoceanographic reconconstruction. Ph.D. Thesis, Lomont Doherty Earth Observatory. Columbia Observatory. New York. 252 pp.

Kohfeld, K.E. and Harrison, S.P. 2000. How well can we simulate past climates? Evaluating models using global palaeoenvironmental datasets. Quaternary Science Reviews, 19: 321-346.

Kohfeld, K.E., Graham, R.M., de Boer, A.M., Sime, L.C., Wolff, E.W., Le Quere, C., and Bopp, L. 2013. Southern Hemisphere westerly wind changes during the Last Glacial Maximum: paleo-data synthesis. Quaternary Science Reviews, 68: 76-95.

Kristensen, K.J. and Jensen, S.E. 1975. A model for estimating actual evapotranspiration from potential evapotranspiration. Royal Veterinary and Agricultural University, Nordic Hydrology, 6: 170-188.

Leij, F.J., Alves, W.J., van Genuchten, M.Th., and Willliams, J.R. 1996. Unsaturated soil hydraulic database, UNSODA 1.0 user's manual. Report EPA/600/R96/095. US Environmental Protection Agency, Ada, Oklahoma.

Lesser, J.M. 1976. Estudio hidrogeologico e hidrogeoquimico de la Peninsual de Yucatan.Proyecto Conacyt-NSF 704, Secretaria de Recursos Hidraulicos, Direccion de Geohidrologia y Zonas Aridas, Mexico, 64 p.

Leyden, B.W., Brenner, M., and Dahlin, B.H. 1998. Cultural and climatic history of Coba, a Lowland Maya city in Quintana Roo, Mexico. Quaternary Research, 49: 111-122.

Li, J., Xie, S.P., Cook, E.R., Huang, G. D'Arrigo, R., Liu, F. Ma, J., and Zheng, X.T. 2011. Interdecadal modulation of El Nino amplitude during the past millennium. Nature Climate Change, 1(2): 114-118.

Mann, M.E., Zhang, Z., Rutherford, S., Bradley, R.S.,Hughes, M.K., Shindell, D., Ammann, C., et al. 2009. Global signatures and dynamical origins of the Little Ice Age and Medieval Climate Anomaly. Science, 326: 1256-1260.

Mantua, N.J. 2002. Pacific Decadal Oscillation (PDO): Volume 1, The Earth system: physical and chemical dimensions of global environmental change. In Encyclopedia of Global Environmental Change. Edited by MacCracken, M.C. and Perry, J.S. John Wiley & Sons, Ltd, Chichester.

McPhaden, M.J., Zebiak, S.E., and Glantz, M.H. 2006. ENSO as an integrating concept in earth science. Science, 314: 1740-1745.

Medina-Elizalde, M., Burns, S.J., Lea, D.W., Asmerom, Y., von Gunten, L., Polyak, V., Vuille, M., et al. 2010. High resolution stalagmite climate record from the Yucatán Peninsula spanning the Maya terminal classic period. Earth and Planetary Science Letters, 298: 255-262.

Medina-Elizalde, M. and Rohling, E.J. 2012. Collapse of Classic Maya civilization related to modest reduction in precipitation. Science, 335: 956-959.

Mendez Ramos, R. 1991. Modelo de compotamiento del acuifero de la cuidad de Merida, Yucatan. Comision Nacional del Agua, Gerencia Estatal Yucatan, Subgerencia de Administracion del Agua, Merid, Yucatan, Mexico.

Mileham, L., Taylor, R., Thompson, J., Todd, M., Tindimugaya, C. 2008. Impact of rainfall distribution on the parameterisation of a soil-moisture balance model of groundwater recharge in equatorial Africa. Journal of Hydrology, 359 (1-2): 46-58.

Mitchell, T. 2005. Pacific Decadal Oscillation (PDO) Index [online]. Available from http://research.jisao.washington.edu/data_sets/pdo/ [cited June 30th, 2016].

Moore, Y.H., Stoessell, R.K., and Easley, D.H. 1992. Fresh-water sea-water relationship within a groundwater-flow system, northeastern coast of the Yucatan Peninsula. Ground Water, 30: 343-350.

National Cooperative Soil Survey. 2016. National cooperative soil characterization database. Available online from http://www.nrcs.usda.gov/wps/portal/nrcs/detail/soils/survey/?cid=nrcs142p2_054 167 [cited June 2016].

Natural Resources Canada. 2010. North American atlas- Basin watersheds. Government of Canada, Natural Resources Canda, Mapping Information Branch, The Atlas of Canada; United States Department of the Interior, U.S. Geological Survey, National Atlas of the United States; Instituto Nacional de Estadistica y Geografia [online]. Available online from http://geogratis.gc.ca/download/frameworkdata/North_America_Atlas10M/waters heds/ [cited May 2016].

NOAA National Weather Service. 2003. The national weather service climate prediction center: Monitoring weather and climate [online]. Available from http://www.cpc.noaa.gov/products/precip/CWlink/daily_ao_index/teleconnecti ons.shtml [cited June 30th, 2016].

Ohno, M., Hamano, Y., Murayama, M., Matsumoto, E., Iwakura, H., Nakamura, T., and Taira, A. 1993. Paleomagnetic record over the past 35,000 years of a sediment core from off Shikoku, Southwest Japan. Geophysical Research Letters, 13: 1395-1398.

Pavia, E.G., Graef, F., and Reyes, J. 2006. PDO–ENSO effects in the climate of Mexico. American Meteorological Society Journal of Climate, 19: 6433-6438.

Perry, E. C., Winter, D.J., Sagar, B., and Wu, B. 1992, The Chicxulub structure: Surface manifestation and possible isotope signature. 23rd Lunar and Planetary Science Conference Abstracts: 1057–1058.

Perry, E., Marin, L., McClain, J., and Velazquez, G. 1995. Ring of Cenotes (sinkholes), northwest Yucatan, Mexico: Its hydrogeologic characteristics and possible association with the Chicxulub impact crater. Geology, 23(1): 17-20.

Perry, E., Velazquez-Oliman, G., and Socki, R.A. 2003. Chapter 7: Hydrogeology of the Yucatan Peninsula. In 21st symposium on plant biology. Edited by Arturo Gomez Pompa and Scott Fedick. The Haworth Press, Inc., 10 Alice Street, Binghamton, NY. pp. 115-138.

Philippsen, B. 2013. The freshwater reservoir effect in radiocarbon dating. Heritage Science, 1(24): 1-19.

Pickett, E.J., et al. 2004. Pollen-based reconstructions of biome distributions for Australia, Southeast Asia and the Pacific (SEAPAC region) at 0, 6000, and 18,000 14C yr BP. Journal of Biogeography, 31: 1381-1444.

Racsko, P., Szeidl, L. and Semenov, M. 1991. A serial approach to local stochastic weather models. Ecological Modelling, 57: 27-41.

Reeve, A. and Perry, E.C. 1990. Aspects and tidal analysis along the western north coast of the Yucatan Peninsula, Mexico. WRA: International Symposium on Tropical Hydrogeology. 23-27, July 1990. San Juan, Puerto Rico.

Rico-Gray, V. and Garcia-Franco, J.G. 1991. The Maya and the vegetation on the Yucatan Peninsula. J. Enthnobiol., 11(1): 135-142.

Roulier, S., Baran, N., Mouvet, C., Stenemo, F., Morvan, X., Albrechtsen, H., Clausen, L., et al. 2005. Controls on atrazine leaching through a soil-unsaturated fractured limestone sequence at Brevilles, France. Journal of Contaminant Hydrology, 84: 81-105.

Scanlon, B.R., Healy, R.W., and Cook, P.G. 2002. Choosing appropriate techniques for quantifying groundwater recharge. Hydrogeology Journal, 10: 18-39.

Schroeder, P. R., Dozier, T.S., Zappi, P.A., McEnroe, B.M.m Sjostrom, J.W., and Peyton, R.L. 1994. The Hydrologic Evaluation of Landfill Performance (HELP) model: User's guide for version 3, EPA/600/R-94/168a. U.S. Environmental Protection Agency Office of Research and Development, Washington, DC

Scibek, J., and Allen, D.M. 2006. Modeled impacts of predicted climate change on recharge and groundwater levels. Water Resources Research, 42: 1-18.

Scurlock, J.M.O., Asner, G.P., and Gower, S.T. 2001. Worldwide historical estimates of leaf area index, 1932-2000. U.S. National Aeronautics and Space Administration (NASA) Environmental Sciences Division, Oak Ridge National Library, Oakridge, Tennessee.

Semenov, M.A. and Barrow, E.M. 2002. LARS-WG: A stochastic weather generator for use in climate impact studies. Version 3.0. User Manual.

Smerdon, B.D., Allen, D.M., and Neilsen, D. 2010. Evaluating the use of a gridded climate surface for modeling groundwater recharge in a semi-arid region (Okanagan Basin, Canada). Hydrological Process, 24: 3087-3100.

Socki, R.A., Gibson, E.K., Perry, E.C., Galindo, C., Golden, D.C., Ming, D.W., McKay, G.A., et al. 2004. Stable isotope composition of carbonates formed in low-temperature terrestrial environments as Martian analogs. Lunar and Planetary Science, 35.

Sorenson, J.P.R., Finch, J.W., Ireson, A.M., and Jackson, C.R. 2014. Comparison of varied complexity models simulating recharge at the field scale. Hydrological Processes, 28: 2091-2102.

Stahle, D.W., Diaz, J.V., Burnette, D.J., Paredes, J.C., Heim Jr., R.R., Fye, F.K., Soto, R.A., et al. 2011. Major Mesoamerican droughts of the past millennium. Geophysical Research Letters, 38: 1-4.

Stahle, D.W., Burnette, D.J., Diaz, J.V., Heim Jr., R.R., Fye, F.K., Paredes, J.C., Soto, R.A., et al. 2012. Pacific and Atlantic influences on Mesoamerican climate over the past millennium. Climate Dynamics, 39: 1431-1446.

Steinich, B. and Marin, L.E. 1997. Determination of flow characteristics in the aquifer of the northwestern Peninsula of Yucatan, Mexico. Journal of Hydrology, 191: 315-331.

Street-Perrott, F.A., Marchand, D.S., Roberts, N., Harrison, S.P. 1989. Global lake level variations from 18,000 to 0 years ago: a paleooclimatic analysis. U.S. Technical Report 46. U. S. Department of Energy, Washington, DC, pp. 213.

Stuiver, M. 1980. Solar variability and climatic change during the current millennium. Nature, 286: 868-871.

Taylor, K.E., Stouffer, R.J., and Meehl, G.A. 2009. A summary of the CMIP5 Experiment Design. World Climate Research Programme.

Taylor, K.E. 2013. CMIP5 standard output document [online]. Available from http://cmip-pcmdi.llnl.gov/cmip5/data_description.html [cited May 17, 2016].

Telford, R.J., Heegaard, E., and Birks, H.J.B. 2004. All age-depth models are wrong: but how badly? Quaternary Science Reviews, 23: 1-5.

The Weather Company. 2016. Weather underground: Merida, Mexico [online]. Available from http://www.wunderground.com/weather-forecast/zmw:00000.1.76644 [cited April 19, 2016].

Thomas, B.F., Berranhi, A., and Famiglietti, J.S. 2016. Precipitation intensity effect on groundwater recharge in the southwestern United States. Water, 8: 1-15.

Trabucco, A., and Zomer, R.J. 2009. CGIAR-CSI Global Aridity Index (Global-Aridity) and Global Potential Evapo-Transpiration (Global-PET) climate database. CGIAR Consortium for Spatial Information. Published online, available from the CGIAR-CSI GeoPortal at: http://www.csi.cgiar.org.

Trenberth, K.E., Dai, A., Rasmussen, R.M, and Parsons, D.B. 2003. The changing character of precipitation. American Meteorological Society, 84 (9): 1205-1217.

Turner, B.L. and Sabloff, J.A. 2012. Classic Period collapse of the central Maya lowlands: Insights about human–environment relationships for sustainability. PNAS, 109: 13908-13914.

United Nations Environment Programme (UNEP). 2006. Environmental data explorer [online]. Available from http://geodata.grid.unep.ch/index.php [cited May 2016].

Vaccaro, J.J. 1992. Sensitivity of groundwater recharge estimate to climate variability and change, Columbia Plateau, Washington. Journal of Geophysical Research, 97: 2821-2833.

Wahl, E.R. and Smerdon, J.E. 2012. Comparative performance of paleoclimate field and index reconstructions derived from climate proxies and noise-only predictors. Geophysical Research Letters, 39: 1-5.

Wassenaar, L.I, Van Wilgenburg, S.L., Larson, K., and Hobson, K.A. 2009. A groundwater isoscape, (dD, d18O) for Mexico. Journal of Geochemical Exploration, 102: 123-136.

Weidie, A.E. 1985. Geology of the Yucatan Platform (Part 1). University of New Orleans. 1-19.

Wilby, R.L., Dawson, C.W., and Barrow, E.M. 2002. SDSM — a decision support tool for the assessment of regional climate change impacts. Environmental Modeling and Software, 17: 147-159.

Zender, C. 1995-2016. NCO User guide: A suite of netCDF operators [online]. Available from http://nco.sourceforge.net/ [cited April 4, 2016].

Zhang, C. 2005. Madden-Julian Oscillation. Reviews of Geophysics, 43: 1-36.

Appendix A.   Graphs for all proxy data sets used for qualitative analysis

Figures A1 to A14: Cross correlation results for all proxy data sets, showing the lag time with the maximum correlation between each proxy and precipitation. A negative lag indicates the proxy record is lagged behind the precipitation record.
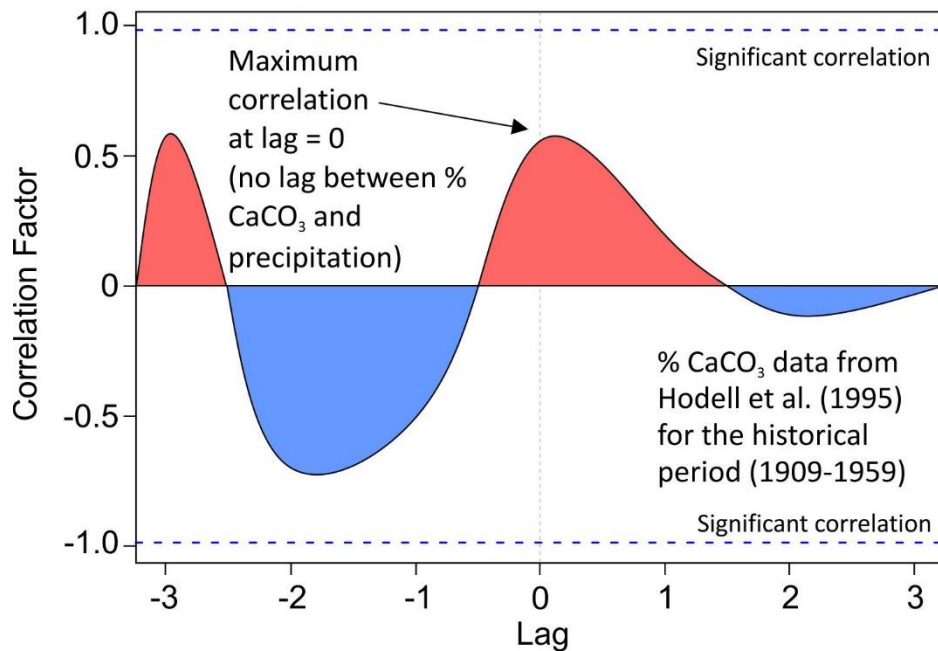
Figure A1. **Cross correlation analysis between % Calcium Carbonate and the historical precipitation record (1900-2002).**
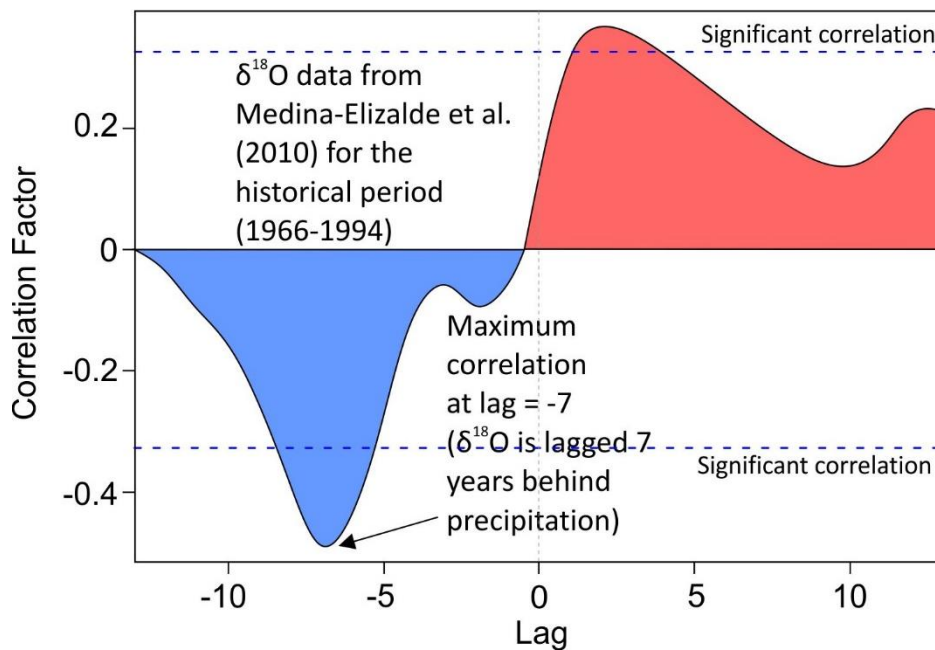
Figure A2. **Cross correlation analysis between Speleothem δ^{18}O and the historical precipitation record (1900-2002).**
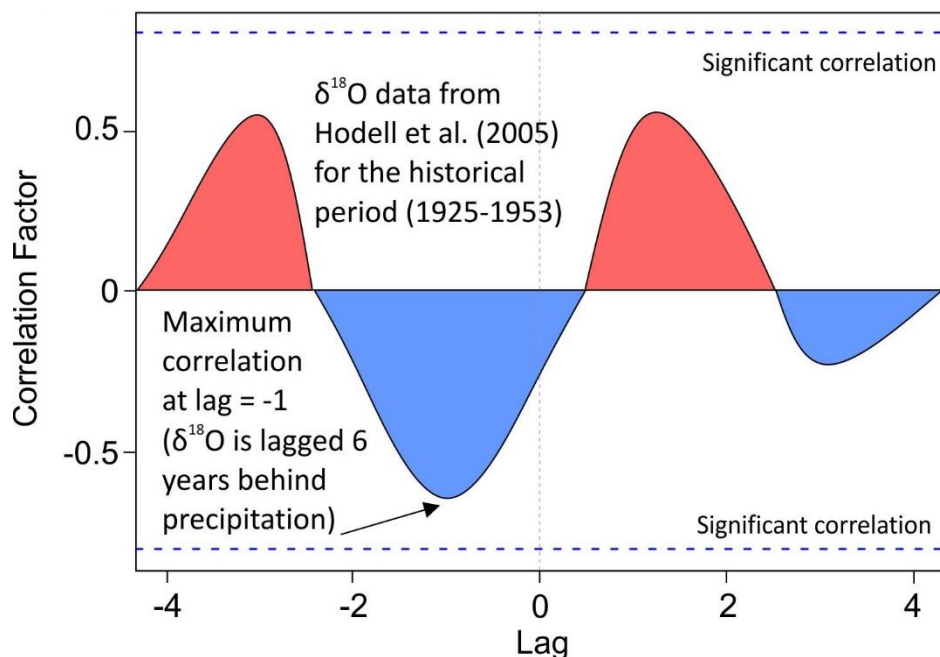
Figure A3. Cross correlation analysis between Chara δ^{18}O and the historical precipitation record (1900-2002).
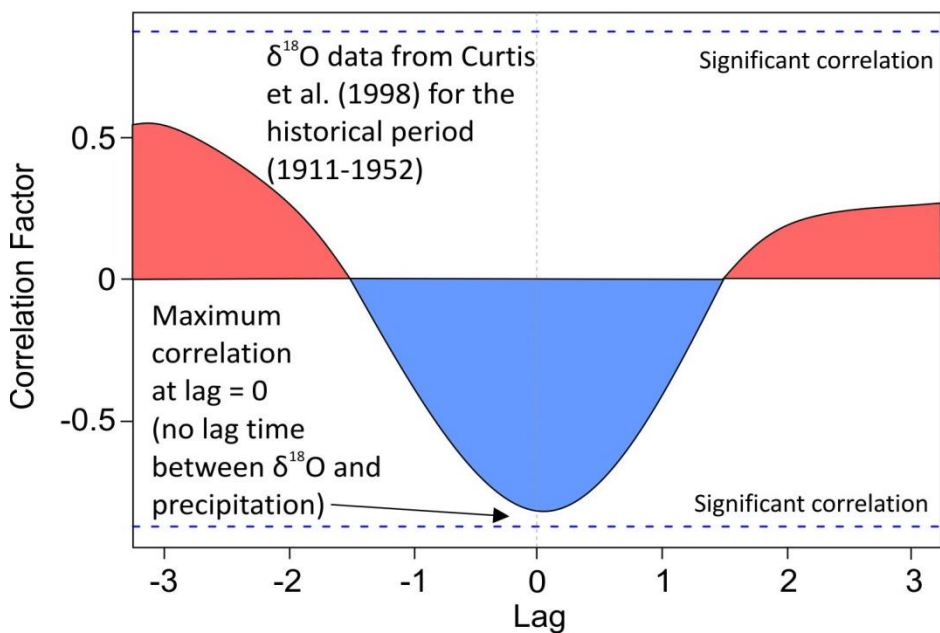
Figure A4. Cross correlation analysis between *Cochliopina sp.* δ^{18}O and the historical precipitation record (1900-2002).
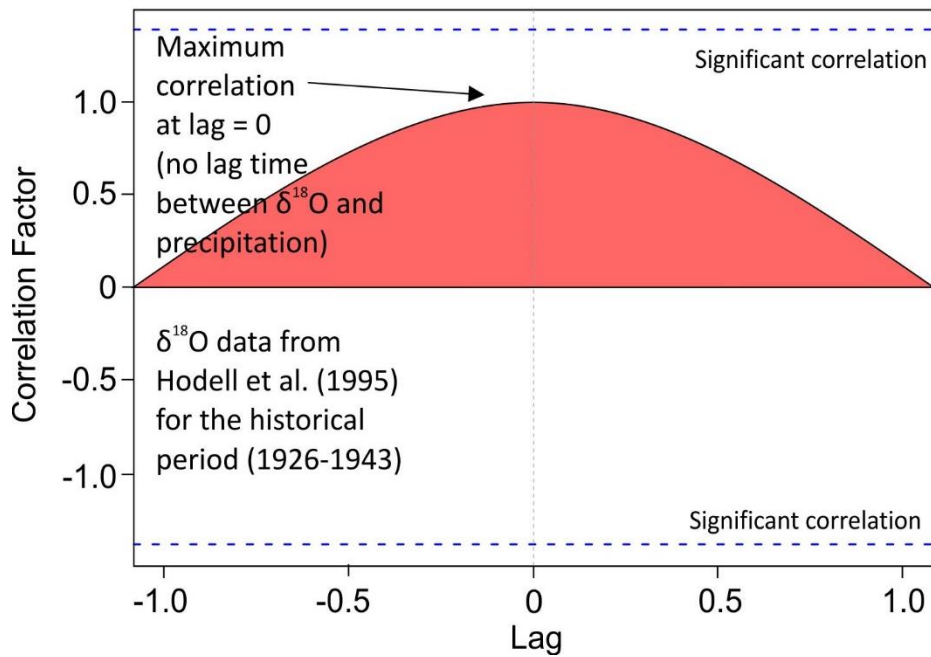
Figure A5. Cross correlation analysis between *Cyprinotus sp.* δ^{18}O and the historical precipitation record (1900-2002).
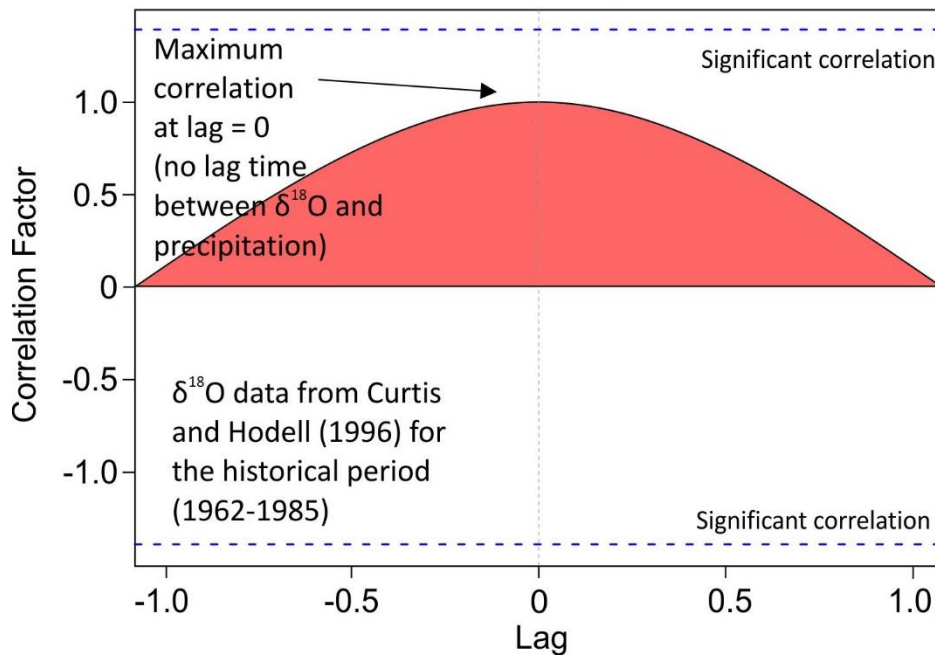
Figure A6. Cross correlation analysis between *Cytheridella ilosvayi* δ^{18}O and the historical precipitation record (1900-2002).
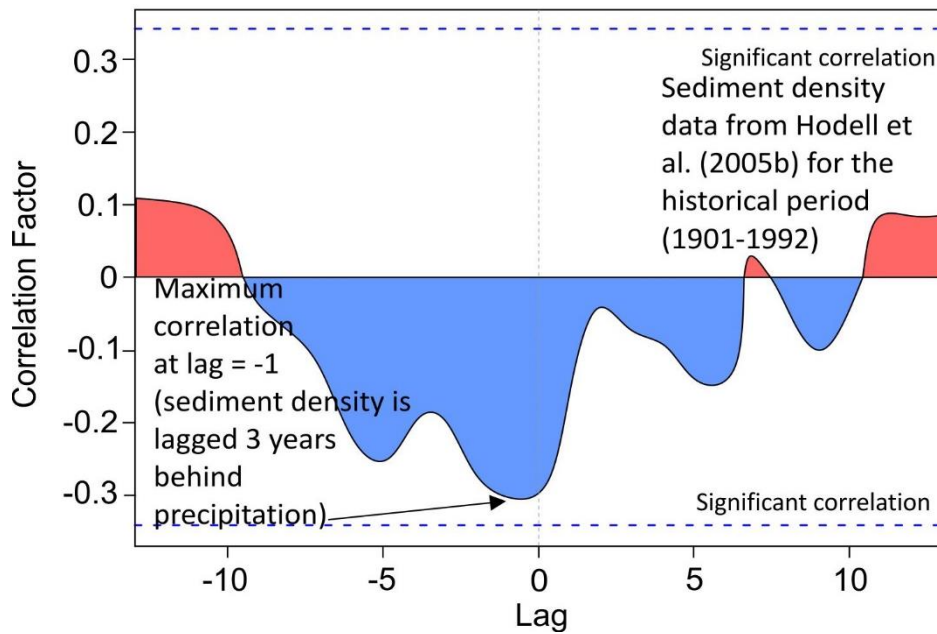
Figure A7.   Cross correlation analysis between sediment density and the historical precipitation record (1900-2002).
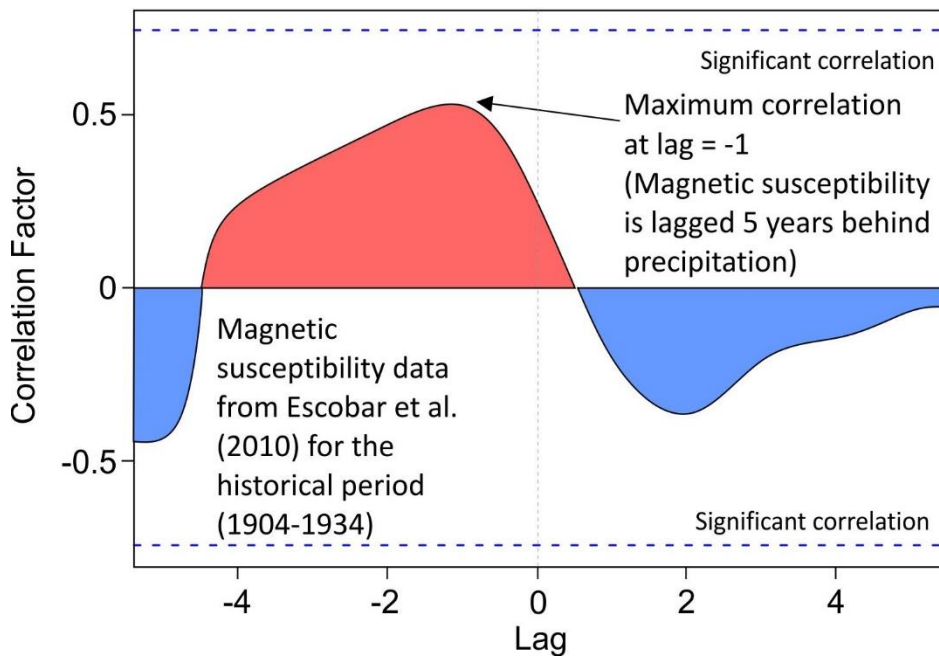
Figure A8.   Cross correlation analysis between magnetic susceptibility and the historical precipitation record (1900-2002).
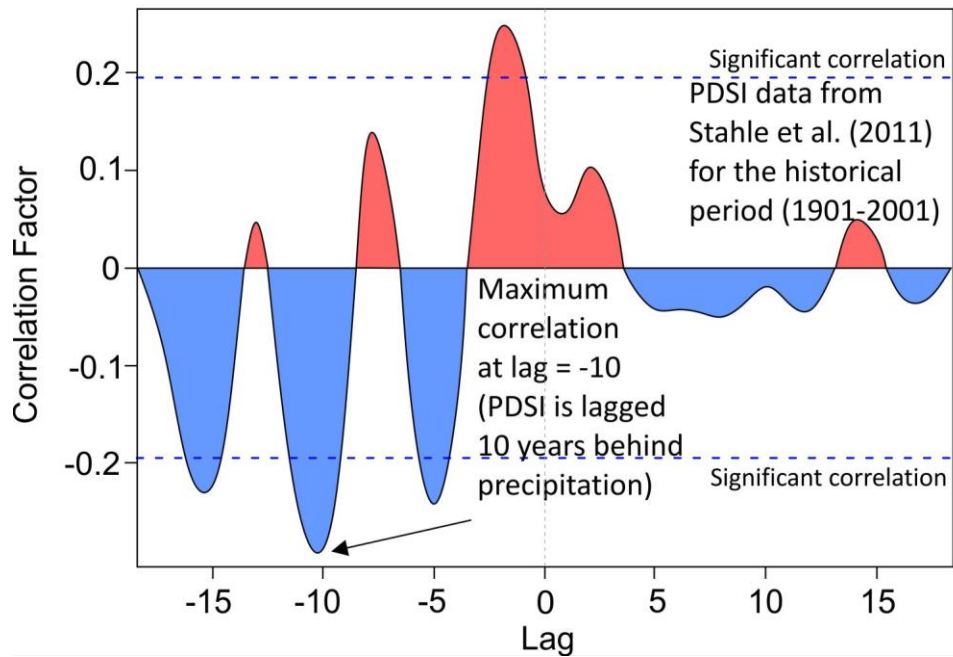
Figure A9. Cross correlation analysis between PDSI and the historical precipitation record (1900-2002).
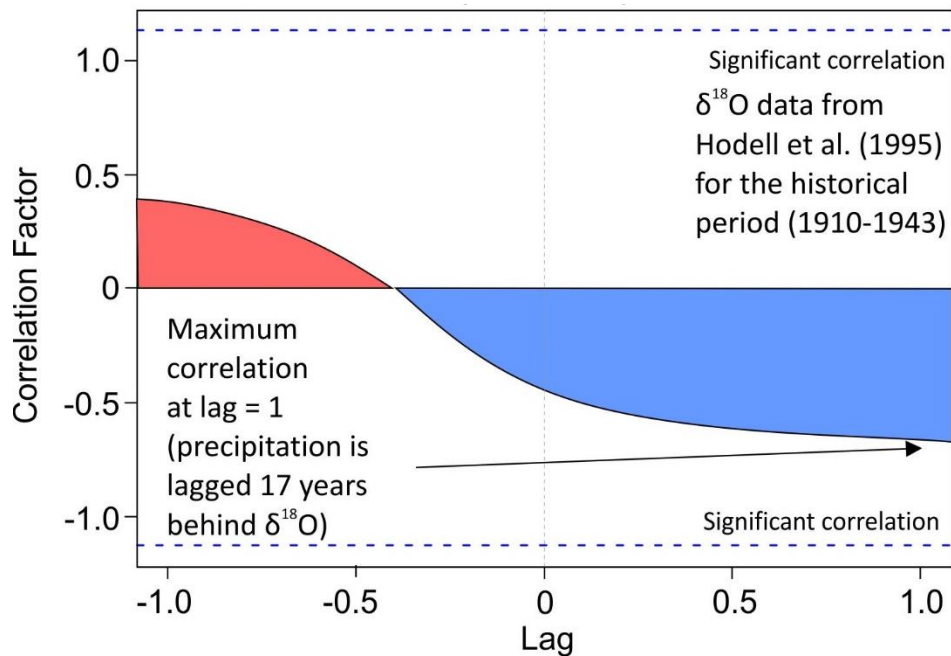
Figure A10. Cross correlation analysis between *Physocypria sp.* δ^{18}O and the historical precipitation record (1900-2002).

135
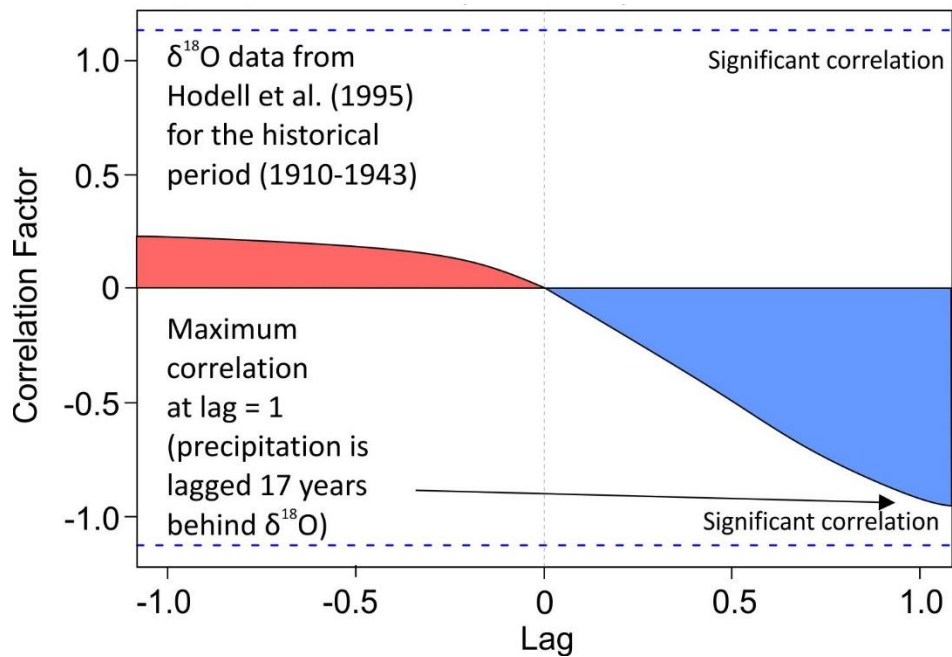
Figure A11. Cross correlation analysis between *Pyrgophorus sp.* $\delta^{18}O$ and the historical precipitation record (1900-2002).
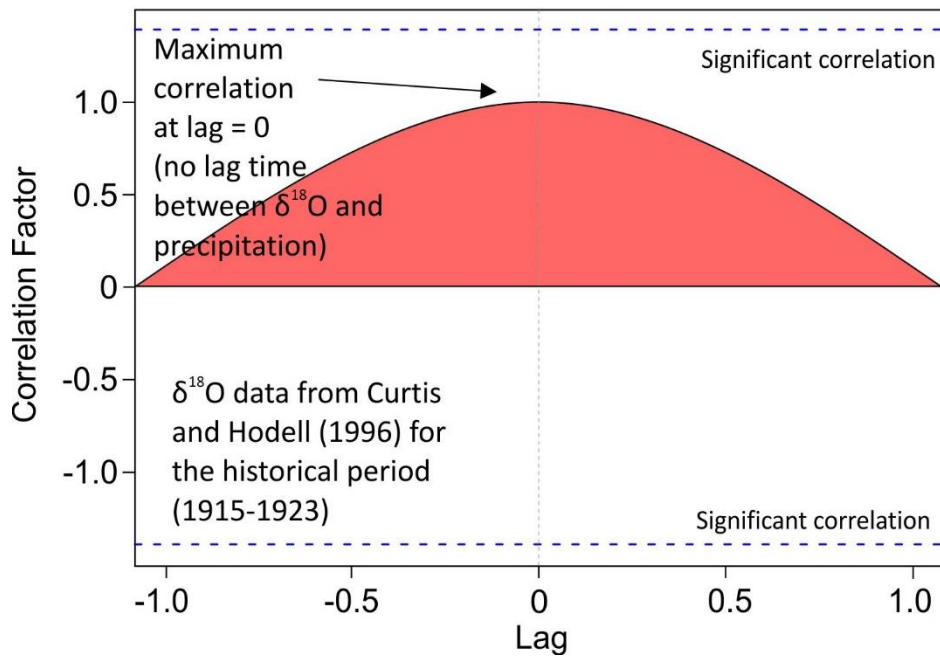
Figure A12. Cross correlation analysis between *Pyrgophorus coronatus* $\delta^{18}O$ and the historical precipitation record (1900-2002).
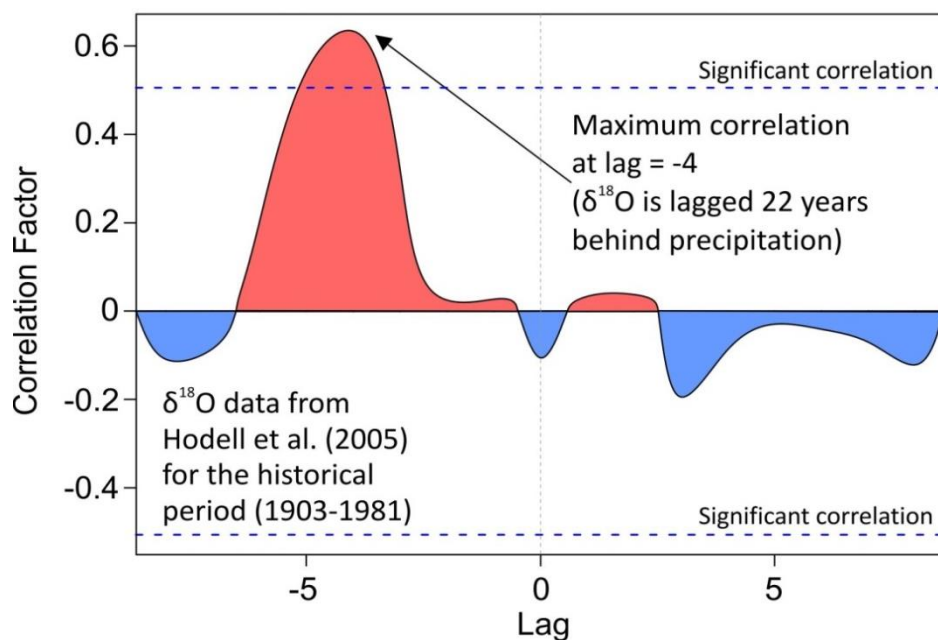
Figure A13. Cross correlation analysis between *Pyrgophorus coronatus* $\delta^{18}O$ and the historical precipitation record (1900-2002).
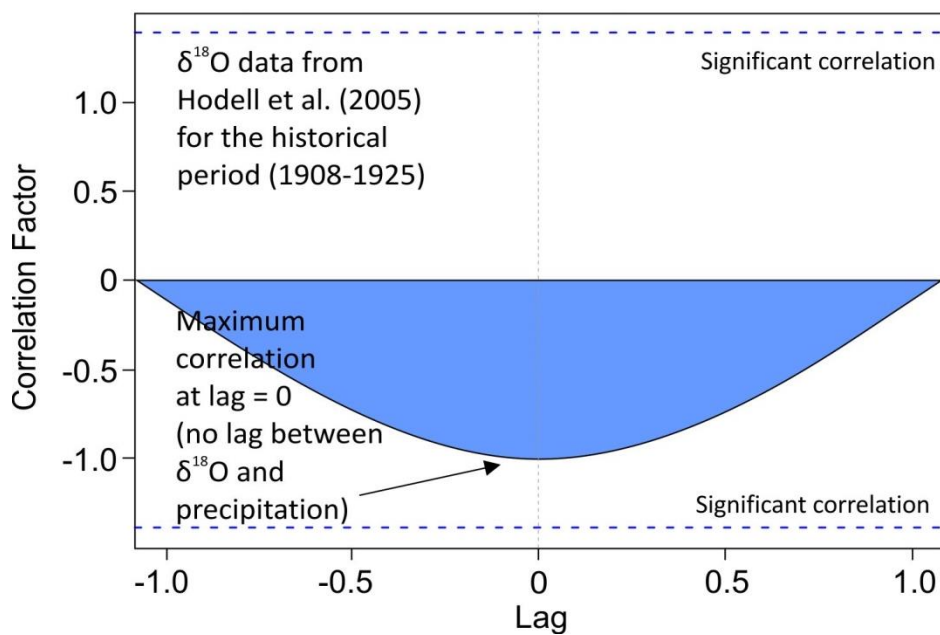
Figure A14. Cross correlation analysis between *D. stevensoni* $\delta^{18}O$ and the historical precipitation record (1900-2002).

Figures A15 to A28: Scatter graphs of all proxy data sets against precipitation at the specified lag time, showing the equation used for each to calculate precipitation. A negative lag indicates that the proxy record is lagged behind the precipitation record.
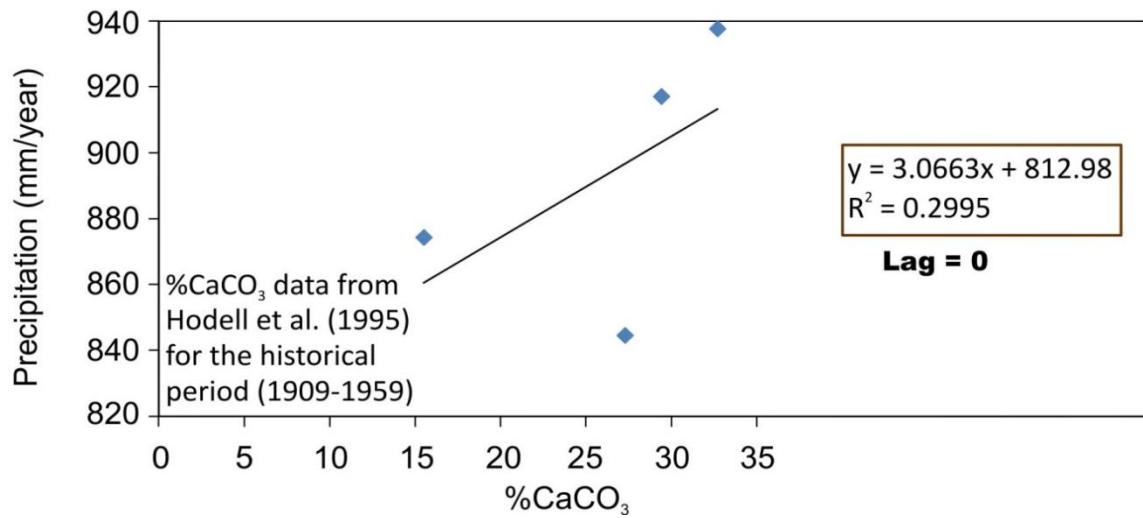
Figure A15.   Linear correlation between % Calcium Carbonate and the historical precipitation record (1900-2002).
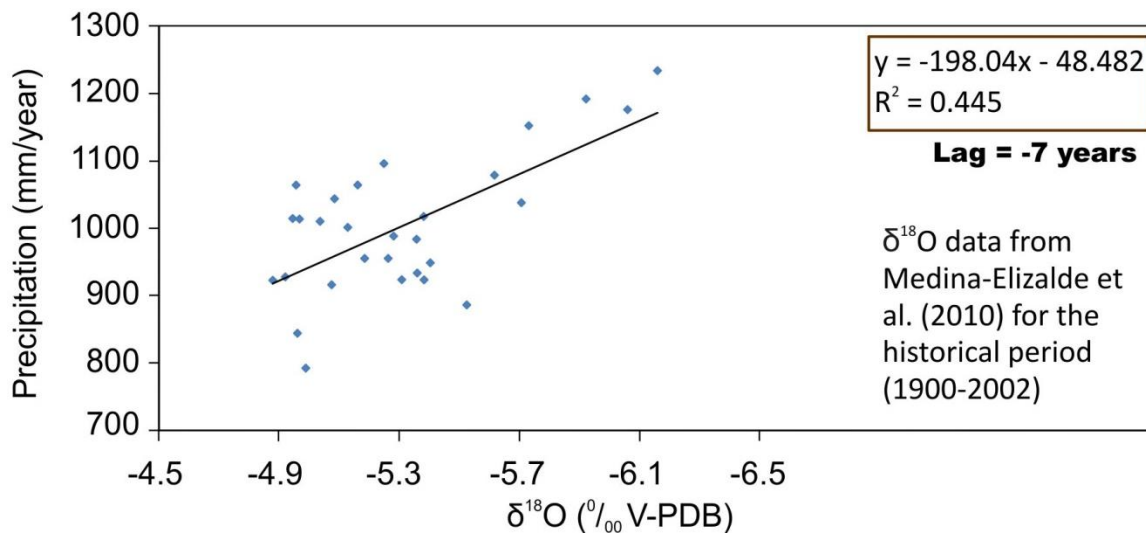
Figure A16.   Linear correlation between Speleothem δ^{18}O and the historical precipitation record (1900-2002).
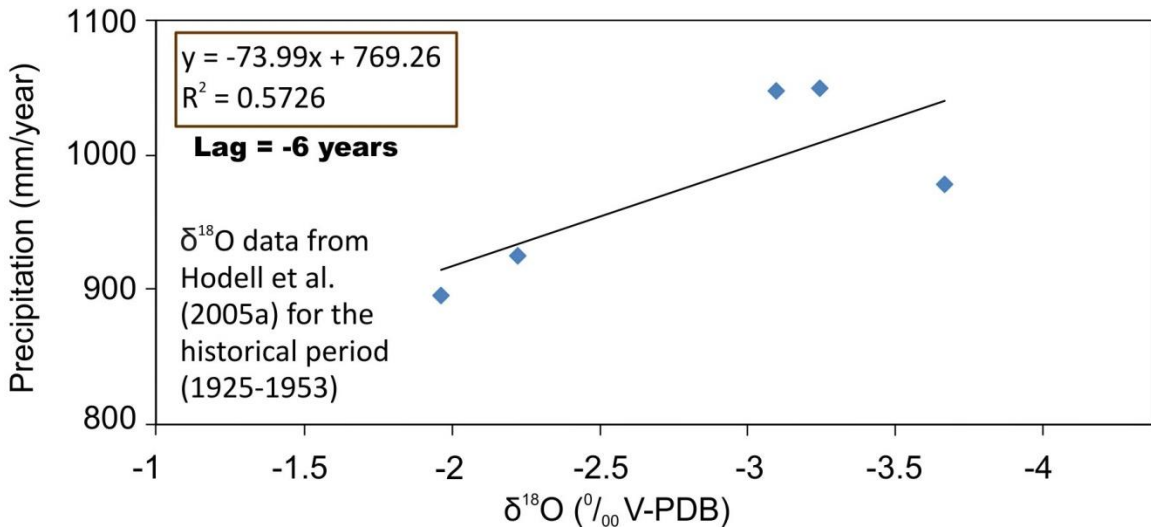
Figure A17. Linear correlation between Chara δ^{18}O and the historical precipitation record (1900-2002).
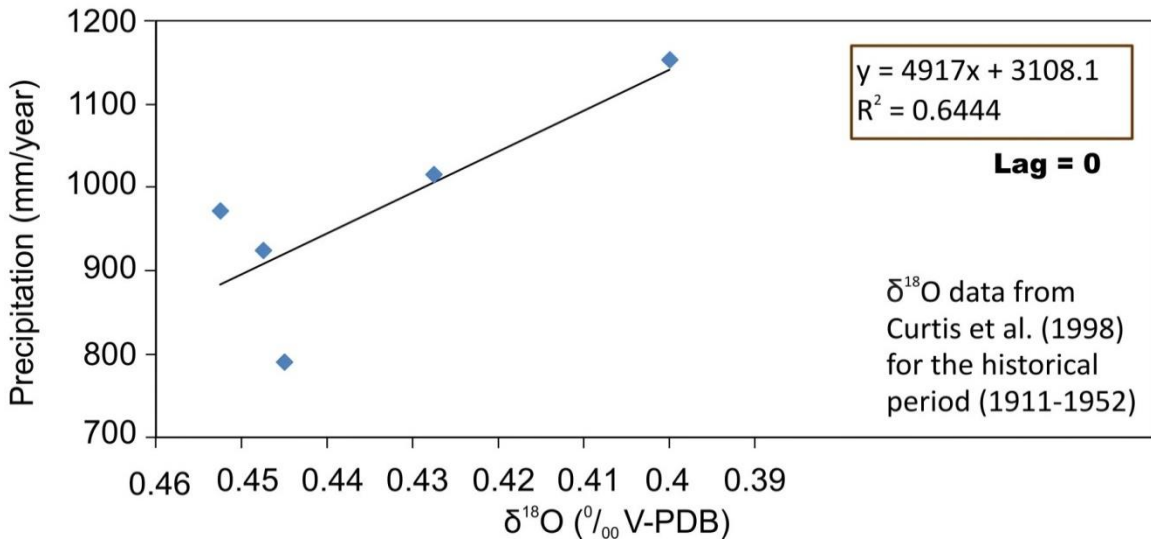
Figure A18. Linear correlation between *Cochliopina sp.* δ^{18}O and the historical precipitation record (1900-2002).
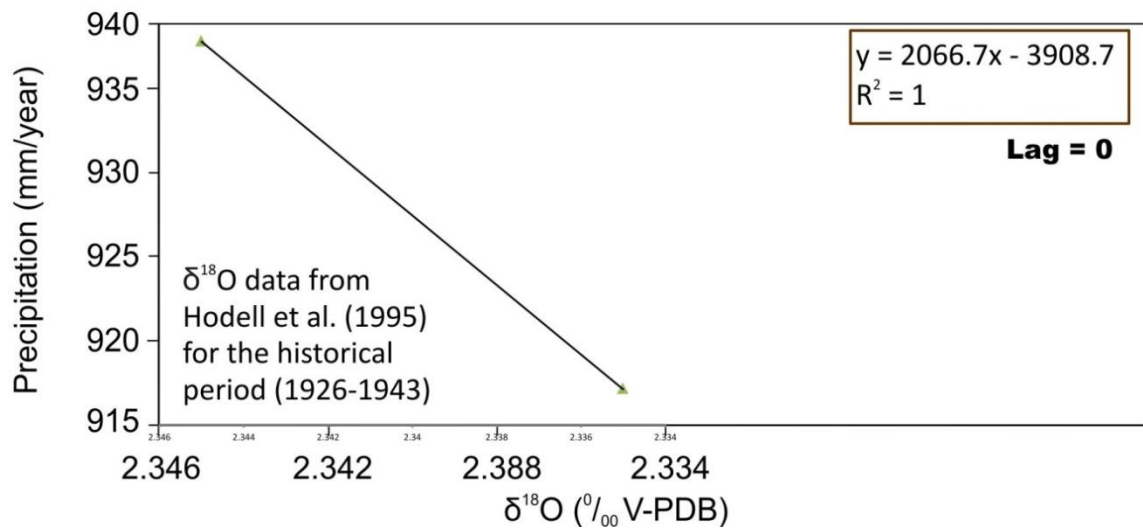
Figure A19. **Linear correlation between *Cyprinotus sp.* δ¹⁸O and the historical precipitation record (1900-2002).**
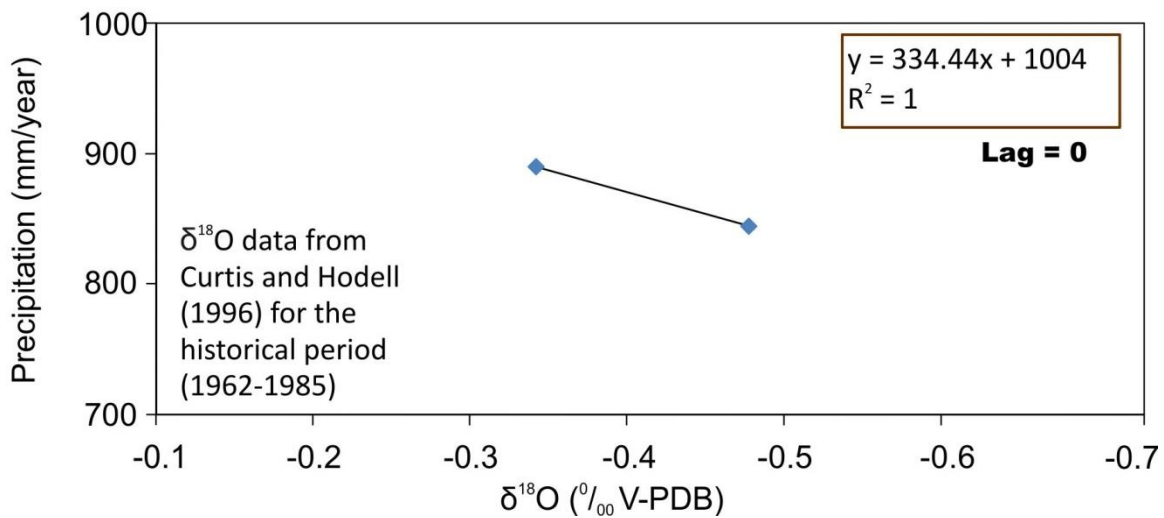
Figure A20. **Linear correlation between *Cytheridella ilosvayi* δ¹⁸O and the historical precipitation record (1900-2002).**
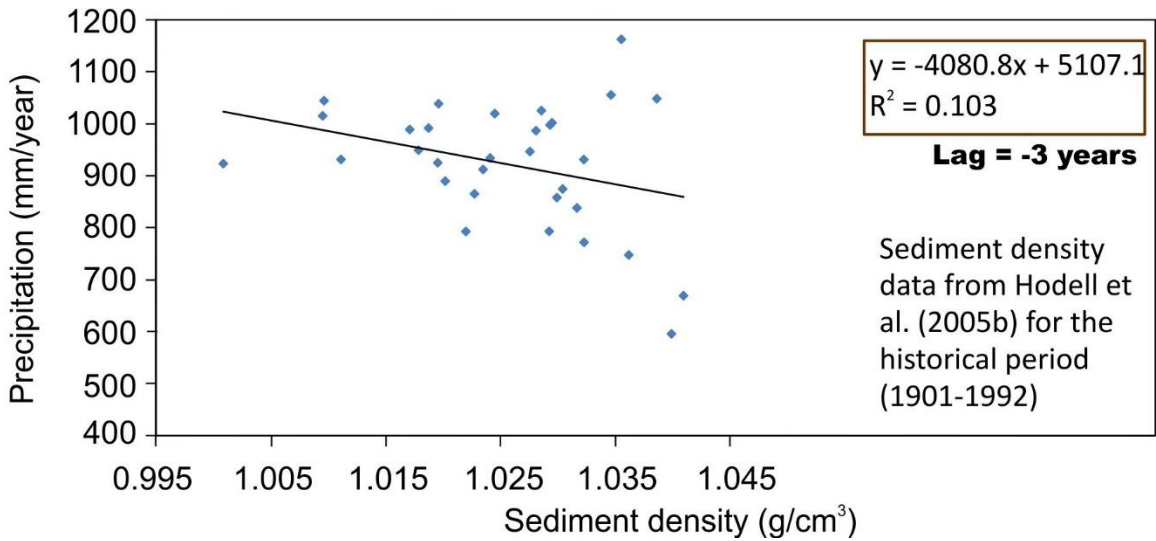
Figure A21. Linear correlation between sediment density and the historical precipitation record (1900-2002).
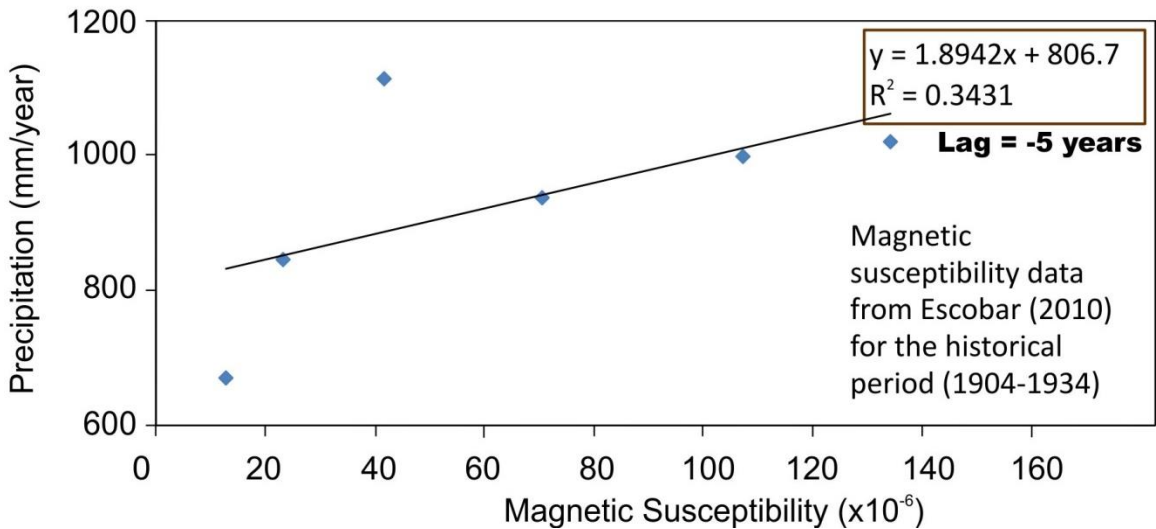
Figure A22. Linear correlation between magnetic susceptibility and the historical precipitation record (1900-2002).
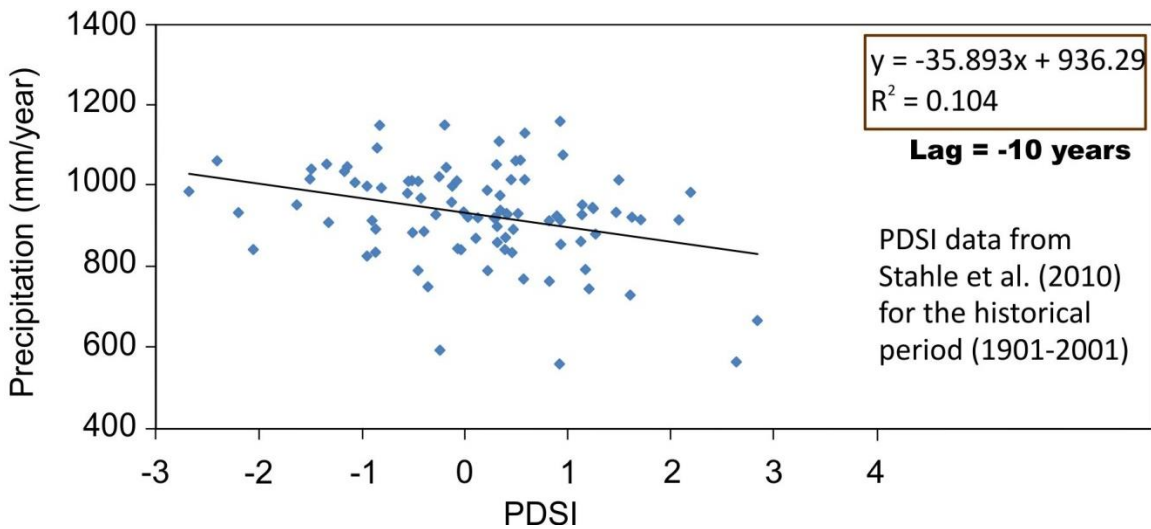
Figure A23.   Linear correlation between PDSI and the historical precipitation record (1900-2002).
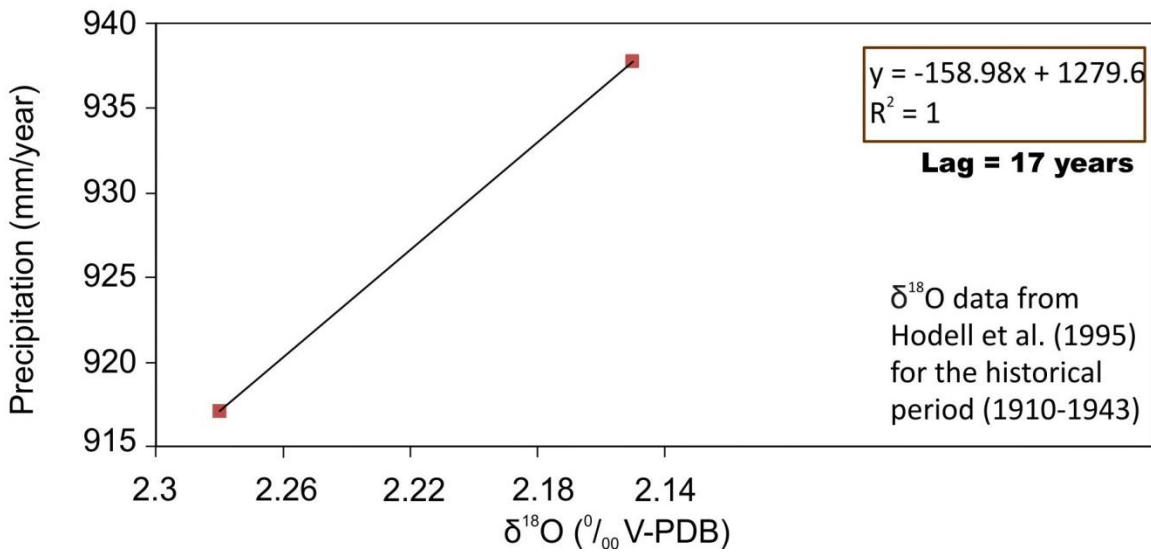
Figure A24.   Linear correlation between *Physocypria sp.* δ^18O and the historical precipitation record (1900-2002).

143
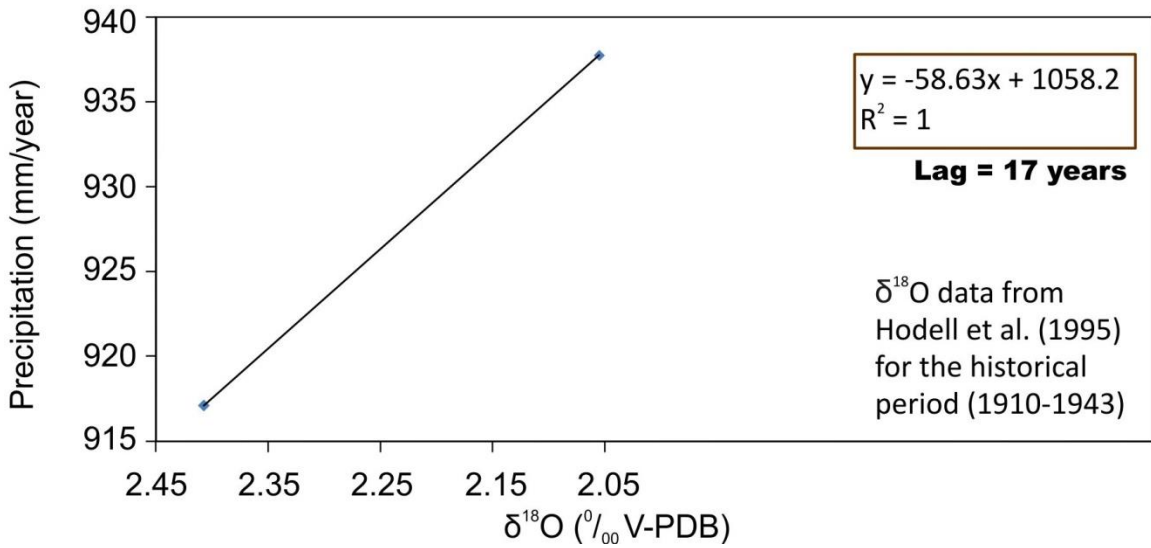
Figure A25. Linear correlation between *Pyrgophorus sp.* δ^{18}O and the historical precipitation record (1900-2002).
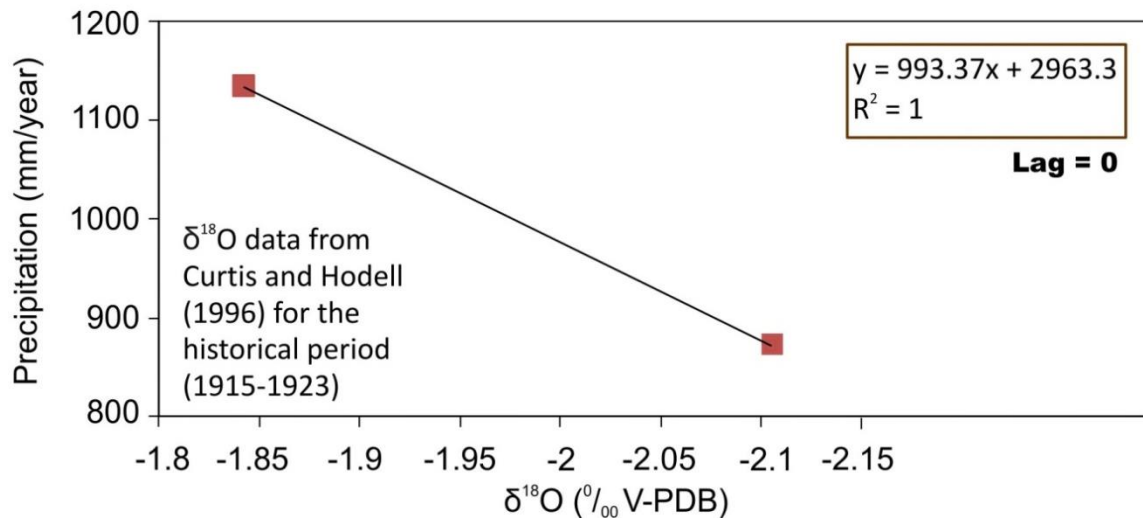
Figure A26. Linear correlation between *Pyrgophorus coronatus* δ^{18}O and the historical precipitation record (1900-2002).

144
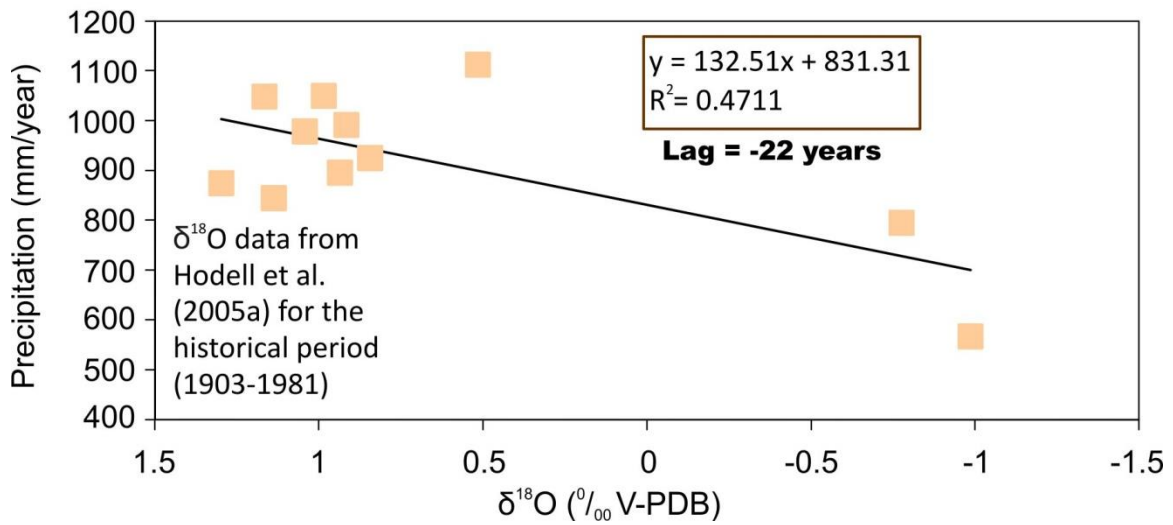
Figure A27. Linear correlation between *Pyrgophorus coronatus* δ^{18}O and the historical precipitation record (1900-2002).
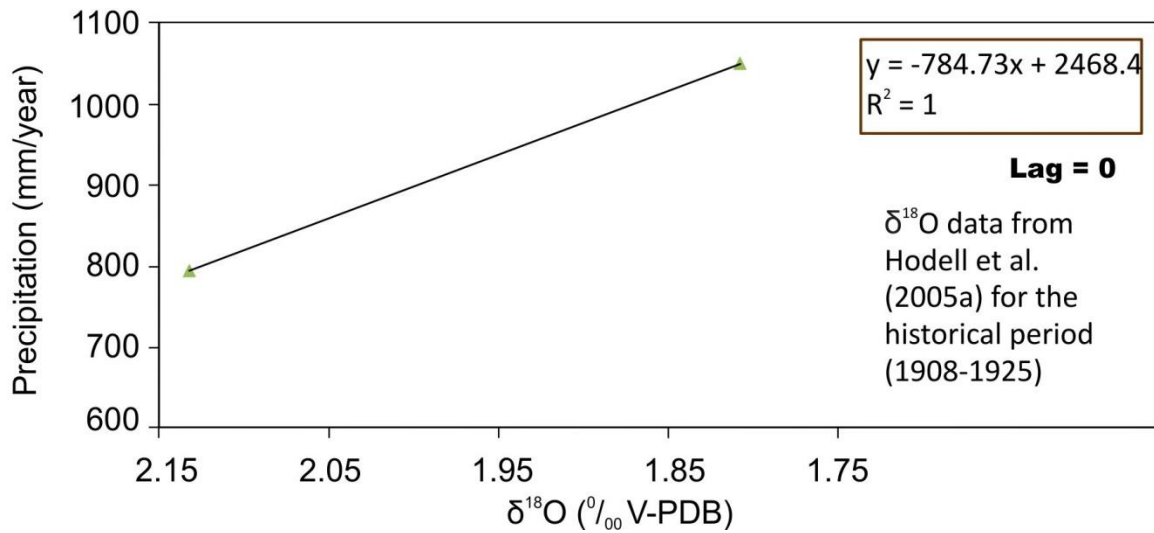
Figure A28. Linear correlation between *D. stevensoni* δ^{18}O and the historical precipitation record (1900-2002).

# Appendix B.   LARS-WG output

Supplementary Material B1-B3: statistical characteristics (.stx files) of the observed climate data (1979-2002), the historical experiment model output (1981-2008), and the past1000 model output (850-1000 AD).   The .stx files provide additional statistical information based on the amount of precipitation, minimum and maximum temperatures, length of wet and dry series, and length of frost spells and heat waves. This information includes semi-empirical distributions, minimum and maximum values, and average values with standard deviations. The monthly statistics for rainfall from these files were used to create shift factors and are included here; the mean monthly precipitation is shown in bold in the historical experiment and past1000 experiment .stx files (this information is also found in the .wgx files, B4-B5).

Supplementary Material B1. The statistical characteristics of the observed daily climate time series from Merida Airport.

```
[VERSION]
LARS-WG5.5
[NAME]
Merida
[LAT, LON and ALT]
20.98 89.65 11.00
[YEARS]
1981  2010
[SERIES seasonal distributions: WET and DRY]
[DJF]
     261   23    1.80  1.99  2.12  1.84
     0.000 0.690 0.877 0.880 0.882 0.884 0.887 0.889 0.891 0.894 0.896
     0.898 0.901 0.903 0.905 0.908 0.910 0.940 0.965 0.980 0.990 0.996
     0.999 1.000
     1.00  2.00  2.00  3.00  3.00  3.00  3.00  3.00  3.00  3.00  3.00
     3.00  3.00  3.00  3.00  3.00  3.00  5.00  7.00  11.00 11.00 11.00
     13.00 13.00
     263   23    8.90  11.40 8.84  10.64
     0.000 0.209 0.350 0.390 0.430 0.470 0.510 0.550 0.590 0.630 0.670
     0.710 0.750 0.790 0.830 0.870 0.910 0.940 0.965 0.980 0.990 0.996
     0.999 1.000
     1.00  1.00  2.00  3.00  4.00  4.00  5.00  6.00  7.00  7.00  9.00
     11.00 13.00 15.00 17.00 18.00 21.00 24.00 27.00 53.00 59.00 74.00
     87.00 87.00
[MAM]
     210   23    2.10  2.84  2.07  3.25
     0.000 0.614 0.805 0.812 0.820 0.827 0.835 0.842 0.850 0.857 0.865
     0.872 0.880 0.887 0.895 0.902 0.910 0.940 0.965 0.980 0.990 0.996
     0.999 1.000
     1.00  1.00  2.00  3.00  3.00  3.00  3.00  3.00  3.00  3.00  3.00
     3.00  3.00  3.00  3.00  4.00  4.00  6.00  8.00  9.00  12.00 31.00
     31.00 31.00
     209   23    9.81  12.69 9.63  12.20
```

146

```
       0.000 0.225 0.344 0.385 0.425 0.466 0.506 0.546 0.587 0.627 0.668
       0.708 0.748 0.789 0.829 0.870 0.910 0.940 0.965 0.980 0.990 0.996
       0.999 1.000
       1.00  1.00  3.00  3.00  4.00  5.00  5.00  5.00  6.00  8.00  9.00
       11.00 13.00 15.00 18.00 21.00 26.00 30.00 43.00 50.00 64.00 76.00
       76.00 76.00
[JJA]
       445   23    2.20  3.38  2.53  2.21
       0.000 0.526 0.793 0.802 0.810 0.818 0.827 0.835 0.843 0.852 0.860
       0.868 0.877 0.885 0.893 0.902 0.910 0.940 0.965 0.980 0.990 0.996
       0.999 1.000
       1.00  2.00  3.00  3.00  3.00  3.00  3.00  3.00  3.00  3.00  3.00
       3.00  4.00  4.00  4.00  4.00  4.00  5.00  6.00  8.00  13.00 26.00
       55.00 55.00
       449   23    3.73  4.41  3.84  3.85
       0.000 0.345 0.528 0.555 0.582 0.610 0.637 0.664 0.692 0.719 0.746
       0.774 0.801 0.828 0.855 0.883 0.910 0.940 0.965 0.980 0.990 0.996
       0.999 1.000
       1.00  2.00  3.00  3.00  3.00  3.00  4.00  4.00  4.00  4.00  5.00
       5.00  5.00  6.00  6.00  7.00  8.00  10.00 12.00 18.00 23.00 39.00
       41.00 41.00
[SON]
       358   23    2.04  2.38  2.33  2.28
       0.000 0.598 0.788 0.796 0.805 0.814 0.823 0.831 0.840 0.849 0.858
       0.866 0.875 0.884 0.893 0.901 0.910 0.940 0.965 0.980 0.990 0.996
       0.999 1.000
       1.00  2.00  2.00  3.00  3.00  3.00  3.00  3.00  3.00  3.00  3.00
       3.00  3.00  3.00  3.00  4.00  4.00  4.00  6.00  12.00 14.00 15.00
       25.00 25.00
       362   23    5.97  9.07  6.38  10.37
       0.000 0.331 0.475 0.506 0.537 0.568 0.599 0.630 0.662 0.693 0.724
       0.755 0.786 0.817 0.848 0.879 0.910 0.940 0.965 0.980 0.990 0.996
       0.999 1.000
       1.00  1.00  3.00  3.00  3.00  3.00  4.00  4.00  5.00  5.00  6.00
       6.00  7.00  9.00  10.00 13.00 16.00 21.00 29.00 37.00 51.00 55.00
       83.00 83.00
[RAIN distributions]
       169   23    4.86  16.64 6.12  22.36
       0.000 0.479 0.580 0.603 0.627 0.651 0.674 0.698 0.721 0.745 0.769
       0.792 0.816 0.839 0.863 0.886 0.910 0.940 0.965 0.980 0.990 0.996
       0.999 1.000
       0.10  0.50  0.90  1.20  1.20  2.18  2.49  2.50  2.69  2.89  3.60
       4.80  5.10  5.65  7.23  8.85  10.30 18.05 29.35 43.76 119.04
       180.10      180.10      180.10
       139   23    5.56  16.16 6.51  20.01
       0.000 0.396 0.475 0.506 0.537 0.568 0.599 0.630 0.661 0.692 0.723
       0.755 0.786 0.817 0.848 0.879 0.910 0.940 0.965 0.980 0.990 0.996
       0.999 1.000
```

```
0.10  0.50  1.00  1.10  1.26  1.59  2.30  2.46  2.70  2.80  3.16
4.04  4.84  5.25  6.27  9.24  13.00 23.95 44.39 58.25 119.83
154.10      154.10      154.10
135   23    7.54  24.87 8.36  24.74
0.000 0.422 0.526 0.553 0.581 0.608 0.636 0.663 0.691 0.718 0.745
0.773 0.800 0.828 0.855 0.883 0.910 0.940 0.965 0.980 0.990 0.996
0.999 1.000
0.10  0.50  1.00  1.10  1.44  2.00  2.18  2.35  2.50  2.69  2.86
4.33  4.60  4.80  5.00  9.80  11.41 40.93 72.40 136.40
154.00      154.80      154.80      154.80
123   23    7.53  23.56 7.74  23.93
0.000 0.325 0.407 0.442 0.478 0.514 0.550 0.586 0.622 0.658 0.694
0.730 0.766 0.802 0.838 0.874 0.910 0.940 0.965 0.980 0.990 0.996
0.999 1.000
0.10  0.50  1.00  1.44  1.50  1.70  2.17  2.30  2.30  2.40  2.50
2.90  3.43  4.80  5.37  7.60  18.08 29.16 77.98 112.46
171.27      183.50      183.50      183.50
167   23    13.25 36.05 13.65 37.61
0.000 0.293 0.365 0.404 0.443 0.482 0.521 0.560 0.599 0.638 0.677
0.715 0.754 0.793 0.832 0.871 0.910 0.940 0.965 0.980 0.990 0.996
0.999 1.000
0.10  0.50  0.90  1.45  1.90  2.30  2.30  2.40  2.50  2.70  3.49
4.60  4.90  7.34  8.90  14.77 45.12 67.91 127.64      184.68
194.16      203.40      203.40      203.40
321   23    15.62 46.60 18.37 54.51
0.000 0.262 0.374 0.412 0.450 0.489 0.527 0.565 0.604 0.642 0.680
0.719 0.757 0.795 0.833 0.872 0.910 0.940 0.965 0.980 0.990 0.996
0.999 1.000
0.10  0.50  1.00  1.33  2.00  2.30  2.50  2.70  3.48  4.60  5.20
6.33  7.20  9.42  13.26 20.26 38.49 68.55 151.32      191.98
256.74      403.67      441.80      441.80
344   23    15.29 36.36 14.83 35.25
0.000 0.238 0.352 0.392 0.431 0.471 0.511 0.551 0.591 0.631 0.671
0.711 0.750 0.790 0.830 0.870 0.910 0.940 0.965 0.980 0.990 0.996
0.999 1.000
0.10  0.50  1.00  1.20  1.50  1.72  2.30  2.70  3.16  3.90  4.75
5.85  7.96  13.59 22.70 30.60 51.90 70.43 134.69      180.76
194.43      203.28      204.90      204.90
316   23    14.46 40.25 16.33 44.46
0.000 0.266 0.380 0.418 0.455 0.493 0.531 0.569 0.607 0.645 0.683
0.721 0.758 0.796 0.834 0.872 0.910 0.940 0.965 0.980 0.990 0.996
0.999 1.000
0.10  0.50  1.00  1.30  1.40  1.80  2.30  2.48  2.70  3.28  4.90
6.14  7.67  10.30 16.82 22.80 35.29 66.10 116.38      193.33
202.30      335.43      381.30      381.30
347   23    14.87 39.80 17.38 45.03
0.000 0.280 0.415 0.450 0.486 0.521 0.556 0.592 0.627 0.662 0.698
0.733 0.769 0.804 0.839 0.875 0.910 0.940 0.965 0.980 0.990 0.996
0.999 1.000
```

```
0.10  0.50  1.00  1.33  1.65  1.98  2.30  2.60  2.70  3.38  4.80
5.20  7.20  12.80 20.10 22.70 39.59 83.41 131.40     184.37
205.32     276.91     294.60     294.60
219   23    17.00 45.75 17.44 49.43
0.000 0.269 0.374 0.413 0.451 0.489 0.527 0.566 0.604 0.642 0.680
0.719 0.757 0.795 0.833 0.872 0.910 0.940 0.965 0.980 0.990 0.996
0.999 1.000
0.10  0.50  1.00  1.34  2.20  2.30  2.50  2.60  3.75  4.70  5.20
6.72  8.53  12.82 19.23 28.10 58.18 78.69 154.30     200.56
222.40     404.00     404.00     404.00
175   23    7.73  24.77 7.12  22.54
0.000 0.343 0.463 0.495 0.527 0.559 0.591 0.623 0.654 0.686 0.718
0.750 0.782 0.814 0.846 0.878 0.910 0.940 0.965 0.980 0.990 0.996
0.999 1.000
0.10  0.50  1.00  1.20  1.42  2.00  2.30  2.40  2.50  2.71  3.81
4.66  4.99  6.00  7.81  13.22 16.85 26.80 50.35 111.51
185.35     200.50     200.50     200.50
166   23    8.47  30.19 9.31  31.68
0.000 0.398 0.482 0.513 0.543 0.574 0.604 0.635 0.665 0.696 0.727
0.757 0.788 0.818 0.849 0.879 0.910 0.940 0.965 0.980 0.990 0.996
0.999 1.000
0.10  0.50  1.00  1.52  2.30  2.30  2.50  2.54  2.60  2.75  3.60
4.60  4.80  5.08  7.30  9.00  12.96 20.20 68.34 179.62
198.88     200.60     200.60     200.60
```
[RAIN monthly statistics: monthly total max and min, N of observations, monthly mean and sd]
```
261.7      257.9      308.3      428.2      731.4      922.1
954.0      960.9      1133.2     1077.1     229.1      279.9
0.0   0.0  0.0   0.0  0.0   0.0  0.2   0.1  0.1   0.0  0.0
0.0
30    30   29    29   30    30   30    30   30    30   30
30
27.370     25.783     35.100     31.938     73.750
167.177    175.350    152.287    172.007    124.133
45.083     46.857
52.840     56.819     69.524     80.516     173.047
262.915    250.031    226.407    276.982    252.377
69.156     73.042
```
[RAIN daily maxima: median, 95 percentile and maximum]
```
1.80 2.00 1.70 1.70 6.00 13.40 16.70 9.40 21.50 4.70 2.70 8.90
91.60 56.00 152.50     86.40 189.60     307.50     200.60
198.60     209.50     217.70     180.30     198.00
180.10     154.10     154.80     183.50     203.40     441.80
204.90     207.50     294.60     404.00     200.50
200.60
```
[END]
```
                    149
```

Supplementary Material B2. Statistical characteristics of the historical experiment model output. Mean monthly precipitation is shown in bold. This file also includes the seasonal distribution of wet and dry series, which show up as 0 (or empty), indicating that LARS-WG was unable to find any wet or dry series in the data.

```
[VERSION]
LARS-WG5.5
[NAME]
MeridaC
[LAT, LON and ALT]
20.98 89.65 11.00
[YEARS]
1979  2005
[SERIES seasonal distributions: WET and DRY]
[DJF]
     0     0
 se-D is empty
     0     0
 se-D is empty
[MAM]
     0     0
 se-D is empty
     0     0
 se-D is empty
[JJA]
     0     0
 se-D is empty
     0     0
 se-D is empty
[SON]
     0     0
 se-D is empty
     0     0
 se-D is empty
[RAIN distributions]
    836    23    2.76 1.03 2.70 0.94
    0.000 -0.001     0.012 0.076 0.140 0.204 0.269 0.333 0.397 0.461
    0.525 0.589 0.653 0.718 0.782 0.846 0.910 0.940 0.965 0.980 0.990
    0.996 0.999 1.000
    0.55 0.00 1.00 1.53 1.80 1.97 2.11 2.23 2.37 2.49 2.66
    2.83 3.01 3.21 3.44 3.72 4.15 4.51 5.05 5.42 5.87 6.65
    9.42 9.42
    756    23    2.30 0.95 2.26 0.92
    0.000 0.004 0.050 0.112 0.173 0.234 0.296 0.357 0.419 0.480 0.542
    0.603 0.664 0.726 0.787 0.849 0.910 0.940 0.965 0.980 0.990 0.996
    0.999 1.000
    0.29 0.45 1.00 1.24 1.42 1.57 1.73 1.90 2.02 2.14 2.28
    2.42 2.60 2.77 2.92 3.20 3.61 3.90 4.34 4.60 5.01 5.88
    7.34 7.34
```

```
837   23    1.44  0.74  1.39  0.77
0.000 0.055 0.333 0.375 0.416 0.457 0.498 0.539 0.580 0.622 0.663
0.704 0.745 0.786 0.828 0.869 0.910 0.940 0.965 0.980 0.990 0.996
0.999 1.000
0.17  0.50  1.00  1.09  1.16  1.24  1.30  1.38  1.47  1.56  1.66
1.75  1.87  2.00  2.11  2.26  2.49  2.71  3.09  3.24  3.50  4.13
5.91  5.91
810   23    1.19  0.66  1.17  0.70
0.000 0.080 0.507 0.536 0.565 0.594 0.622 0.651 0.680 0.709 0.737
0.766 0.795 0.824 0.852 0.881 0.910 0.940 0.965 0.980 0.990 0.996
0.999 1.000
0.22  0.50  1.00  1.05  1.11  1.14  1.18  1.24  1.30  1.35  1.42
1.50  1.59  1.75  1.88  2.04  2.30  2.51  2.73  3.02  3.34  3.76
4.34  4.34
837   23    1.17  0.68  1.14  0.66
0.000 0.115 0.532 0.559 0.586 0.613 0.640 0.667 0.694 0.721 0.748
0.775 0.802 0.829 0.856 0.883 0.910 0.940 0.965 0.980 0.990 0.996
0.999 1.000
0.19  0.50  1.00  1.05  1.12  1.18  1.23  1.28  1.36  1.42  1.52
1.62  1.71  1.80  1.89  2.02  2.14  2.42  2.75  3.05  3.61  3.99
4.22  4.22
810   23    1.29  0.62  1.28  0.65
0.000 0.049 0.367 0.405 0.444 0.483 0.522 0.561 0.600 0.638 0.677
0.716 0.755 0.794 0.832 0.871 0.910 0.940 0.965 0.980 0.990 0.996
0.999 1.000
0.19  0.50  1.00  1.05  1.11  1.14  1.21  1.26  1.33  1.38  1.45
1.52  1.61  1.73  1.87  2.04  2.18  2.40  2.64  2.85  3.17  3.77
4.80  4.80
837   23    1.90  0.76  1.87  0.83
0.000 -0.001      0.063 0.124 0.184 0.245 0.305 0.366 0.426 0.487
0.547 0.608 0.668 0.729 0.789 0.850 0.910 0.940 0.965 0.980 0.990
0.996 0.999 1.000
0.54  0.00  1.00  1.16  1.26  1.37  1.47  1.57  1.66  1.75  1.85
1.96  2.09  2.23  2.38  2.61  2.90  3.08  3.48  3.71  4.47  5.23
8.33  8.33
837   23    2.70  1.06  2.67  1.04
0.000 -0.001      0.000 0.065 0.130 0.195 0.260 0.325 0.390 0.455
0.520 0.585 0.650 0.715 0.780 0.845 0.910 0.940 0.965 0.980 0.990
0.996 0.999 1.000
0.92  0.00  0.92  1.49  1.71  1.83  1.97  2.09  2.25  2.40  2.56
2.71  2.89  3.04  3.30  3.58  4.15  4.63  5.24  5.72  6.45  7.15
8.04  8.04
810   23    3.71  1.38  3.57  1.44
0.000 -0.001     -0.001      0.064 0.129 0.194 0.259 0.324 0.389
0.454 0.519 0.585 0.650 0.715 0.780 0.845 0.910 0.940 0.965 0.980
0.990 0.996 0.999 1.000
1.12  0.00  0.00  2.09  2.44  2.63  2.80  2.97  3.19  3.35  3.51
3.73  3.92  4.15  4.41  4.84  5.60  6.02  6.60  7.34  8.57  10.68
11.58 11.58
837   23    3.98  1.41  3.86  1.48
```

```
0.000 -0.001     -0.001     0.064 0.129 0.194 0.259 0.324 0.389
0.454 0.519 0.585 0.650 0.715 0.780 0.845 0.910 0.940 0.965 0.980
0.990 0.996 0.999 1.000
1.37  0.00  0.00  2.27  2.59  2.80  3.02  3.25  3.44  3.63  3.80
3.96  4.18  4.44  4.83  5.23  6.01  6.55  7.26  7.65  8.58  10.11
10.54 10.54
810   23    3.56  1.29  3.54  1.34
0.000 -0.001     0.006 0.071 0.135 0.200 0.264 0.329 0.394 0.458
0.523 0.587 0.652 0.716 0.781 0.845 0.910 0.940 0.965 0.980 0.990
0.996 0.999 1.000
0.62  0.00  1.00  1.95  2.33  2.49  2.71  2.90  3.06  3.25  3.42
3.59  3.82  4.11  4.40  4.79  5.39  5.96  6.47  7.07  7.60  7.93
8.07  8.07
837   23    3.09  1.06  3.14  1.14
0.000 -0.001     0.002 0.067 0.132 0.197 0.262 0.327 0.391 0.456
0.521 0.586 0.651 0.716 0.780 0.845 0.910 0.940 0.965 0.980 0.990
0.996 0.999 1.000
0.88  0.00  0.93  1.70  2.00  2.19  2.38  2.54  2.71  2.85  2.99
3.14  3.34  3.56  3.82  4.10  4.63  4.89  5.37  5.65  6.14  7.14
8.14  8.14
```
[RAIN monthly statistics: monthly total max and min, N of
observations, monthly mean and sd]
```
103.2      82.2  64.2  47.5  61.8  60.8  71.8  108.0      154.6
158.2      155.2       116.1
52.9  46.2  28.5  26.6  20.9  28.6  47.3  66.8  79.9  100.0
82.9  77.4
27    27    27    27    27    27    27    27    27    27    27
27
```
85.509   64.372   44.515   35.691   36.278
38.653   58.863   83.802   111.259   123.266
106.790   95.848
```
10.598      10.579      7.903       6.250       10.659      6.949
6.298       9.738       14.498      13.114      15.088      9.556
```
[RAIN daily maxima: median, 95 percentile and maximum]
```
5.25 4.44 3.20 2.82 2.44 2.71 3.61 5.03 6.74 7.33 6.50 5.50
8.81 5.89 4.20 3.94 4.10 4.63 6.60 7.72 11.23 10.49 7.93 7.86
9.42 7.15 5.91 4.34 4.22 4.80 8.33 8.04 11.58 10.54 8.00 8.14
```
 [END]
```

**Supplementary Material B3.** **Statistical characteristics of the past1000 experiment model output. Mean monthly precipitation is shown in bold. LARS-WG did calculate wet and dry series for this dataset (found under SERIES seasonal distributions: WET and DRY); however, the length of wet series are much longer than those of the observed climate. The average length of the seasonal wet series is also shown in bold.**

```
[VERSION]
LARS-WG5.5
[NAME]
MeridaTCP
[LAT, LON and ALT]
20.98 89.65 11.00
[YEARS]
850   999
[SERIES seasonal distributions: WET and DRY]
[DJF]
    10    23    108.70      220.28      109.86      214.58
    0.000 0.043 0.087 0.130 0.174 0.217 0.261 0.304 0.348 0.391 0.435
    0.478 0.522 0.565 0.609 0.652 0.696 0.739 0.783 0.826 0.870 0.913
    0.957 1.000
    8.00  8.00  8.00  20.00 20.00 22.00 22.00 30.00 30.00 30.00 32.00
    32.00 33.00 33.00 39.00 39.00 39.00 54.00 54.00 82.00 82.00
    767.00      767.00      767.00
    17    23    1.29  0.46  1.25  0.43
    0.000 0.043 0.087 0.130 0.174 0.217 0.261 0.304 0.348 0.391 0.435
    0.478 0.522 0.565 0.609 0.652 0.696 0.739 0.783 0.826 0.870 0.913
    0.957 1.000
    1.00  1.00  1.00  1.00  1.00  1.00  1.00  1.00  1.00  1.00  1.00
    1.00  1.00  1.00  1.00  1.00  1.00  2.00  2.00  2.00  2.00  2.00
    2.00  2.00
[MAM]
    25    23    302.84      256.62      312.34      260.35
    0.000 0.043 0.087 0.130 0.174 0.217 0.261 0.304 0.348 0.391 0.435
    0.478 0.522 0.565 0.609 0.652 0.696 0.739 0.783 0.826 0.870 0.913
    0.957 1.000
    1.00  3.00  11.00 26.00 26.00 29.00 46.00 61.00 62.00 116.00
    199.00      281.00      361.00      366.00      372.00
    377.00      393.00      398.00      633.00      644.00
    700.00      711.00      713.00      715.00
    38    23    1.42  0.75  1.33  0.72
    0.000 0.711 0.895 0.896 0.897 0.898 0.899 0.900 0.901 0.902 0.903
    0.905 0.906 0.907 0.908 0.909 0.910 0.940 0.965 0.980 0.990 0.996
    0.999 1.000
    1.00  1.00  2.00  3.00  3.00  3.00  3.00  3.00  3.00  3.00  3.00
    3.00  3.00  3.00  3.00  3.00  3.00  3.00  3.00  4.00  4.00  4.00
    4.00  4.00
[JJA]
    12    23    321.25      303.36      315.98      293.83
```

```
0.000 0.043 0.087 0.130 0.174 0.217 0.261 0.304 0.348 0.391 0.435
0.478 0.522 0.565 0.609 0.652 0.696 0.739 0.783 0.826 0.870 0.913
0.957 1.000
40.00 40.00 67.00 67.00 83.00 83.00 100.00     100.00
142.00      142.00      191.00      191.00      217.00
217.00      236.00      236.00      442.00      442.00
470.00      470.00      909.00      909.00      958.00
958.00
0     0
se-D is empty
[SON]
8     23     387.25       261.09       378.19       238.08
0.000 0.043 0.087 0.130 0.174 0.217 0.261 0.304 0.348 0.391 0.435
0.478 0.522 0.565 0.609 0.652 0.696 0.739 0.783 0.826 0.870 0.913
0.957 1.000
49.00 49.00 49.00 134.00      134.00      134.00      167.00
167.00      167.00      317.00      317.00      317.00
450.00      450.00      450.00      530.00      530.00
530.00      552.00      552.00      552.00      899.00
899.00      899.00
1     23     2.00  0.00  2.00  0.00
0.000 0.043 0.087 0.130 0.174 0.217 0.261 0.304 0.348 0.391 0.435
0.478 0.522 0.565 0.609 0.652 0.696 0.739 0.783 0.826 0.870 0.913
0.957 1.000
2.00  2.00  2.00  2.00  2.00  2.00  2.00  2.00  2.00  2.00  2.00
2.00  2.00  2.00  2.00  2.00  2.00  2.00  2.00  2.00  2.00  2.00
2.00  2.00
[RAIN distributions]
4644 23     2.95  2.19  3.00  2.23
0.000 0.060 0.156 0.210 0.263 0.317 0.371 0.425 0.479 0.533 0.587
0.641 0.694 0.748 0.802 0.856 0.910 0.940 0.965 0.980 0.990 0.996
0.999 1.000
0.09  0.43  0.95  1.30  1.56  1.81  1.99  2.25  2.42  2.59  2.85
3.11  3.46  3.80  4.23  4.92  5.79  6.65  7.69  9.08  10.76 13.03
19.53 24.71
4185 23     2.44  2.10  2.42  2.06
0.000 0.128 0.259 0.306 0.352 0.399 0.445 0.492 0.538 0.585 0.631
0.678 0.724 0.771 0.817 0.864 0.910 0.940 0.965 0.980 0.990 0.996
0.999 1.000
0.09  0.43  0.95  1.21  1.38  1.56  1.73  1.90  2.07  2.33  2.51
2.76  3.11  3.46  3.89  4.41  5.18  6.05  7.26  8.64  10.38 12.31
15.68 16.59
4625 23     1.61  1.68  1.52  1.73
0.000 0.251 0.457 0.489 0.522 0.554 0.586 0.619 0.651 0.683 0.716
0.748 0.781 0.813 0.845 0.878 0.910 0.940 0.965 0.980 0.990 0.996
0.999 1.000
0.09  0.43  0.95  1.12  1.21  1.30  1.38  1.56  1.64  1.81  1.99
2.07  2.25  2.56  2.85  3.20  3.80  4.45  5.53  6.74  8.12  9.76
13.98 25.06
4477 23     1.35  1.62  1.33  1.58
```

```
0.000 0.341 0.579 0.603 0.627 0.650 0.674 0.697 0.721 0.745 0.768
0.792 0.816 0.839 0.863 0.886 0.910 0.940 0.965 0.980 0.990 0.996
0.999 1.000
0.09  0.43  0.95  1.04  1.12  1.21  1.30  1.38  1.47  1.64  1.81
1.90  2.16  2.33  2.68  3.02  3.37  4.15  5.18  6.57  8.06  10.22
12.75 17.80
4643  23    1.32  1.68  1.26  1.64
0.000 0.351 0.594 0.617 0.639 0.662 0.684 0.707 0.730 0.752 0.775
0.797 0.820 0.842 0.865 0.887 0.910 0.940 0.965 0.980 0.990 0.996
0.999 1.000
0.09  0.43  0.95  1.04  1.12  1.21  1.30  1.38  1.47  1.64  1.73
1.90  2.07  2.25  2.51  2.76  3.20  3.97  5.18  6.65  8.79  11.22
15.05 19.44
4500  23    1.53  1.48  1.53  1.61
0.000 0.197 0.446 0.480 0.513 0.546 0.579 0.612 0.645 0.678 0.711
0.744 0.778 0.811 0.844 0.877 0.910 0.940 0.965 0.980 0.990 0.996
0.999 1.000
0.09  0.43  0.95  1.04  1.12  1.21  1.30  1.47  1.56  1.64  1.81
1.99  2.16  2.33  2.59  2.85  3.28  3.89  4.75  5.79  7.43  9.33
12.62 27.91
4650  23    2.15  1.79  2.22  1.81
0.000 0.067 0.239 0.287 0.335 0.383 0.431 0.479 0.527 0.575 0.622
0.670 0.718 0.766 0.814 0.862 0.910 0.940 0.965 0.980 0.990 0.996
0.999 1.000
0.09  0.43  0.95  1.12  1.21  1.38  1.47  1.64  1.81  1.90  2.16
2.33  2.59  2.85  3.20  3.63  4.23  4.92  6.13  7.17  9.33  12.39
16.16 21.17
4650  23    2.96  2.39  3.07  2.75
0.000 0.016 0.102 0.160 0.217 0.275 0.333 0.391 0.448 0.506 0.564
0.621 0.679 0.737 0.795 0.852 0.910 0.940 0.965 0.980 0.990 0.996
0.999 1.000
0.17  0.43  0.95  1.21  1.47  1.64  1.81  1.99  2.25  2.42  2.68
2.85  3.20  3.46  3.97  4.58  5.53  6.48  8.04  10.02 12.01 16.11
22.84 45.27
4500  23    3.81  2.89  3.88  3.06
0.000 0.004 0.040 0.103 0.165 0.227 0.289 0.351 0.413 0.475 0.537
0.599 0.662 0.724 0.786 0.848 0.910 0.940 0.965 0.980 0.990 0.996
0.999 1.000
0.17  0.43  0.95  1.38  1.73  1.99  2.25  2.47  2.68  2.94  3.20
3.54  3.97  4.41  5.01  5.84  7.26  8.47  10.15 12.70 15.38 18.84
22.60 53.74
4648  23    4.13  3.12  4.06  2.89
0.000 0.017 0.068 0.128 0.188 0.249 0.309 0.369 0.429 0.489 0.549
0.609 0.669 0.730 0.790 0.850 0.910 0.940 0.965 0.980 0.990 0.996
0.999 1.000
0.09  0.43  0.95  1.38  1.73  1.99  2.33  2.62  2.94  3.28  3.63
4.06  4.58  5.10  5.79  6.83  8.29  9.59  11.32 12.96 15.72 19.56
21.61 40.95
4500  23    3.80  2.94  3.71  2.94
```

```
0.000 0.032 0.113 0.170 0.227 0.284 0.341 0.398 0.455 0.511 0.568
0.625 0.682 0.739 0.796 0.853 0.910 0.940 0.965 0.980 0.990 0.996
0.999 1.000
0.09  0.43  0.95  1.30  1.64  1.90  2.16  2.42  2.76  3.20  3.54
3.89  4.41  5.01  5.70  6.57  7.78  8.73  10.37 11.84 14.08 17.11
21.13 35.60
4649 23   3.35  2.55  3.43  2.87
0.000 0.049 0.125 0.181 0.237 0.293 0.349 0.405 0.462 0.518 0.574
0.630 0.686 0.742 0.798 0.854 0.910 0.940 0.965 0.980 0.990 0.996
0.999 1.000
0.09  0.43  0.95  1.30  1.56  1.81  2.07  2.33  2.59  2.85  3.11
3.46  3.89  4.32  4.92  5.70  6.83  7.61  9.10  10.63 12.40 14.38
21.73 29.64
```

[RAIN monthly statistics: monthly total max and min, N of observations, monthly mean and sd]

```
    188.1       165.0       106.9       101.8       113.3        97.3
    120.6       175.9       193.6       241.2       189.3       172.2
    35.1 12.8 14.6 6.7   12.0 16.1 35.4 51.8 64.9 46.9 47.8
    38.5
    150   150  150   150   150   150   150   150   150   150   150
    150
    91.237      68.125      49.764      40.208      40.752
    45.856      66.743      91.733      114.309     128.009
    113.955     103.816
    23.812      24.120      17.545      18.593      21.231
    15.758      16.999      21.472      25.907      38.385
    27.638      27.270
```

[RAIN daily maxima: median, 95 percentile and maximum]

```
7.95  7.00  5.36  4.92  4.58  4.41  6.13  8.38  9.85  10.89 10.97 9.24
14.00 13.91 10.97 11.66 12.70 10.02 14.52 21.43 20.56 21.00 18.75 17.19
24.71 16.59 25.06 17.80 19.44 27.91 21.17 45.27 24.11 40.95 35.60 29.64
 [END]
```

Supplementary Material B4-B6: parameter files (.wgx files) of the observed climate data (1979-2002), the historical experiment model output (1981-2008), and the past1000 model output (850-1000 AD). These files are used by LARS-WG to generate new climate series. These files include monthly distributions for the length of wet and dry series; minimum and maximum temperature; and precipitation. The relative change in the length of wet and dry series would be calculated using the monthly mean length of wet and dry series from the historical and past1000 experiment .wgx files; however, LARS-WG was not able to calculate the length of wet and dry series for the historical experiment (and some months of the past1000 experiment).

Supplementary Material B4. Parameter file for the observed daily climate time series from Merida Airport. The mean monthly length of wet and dry series are shown in bold.

```
[VERSION]
LARS-WG5.5
[NAME]
Merida
[LAT, LON and ALT]
     20.98 89.65 11.00
[YEARS]
     1981  2010
[SERIES WET]
     92    23    1.84  2.15  2.23  1.93
     0.000 0.707 0.891 0.893 0.894 0.895 0.897 0.898 0.899 0.901 0.902
     0.903 0.905 0.906 0.907 0.909 0.910 0.940 0.965 0.980 0.990 0.996
     0.999 1.000
     1.00  2.00  3.00  3.00  3.00  3.00  3.00  3.00  3.00  3.00  3.00
     3.00  3.00  3.00  3.00  3.00  3.00  7.00  8.00  11.00 13.00 13.00
     13.00 13.00
     76    23    1.89  2.06  1.89  2.17
     0.000 0.658 0.855 0.859 0.863 0.867 0.871 0.875 0.879 0.883 0.887
     0.890 0.894 0.898 0.902 0.906 0.910 0.940 0.965 0.980 0.990 0.996
     0.999 1.000
     1.00  1.00  3.00  3.00  3.00  3.00  3.00  3.00  3.00  3.00  3.00
     3.00  3.00  3.00  3.00  3.00  3.00  6.00  10.00 11.00 11.00 11.00
     11.00 11.00
     69    23    1.88  2.29  2.08  1.86
     0.000 0.638 0.855 0.859 0.863 0.867 0.871 0.875 0.879 0.883 0.886
     0.890 0.894 0.898 0.902 0.906 0.910 0.940 0.965 0.980 0.990 0.996
     0.999 1.000
     1.00  2.00  2.00  3.00  3.00  3.00  3.00  3.00  3.00  3.00  3.00
     3.00  3.00  3.00  3.00  3.00  3.00  4.00  5.00  12.00 16.00 16.00
     16.00 16.00
     65    23    1.88  1.97  2.43  2.07
     0.000 0.692 0.846 0.851 0.855 0.860 0.864 0.869 0.874 0.878 0.883
     0.887 0.892 0.896 0.901 0.905 0.910 0.940 0.965 0.980 0.990 0.996
     0.999 1.000
     1.00  2.00  3.00  3.00  3.00  3.00  3.00  3.00  3.00  3.00  3.00
     3.00  3.00  4.00  4.00  4.00  5.00  6.00  8.00  9.00  11.00 11.00
     11.00 11.00
     75    23    2.47  3.77  3.05  4.29
     0.000 0.547 0.747 0.758 0.770 0.782 0.793 0.805 0.817 0.828 0.840
     0.852 0.863 0.875 0.887 0.898 0.910 0.940 0.965 0.980 0.990 0.996
     0.999 1.000
     1.00  2.00  3.00  3.00  3.00  3.00  3.00  3.00  3.00  3.00  3.00
     3.00  3.00  3.00  4.00  5.00  6.00  7.00  9.00  9.00  31.00 31.00
     31.00 31.00
     133   23    2.41  3.09  2.78  2.78
```

```
0.000 0.459 0.744 0.756 0.768 0.780 0.792 0.804 0.815 0.827 0.839
0.851 0.863 0.875 0.886 0.898 0.910 0.940 0.965 0.980 0.990 0.996
0.999 1.000
1.00  2.00  3.00  3.00  3.00  3.00  3.00  3.00  3.00  3.00  3.00
4.00  4.00  4.00  4.00  4.00  4.00  5.00  8.00  10.00 22.00 26.00
26.00 26.00
165   23   2.21  4.39  2.50  3.26
0.000 0.533 0.806 0.813 0.821 0.828 0.836 0.843 0.851 0.858 0.865
0.873 0.880 0.888 0.895 0.903 0.910 0.940 0.965 0.980 0.990 0.996
0.999 1.000
1.00  2.00  3.00  3.00  3.00  3.00  3.00  3.00  3.00  3.00  3.00
3.00  3.00  3.00  3.00  4.00  4.00  5.00  6.00  6.00  13.00 55.00
55.00 55.00
145   23   1.97  2.06  2.37  1.88
0.000 0.579 0.814 0.821 0.828 0.834 0.841 0.848 0.855 0.862 0.869
0.876 0.883 0.889 0.896 0.903 0.910 0.940 0.965 0.980 0.990 0.996
0.999 1.000
1.00  2.00  3.00  3.00  3.00  3.00  3.00  3.00  3.00  3.00  3.00
4.00  4.00  4.00  4.00  4.00  4.00  5.00  6.00  8.00  9.00  20.00
20.00 20.00
156   23   2.27  2.63  2.61  2.31
0.000 0.513 0.718 0.732 0.745 0.759 0.773 0.787 0.800 0.814 0.828
0.841 0.855 0.869 0.883 0.896 0.910 0.940 0.965 0.980 0.990 0.996
0.999 1.000
1.00  2.00  3.00  3.00  3.00  3.00  3.00  3.00  3.00  3.00  3.00
3.00  3.00  3.00  4.00  4.00  4.00  5.00  7.00  10.00 13.00 25.00
25.00 25.00
107   23   1.93  2.23  1.90  2.47
0.000 0.645 0.841 0.846 0.851 0.856 0.861 0.866 0.871 0.876 0.880
0.885 0.890 0.895 0.900 0.905 0.910 0.940 0.965 0.980 0.990 0.996
0.999 1.000
1.00  1.00  2.00  3.00  3.00  3.00  3.00  3.00  3.00  3.00  3.00
3.00  3.00  3.00  3.00  3.00  3.00  5.00  8.00  13.00 13.00 14.00
14.00 14.00
95    23   1.73  1.65  1.78  1.93
0.000 0.663 0.842 0.847 0.852 0.857 0.862 0.866 0.871 0.876 0.881
0.886 0.891 0.895 0.900 0.905 0.910 0.940 0.965 0.980 0.990 0.996
0.999 1.000
1.00  1.00  3.00  3.00  3.00  3.00  3.00  3.00  3.00  3.00  3.00
3.00  3.00  3.00  3.00  3.00  3.00  4.00  4.00  6.00  14.00 14.00
14.00 14.00
96    23   1.82  2.19  2.32  2.19
0.000 0.698 0.875 0.877 0.880 0.882 0.885 0.887 0.890 0.892 0.895
0.897 0.900 0.902 0.905 0.907 0.910 0.940 0.965 0.980 0.990 0.996
0.999 1.000
1.00  2.00  3.00  3.00  3.00  3.00  3.00  3.00  3.00  3.00  3.00
3.00  3.00  3.00  3.00  3.00  3.00  5.00  7.00  11.00 15.00 15.00
15.00 15.00
[SERIES DRY]
96    23   9.33  11.96 9.46  11.87
```

0.000 0.229 0.333 0.375 0.416 0.457 0.498 0.539 0.580 0.622 0.663
0.704 0.745 0.786 0.828 0.869 0.910 0.940 0.965 0.980 0.990 0.996
0.999 1.000
1.00 2.00 3.00 3.00 3.00 4.00 5.00 6.00 7.00 7.00 9.00
9.00 12.00 15.00 18.00 21.00 24.00 27.00 33.00 59.00 74.00 74.00
74.00 74.00
75   23   **10.04** 14.44 10.66 15.68
0.000 0.200 0.347 0.387 0.427 0.467 0.508 0.548 0.588 0.628 0.669
0.709 0.749 0.789 0.830 0.870 0.910 0.940 0.965 0.980 0.990 0.996
0.999 1.000
1.00 2.00 2.00 3.00 3.00 5.00 6.00 7.00 7.00 8.00 10.00
12.00 13.00 14.00 15.00 19.00 22.00 25.00 54.00 59.00 87.00 87.00
87.00 87.00
71   23   **10.27** 14.15 9.98 13.09
0.000 0.197 0.310 0.353 0.396 0.438 0.481 0.524 0.567 0.610 0.653
0.696 0.739 0.781 0.824 0.867 0.910 0.940 0.965 0.980 0.990 0.996
0.999 1.000
1.00 2.00 3.00 3.00 4.00 5.00 5.00 6.00 7.00 8.00 9.00
10.00 11.00 15.00 17.00 20.00 26.00 28.00 49.00 74.00 76.00 76.00
76.00 76.00
67   23   **11.58** 12.90 12.46 13.40
0.000 0.254 0.343 0.384 0.424 0.465 0.505 0.546 0.586 0.627 0.667
0.708 0.748 0.789 0.829 0.870 0.910 0.940 0.965 0.980 0.990 0.996
0.999 1.000
1.00 1.00 3.00 4.00 5.00 5.00 6.00 7.00 10.00 12.00 14.00
15.00 18.00 18.00 23.00 26.00 30.00 35.00 46.00 50.00 55.00 55.00
55.00 55.00
66   23   **8.26** 10.86 8.59 10.85
0.000 0.212 0.364 0.403 0.442 0.481 0.520 0.559 0.598 0.637 0.676
0.715 0.754 0.793 0.832 0.871 0.910 0.940 0.965 0.980 0.990 0.996
0.999 1.000
1.00 2.00 3.00 3.00 3.00 4.00 5.00 5.00 5.00 6.00 8.00
9.00 11.00 13.00 14.00 18.00 23.00 28.00 29.00 43.00 64.00 64.00
64.00 64.00
136   23   **3.88** 4.40 3.87 4.62
0.000 0.360 0.493 0.522 0.552 0.582 0.612 0.642 0.672 0.701 0.731
0.761 0.791 0.821 0.850 0.880 0.910 0.940 0.965 0.980 0.990 0.996
0.999 1.000
1.00 1.00 2.00 3.00 3.00 3.00 4.00 4.00 4.00 4.00 5.00
5.00 6.00 6.00 7.00 7.00 9.00 10.00 12.00 15.00 17.00 39.00
39.00 39.00
166   23   **3.51** 4.69 3.70 4.42
0.000 0.361 0.566 0.591 0.615 0.640 0.664 0.689 0.714 0.738 0.763
0.787 0.812 0.836 0.861 0.885 0.910 0.940 0.965 0.980 0.990 0.996
0.999 1.000
1.00 2.00 2.00 3.00 3.00 3.00 3.00 4.00 4.00 4.00 4.00
5.00 5.00 5.00 6.00 6.00 7.00 8.00 10.00 19.00 30.00 41.00
41.00 41.00
147   23   **3.78** 3.91 3.59 3.80

```
0.000 0.313 0.524 0.551 0.579 0.607 0.634 0.662 0.689 0.717 0.744
0.772 0.800 0.827 0.855 0.882 0.910 0.940 0.965 0.980 0.990 0.996
0.999 1.000
1.00  1.00  3.00  3.00  3.00  3.00  3.00  4.00  4.00  4.00  5.00
5.00  6.00  6.00  7.00  7.00  9.00  11.00 12.00 20.00 22.00 23.00
23.00 23.00
155   23    3.72  4.62  3.86  4.38
0.000 0.400 0.581 0.604 0.628 0.651 0.675 0.698 0.722 0.745 0.769
0.792 0.816 0.839 0.863 0.886 0.910 0.940 0.965 0.980 0.990 0.996
0.999 1.000
1.00  2.00  2.00  3.00  3.00  3.00  4.00  4.00  4.00  4.00  5.00
5.00  6.00  6.00  6.00  8.00  9.00  10.00 17.00 18.00 27.00 30.00
30.00 30.00
118   23    7.96  12.46 7.85  12.89
0.000 0.288 0.407 0.443 0.479 0.515 0.551 0.587 0.622 0.658 0.694
0.730 0.766 0.802 0.838 0.874 0.910 0.940 0.965 0.980 0.990 0.996
0.999 1.000
1.00  1.00  2.00  3.00  3.00  4.00  4.00  4.00  5.00  6.00  6.00
7.00  8.00  9.00  12.00 18.00 26.00 33.00 38.00 51.00 51.00 83.00
83.00 83.00
96    23    7.23  8.62  7.40  8.79
0.000 0.281 0.375 0.413 0.451 0.490 0.528 0.566 0.604 0.642 0.681
0.719 0.757 0.795 0.834 0.872 0.910 0.940 0.965 0.980 0.990 0.996
0.999 1.000
1.00  2.00  3.00  3.00  3.00  4.00  4.00  5.00  5.00  6.00  7.00
10.00 11.00 12.00 14.00 16.00 20.00 25.00 26.00 29.00 55.00 55.00
55.00 55.00
90    23    7.26  6.85  7.60  6.76
0.000 0.189 0.378 0.416 0.454 0.492 0.530 0.568 0.606 0.644 0.682
0.720 0.758 0.796 0.834 0.872 0.910 0.940 0.965 0.980 0.990 0.996
0.999 1.000
1.00  2.00  3.00  3.00  4.00  4.00  5.00  6.00  7.00  7.00  8.00
11.00 13.00 15.00 16.00 17.00 18.00 19.00 21.00 22.00 33.00 33.00
33.00 33.00
```
[END]

Supplementary Material B5. The parameter file for the historical experiment model output. Note that the information for the length of wet and dry series appears as 0 or empty, indicating that LARS-WG did not detect any wet or dry series for this dataset.

```
[VERSION]
LARS-WG5.5
[NAME]
MeridaC
[LAT, LON and ALT]
     20.98 89.65 11.00
[YEARS]
     1979  2005
[SERIES WET]
     0     0
 se-D is empty
     0     0
 se-D is empty
     0     0
 se-D is empty
     0     0
 se-D is empty
     0     0
 se-D is empty
     0     0
 se-D is empty
     0     0
 se-D is empty
     0     0
 se-D is empty
     0     0
 se-D is empty
     0     0
 se-D is empty
     0     0
 se-D is empty
     0     0
 se-D is empty
[SERIES DRY]
     0     0
 se-D is empty
     0     0
 se-D is empty
     0     0
 se-D is empty
     0     0
 se-D is empty
     0     0
 se-D is empty
     0     0
```

```
se-D is empty
     0      0
se-D is empty
     0      0
se-D is empty
     0      0
se-D is empty
     0      0
se-D is empty
     0      0
se-D is empty
     0      0
se-D is empty
 [END]
```

Supplementary Material B6. Parameter file for the past100 experiment model output. LARS-WG did not find and wet series for September-October or any dry series for June-September and November for this dataset. The mean monthly length of wet and dry series are shown in bold.

```
[VERSION]
LARS-WG5.5
[NAME]
MeridaTCP
[LAT, LON and ALT]
     20.98 89.65 11.00
[YEARS]
     850   999
[SERIES WET]
     5      23     193.60       287.28       194.92       282.72
     0.000 0.043 0.087 0.130 0.174 0.217 0.261 0.304 0.348 0.391 0.435
     0.478 0.522 0.565 0.609 0.652 0.696 0.739 0.783 0.826 0.870 0.913
     0.957 1.000
     32.00 32.00 32.00 32.00 32.00 33.00 33.00 33.00 33.00 33.00 54.00
     54.00 54.00 54.00 82.00 82.00 82.00 82.00 82.00 767.00
     767.00      767.00       767.00       767.00
     5      23     43.00 37.89 43.15 37.76
     0.000 0.043 0.087 0.130 0.174 0.217 0.261 0.304 0.348 0.391 0.435
     0.478 0.522 0.565 0.609 0.652 0.696 0.739 0.783 0.826 0.870 0.913
     0.957 1.000
     8.00  8.00  8.00  8.00  8.00  22.00 22.00 22.00 22.00 22.00 30.00
     30.00 30.00 30.00 39.00 39.00 39.00 39.00 39.00 116.00
     116.00      116.00       116.00       116.00
     11     23     185.36       217.88       197.85       227.67
     0.000 0.043 0.087 0.130 0.174 0.217 0.261 0.304 0.348 0.391 0.435
     0.478 0.522 0.565 0.609 0.652 0.696 0.739 0.783 0.826 0.870 0.913
     0.957 1.000
```

```
20.00 20.00 20.00 26.00 26.00 26.00 26.00 29.00 29.00 46.00 46.00
61.00 61.00 62.00 62.00 281.00      281.00      377.00
377.00      398.00      398.00      713.00      713.00
713.00
22     23     377.32      284.22      383.97      292.11
0.000 0.043 0.087 0.130 0.174 0.217 0.261 0.304 0.348 0.391 0.435
0.478 0.522 0.565 0.609 0.652 0.696 0.739 0.783 0.826 0.870 0.913
0.957 1.000
1.00  1.00  3.00  11.00 67.00 83.00 142.00      191.00
199.00      236.00      327.00      361.00      366.00
372.00      393.00      442.00      470.00      644.00
700.00      711.00      715.00      909.00      958.00
958.00
4      23     304.25      205.42      303.79      197.93
0.000 0.043 0.087 0.130 0.174 0.217 0.261 0.304 0.348 0.391 0.435
0.478 0.522 0.565 0.609 0.652 0.696 0.739 0.783 0.826 0.870 0.913
0.957 1.000
100.00      100.00      100.00      100.00      100.00
100.00      167.00      167.00      167.00      167.00
167.00      167.00      317.00      317.00      317.00
317.00      317.00      317.00      633.00      633.00
633.00      633.00      633.00      633.00
5      23     431.00      311.31      450.49      308.60
0.000 0.043 0.087 0.130 0.174 0.217 0.261 0.304 0.348 0.391 0.435
0.478 0.522 0.565 0.609 0.652 0.696 0.739 0.783 0.826 0.870 0.913
0.957 1.000
40.00 40.00 40.00 40.00 40.00 134.00      134.00      134.00
134.00      134.00      530.00      530.00      530.00
530.00      552.00      552.00      552.00      552.00
552.00      899.00      899.00      899.00      899.00
899.00
2      23     249.50      200.50      246.72      196.91
0.000 0.043 0.087 0.130 0.174 0.217 0.261 0.304 0.348 0.391 0.435
0.478 0.522 0.565 0.609 0.652 0.696 0.739 0.783 0.826 0.870 0.913
0.957 1.000
49.00 49.00 49.00 49.00 49.00 49.00 49.00 49.00 49.00 49.00 49.00
49.00 450.00      450.00      450.00      450.00      450.00
450.00      450.00      450.00      450.00      450.00
450.00      450.00
1      23     989.00      0.00  989.00      0.00
0.000 0.043 0.087 0.130 0.174 0.217 0.261 0.304 0.348 0.391 0.435
0.478 0.522 0.565 0.609 0.652 0.696 0.739 0.783 0.826 0.870 0.913
0.957 1.000
989.00      989.00      989.00      989.00      989.00
989.00      989.00      989.00      989.00      989.00
989.00      989.00      989.00      989.00      989.00
989.00      989.00      989.00      989.00      989.00
989.00      989.00      989.00      989.00
0      0
se-D is empty
```

```
     0      0
 se-D is empty
     0      0
 se-D is empty
     0      0
 se-D is empty
[SERIES DRY]
     5     23     1.00  0.00  1.00  0.00
     0.000 0.043 0.087 0.130 0.174 0.217 0.261 0.304 0.348 0.391 0.435
     0.478 0.522 0.565 0.609 0.652 0.696 0.739 0.783 0.826 0.870 0.913
     0.957 1.000
     1.00  1.00  1.00  1.00  1.00  1.00  1.00  1.00  1.00  1.00  1.00
     1.00  1.00  1.00  1.00  1.00  1.00  1.00  1.00  1.00  1.00  1.00
     1.00  1.00
    11     23     21.00 61.98 24.35 64.52
     0.000 0.043 0.087 0.130 0.174 0.217 0.261 0.304 0.348 0.391 0.435
     0.478 0.522 0.565 0.609 0.652 0.696 0.739 0.783 0.826 0.870 0.913
     0.957 1.000
     1.00  1.00  1.00  1.00  1.00  1.00  1.00  1.00  1.00  1.00  1.00
     1.00  1.00  2.00  2.00  2.00  2.00  2.00  2.00  2.00  2.00
   217.00       217.00      217.00
    17     23     1.53  0.85  1.59  0.85
     0.000 0.043 0.087 0.130 0.174 0.217 0.261 0.304 0.348 0.391 0.435
     0.478 0.522 0.565 0.609 0.652 0.696 0.739 0.783 0.826 0.870 0.913
     0.957 1.000
     1.00  1.00  1.00  1.00  1.00  1.00  1.00  1.00  1.00  1.00  1.00
     1.00  1.00  1.00  1.00  2.00  2.00  2.00  2.00  2.00  2.00  3.00
     4.00  4.00
    17     23     1.29  0.57  1.27  0.54
     0.000 0.043 0.087 0.130 0.174 0.217 0.261 0.304 0.348 0.391 0.435
     0.478 0.522 0.565 0.609 0.652 0.696 0.739 0.783 0.826 0.870 0.913
     0.957 1.000
     1.00  1.00  1.00  1.00  1.00  1.00  1.00  1.00  1.00  1.00  1.00
     1.00  1.00  1.00  1.00  1.00  1.00  1.00  2.00  2.00  2.00  2.00
     3.00  3.00
     5     23     1.60  0.80  1.62  0.80
     0.000 0.043 0.087 0.130 0.174 0.217 0.261 0.304 0.348 0.391 0.435
     0.478 0.522 0.565 0.609 0.652 0.696 0.739 0.783 0.826 0.870 0.913
     0.957 1.000
     1.00  1.00  1.00  1.00  1.00  1.00  1.00  1.00  1.00  1.00  1.00
     1.00  1.00  1.00  2.00  2.00  2.00  2.00  2.00  3.00  3.00  3.00
     3.00  3.00
     0      0
 se-D is empty
     0      0
 se-D is empty
     0      0
 se-D is empty
     0      0
 se-D is empty
```

```
 1     23    2.00  0.00  2.00  0.00
0.000 0.043 0.087 0.130 0.174 0.217 0.261 0.304 0.348 0.391 0.435
0.478 0.522 0.565 0.609 0.652 0.696 0.739 0.783 0.826 0.870 0.913
0.957 1.000
2.00  2.00  2.00  2.00  2.00  2.00  2.00  2.00  2.00  2.00  2.00
2.00  2.00  2.00  2.00  2.00  2.00  2.00  2.00  2.00  2.00  2.00
2.00  2.00
0     0
se-D is empty
 1     23    1.00  0.00  1.00  0.00
0.000 0.043 0.087 0.130 0.174 0.217 0.261 0.304 0.348 0.391 0.435
0.478 0.522 0.565 0.609 0.652 0.696 0.739 0.783 0.826 0.870 0.913
0.957 1.000
1.00  1.00  1.00  1.00  1.00  1.00  1.00  1.00  1.00  1.00  1.00
1.00  1.00  1.00  1.00  1.00  1.00  1.00  1.00  1.00  1.00  1.00
1.00  1.00
[END]
```

Appendix C.   Recharge model sensitivity analysis

Model sensitivity to K values

The sensitivity of the model to different K values for the limestone was assessed using two model runs of lower and higher K values based on the range for hydraulic conductivity of limestones published in Charvet (2009). The lowest value for limestones at the 100s of kilometres scale was 1×10^{-6} m/s, and the highest value was 6 m/s. These were used for all three limestone types (laja, sascab, coquina).   These two simulations were run for the same period as the initial historical model, from 1979-2005, and used the stochastic historical climate data.   For the purpose of the sensitivity analysis described here, the stochastic historical model run is termed the baseline scenario. The results of these model runs are shown in Table C.

Table C1.   Average annual water balance components for the hydraulic conductivity sensitivity analysis. 6 m/s was used for the high K scenario, 1×10^{-6} m/s was used for the low K scenario, and the baseline scenario (middle K scenario) was 1.2 m/s.

	High K scenario		Low K scenario		Baseline (middle K) scenario	
	Average annual amount (mm)	Percent of precipitation (%)	Average annual amount (mm)	Percent of precipitation (%)	Average annual amount (mm)	Percent of precipitation (%)
Precipitation	2161.19	100.00	2161.19	100.00	2340.77	100.00
Evapotranspiration	652.03	30.17	670.63	31.03	616.07	26.32
Overland boundary flow/runoff	238.11 (out)	11.02 (out)	254.96 (out)	11.80 (out)	273.50 (out)	11.68 (out)
Saturated zone boundary flow	1265.19 (out), -0.52 (in)	58.54 (out), -0.02 (in)	1225.30 (out)	56.70 (out)	1445.76 (out), -0.03 (in)	61.77 (out), 0.00 (in)
Overland storage change	0.30	0.01	0.30	0.01	0.23	0.01
Unsaturated zone storage change	-0.56	-0.03	0.01	0.00	-0.33	-0.01
Recharge	1264.67	58.52	1225.30	56.70	1445.76	61.76
Error	-6.63	-0.31	-8.67	-0.40	-5.53	-0.24

The water balance components for the low K scenario indicate the low hydraulic conductivity has very little effect on the model. There is a slight decrease in recharge from 58.5% (in the middle K scenario) to 56.7% in the low K scenario, as well as a 0.78% increase in runoff and a 1.12% increase in ET. The water balance components for the high K scenario are even more similar to the baseline scenario, indicating that the slight increase in K to 6 m/s has little effect on the water balance components.

The average annual water balance components show that the high K scenario has an identical seasonal distribution of recharge, ET, and runoff to the baseline scenario (Figure C). This could be because the initial K estimate was purposely chosen to be slightly higher than many of the published values, to represent the porosity of fractures at a larger scale. For this reason, a much higher value of K for the scale of the model was not within the published values, and not viable for a sensitivity analysis. The low K scenario has slightly greater runoff than the baseline scenario, with the greatest difference being during the wet season. The seasonal distribution of recharge varies slightly in the low K scenario; four months have greater recharge than the baseline scenario (January, April, July, November), five have lower recharge (March, May, June, August, October) while the rest have the same amount of monthly recharge. This difference in the seasonal distribution of recharge in the low K scenario is interesting, because overall this scenario has slightly lower recharge than both the baseline scenario and the higher K scenario. The seasonal distribution of the low K scenario deviates slightly from the seasonal precipitation pattern, which shows that recharge is not as closely linked to precipitation in this scenario as it is in others. A direct link between precipitation and recharge was expected for the Yucatan Peninsula, as the karst limestone allows rapid infiltration, so this scenario confirms that using a low conductivity and not including macropores somewhat limits the effect of rapid infiltration.

Figure C1. **Average monthly water balance components for the High K (6 m/s),**
Low K (1 x 10^{-6} m/s) and baseline (middle K, 1.2 m/s) scenarios.
Note that the high K and baseline scenarios have identical seasonal
distributions for ET, runoff, and recharge. The stochastic
precipitation data were used for all three simulations.

Model sensitivity to macropores

Two options were available to simulate the fractures/solution cavities in the limestones
on the Yucatan Peninsula, which are known to allow rapid infiltration through the
unsaturated zone and to channel groundwater flow (Back and Hanshaw, 1980). The
final historical model used a mid-range value for K (which is representative of the
limestone at a large scale) to simulate both the low K of the limestone matrix and the
high K of the macropores. A second option explored in this sensitivity analysis is to
assign a macroporosity to the limestones in MIKE SHE, and assign a low value to the
limestone matrix. In the macropore simulation, the low K value of 1 x 10^{-6} m/s used in
the low K sensitivity analysis was used to represent to limestone matrix for all three
limestone types. Porosity of the macropores was set at 20%, which was mid-range of
the values published in Charvet (2009), which ranged from 7 to 41% around Merida
(Gonzalez Herrera, 1984, cited in Steinich and Marin, 1997). Other parameters used in
macropore flow include (DHI, 2007b):

- Conductivity exponent: an empirical exponent related to size distribution, the
  continuity of macropores, and tortuosity. The conductivity exponent ranges

168

from 2-6 (Jarvis, 1994), where lower values represent a coarse soil with a small pore size distribution (i.e. macropores are a similar size as matrix pores), and higher values represent soils with a larger pore size distribution. A value of 6 was chosen to represent karstic limestones on the Yucatan Peninsula, which should have a much higher porosity compare to the matrix.

- Pressure threshold: the capillary pressure in the matrix above which flow can occur in the macropores. This value was left as 0 (air pressure), allowing macropore flow to occur at any time in the model.

- Water transfer coefficient (β_{mp}): describes the distance between macropores (increases with decreasing distance between macropores). The water transfer coefficient for macropores to matrix and matrix to macropores were both assigned as 0.5 m^{-2}, which is a middle value based on a 1 m-long diffusion path and is the default value of the model.

MIKE SHE has two options for macropore flow: full macropore and simplified macropore (bypass flow). Bypass flow allows a portion of infiltrating water to flow through the soil, while the rest directly recharges the groundwater. The amount of water that is allowed to pass through the macropores is determined by a user-specified maximum fraction of precipitation and on the water content of the unsaturated zone (DHI, 2007b). Bypass flow is calculated by:

$$Q_{bypass} = P_{net} P_{frac} \sqrt{\alpha_{10}\beta_{50}} / \Delta t \qquad (C.1)$$

where P_{net} is the net rainfall, P_{frac} is the maximum fraction of rainfall allowed to pass through the macropores (user-specified), and α_{10} and β_{50} are parameters calculated by MIKE SHE to reduce the fraction that bypasses the soil matrix when the soil is dry. α_{10} and β_{50} are assigned numbers between 0 and 1 based on the moisture content 10 and 50 cm below the ground surface. Δt is the change in time (DHI, 2007b).

Full macropore flow involves creating a secondary pore domain (in addition to the soil matrix) in the unsaturated zone (DHI, 2007b). Flow in this domain is related to the pressure head and capillary head in the matrix domain. This method is much more computationally intensive than bypass flow, so for this model bypass flow was decided to be sufficient to simulate the karst features of the Yucatan limestones. The initial parameters used for bypass flow are:

- Maximum bypass constant: the maximum fraction of net rainfall that will infiltrate through the macropores. This value was set at 0.5 to allow a maximum of 50% of infiltration to occur through the macropores.

- Water content for reduced bypass flow: This value was left as the default (0.15) due to a lack of information on the water content necessary to reduce bypass flow.

- Water content limit for bypass flow: The water content below which no bypass flow occurs. This value was also left as the default (0.05).

This simulation was run for the same period as the initial historical simulation, which ran from 1979-2005 and used the stochastic historical climate data. The results from this model run (macropore scenario) are given in (Table C) with the results from the stochastic historical simulation (baseline scenario) for comparison.

Table C2.   Average annual water balance components for the macropore scenario and the baseline scenario.

	Macropore scenario		Baseline scenario	
	Average annual amount (mm)	Percent of precipitation (%)	Average annual amount (mm)	Percent of precipitation (%)
Precipitation	2161.19	100.00	2161.19	100.00
Evapotranspiration	649.11	30.03	651.70	30.15
Overland boundary flow/runoff	120.19 (out)	5.56 (out)	238.11 (out)	11.02 (out)
Saturated zone boundary flow	1389.52 (out)	64.29 (out)	1265.07 (out), -0.04 (in)	58.54 (out), 0.00 (in)
Overland storage change	0.26	0.01	0.30	0.01
Unsaturated zone storage change	1.30	0.06	-0.56	-0.03
Recharge	1389.52	64.29	1265.07	58.54
Error	-0.78	-0.04	-6.59	-0.31

The macropore scenario has an increased percent of recharge compared to the baseline scenario (64% compared to 58%), corresponding with a lower percent of runoff (5% in the macropore scenario compared to 11% in the baseline scenario). This indicates that using the macropores allows more infiltration to occur. For the purpose of this modeling study, a large-scale K estimate (as was done for the initial model) is likely more representative of the regional K value, as detailed information about local fractures and karst dissolution features was not available. The average monthly water balance components for the macropore model also show that the seasonal distribution of ET is nearly identical to the baseline scenario and that all months have lower runoff than the baseline scenario (Figure C). The difference in runoff is the most apparent in the wet season (a difference of up to 20 mm/month), when precipitation is the highest. The differences in recharge are more complex, although overall there is more recharge in the macropore model. Recharge in the macropore scenario is higher than in the baseline scenario in all months except February, March, May, June, and August. The macropore recharge appears to be a slightly smoothed compared to the baseline recharge, although the pattern is still very similar to that of precipitation.

Figure C2. **Average monthly water balance components for the macropore and baseline scenarios. Both scenarios used the stochastic historical climate data.**

Model sensitivity to changes in LAI

The sensitivity of the model to changes in LAI were analyzed to determine the potential for changes in LAI to effect the TCP model simulations, which had a reduced LAI by 25%. Four LAI scenarios were run: the baseline scenario (with stochastic historical precipitation), the baseline scenario using the TCP LAI, the stochastic reconstruction (using the stochastic TCP precipitation), and the stochastic reconstructions without reduced LAI. The seasonal water balance components of these four simulations show that LAI has little to no effect on the model (Figure C). The two historical scenarios (with and without LAI change) are virtually identical, as are the two TCP scenarios (with and without LAI change). Although the LAI was reduced in the TCP models to simulate environmental stress during the Mayan times, this result is desirable because it means the changes seen between the TCP and historical models are not just an effect of the reduced LAI, but also the shifted climate.

171

Figure C3. Average monthly water balance components for the LAI scenarios and the baseline scenario.

Appendix D.   Climate variability on the Yucatan Peninsula

The correlation of precipitation and temperature to the strength of climate cycles (ENSO, PDO) is explored in this Appendix using the Spearman Rank Correlation. This type of correlation is useful for data that are non-linear but monotonic (i.e. one variable increases or decreases as the other variable increases).   The relationship between climate cycle indices and climate variables is not necessarily linear, as the precipitation (or temperature) that occurs in any area is dependent on many variables.   However, in general, El Nino years are cooler and experience more precipitation on the Yucatan Peninsula, and La Nina years are the opposite, which leads to the assumption that the relationship is monotonic.   The Spearman Rank Correlation is conducted by ranking the two variables and determining the correlation between the two ranked series.

Data for these analyses were obtained from the Joint Institute for the Study of the Atmosphere and Ocean (JISAO) website (Mitchell, 2005) and the NOAA Climate Prediction Center (NOAA, 2003).   The Oceanic Nino Index (ONI) data included a record of the strength of El Nino and La Nina events in each year (weak, moderate, strong, or neutral), and these classifications were used to choose a strong El Nino year (1987) and a strong La Nina year (1975) on record.   Observed temperature and precipitation data were compiled from the daily observed record from Merida Airport (used in Chapters 2 and 3).

Analysis of the ONI and observed temperature and precipitation on the Yucatan Peninsula show that temperature and precipitation are not directly linked to the ONI (Figure D). A significant correlation is only found between precipitation and ONI during a strong El Nino year (10% significance level). It is not unexpected that there is no strong correlation in a strong La Nina year, as climate anomalies during La Nina years are known to be less pronounced than those that occur during El Nino years (Pavia et al., 2006).   It may also be difficult to determine if there is a strong correlation between temperature and any climate index, as temperature on the Yucatan Peninsula is not very variable.

Figure D1. Spearman Rank Correlation between precipitation and temperature and the ONI during a strong El Nino and a strong La Nina year in the observed record. The precipitation and ONI correlation in an El Nino year (top right) corresponds to a Spearman Rank Coefficient of 0.4988, which has a 10% significance level.

Other climate cycles (PDO and MJO) also have the potential to affect climate on the Yucatan Peninsula, as they affect sea surface temperature (SST), cyclone activity, temperature, precipitation, and wind patterns. The Southern Oscillation Index (SOI, another measure of ENSO), PDO and MJO indices were compared with observed temperature, precipitation, and storm count to analyze the effects of these three main climate cycles on the climate of the Yucatan Peninsula (Table D). These correlations showed that temperature has a significant correlation with SOI, but precipitation and storm count do not. However, precipitation is significantly correlated with the PDO and MJO indices while temperature is not. Storm count is not significantly correlated to any of these climate cycles.

Table D1. **Spearman Rank Correlation between annual SOI, PDO, MJO and annual observed temperature, precipitation, and storm count on the Yucatan Peninsula (1973-2013).**

	SOI	PDO	MJO
Temperature	**-0.2088**	-0.1589	-0.1593
Precipitation	0.14792	**-0.2587**	**0.2507**
Storm count	-0.2022	0.0056	0.0271

Bold values indicate a 10% significance level (no correlations showed a 5% significance level)

These mixed results suggest that relating precipitation and temperature to any one of these climate indices is an over-simplification of the observed climate patterns. Precipitation and temperature on the Yucatan Peninsula depend on the combination of these cycles, as well as other climate phenomena in the area (such as seasonal shifts in the ITCZ, see Chapter 1). In addition, these comparisons were conducted at an annual scale, but it is possible that SOI, PDO, and MJO have a more seasonal effect on these climate variables. Future analysis of the effects of climate cycles on temperature, precipitation, and storm count could focus on the dry season (November-April) to determine the possible effects of these climate cycles on dry season droughts.

A reconstruction of ENSO index (Li et al., 2011) was also compared to the reconstructed precipitation from the speleothem record from Medina-Elizalde et al. (2010). This precipitation reconstruction was identified in Chapter 2 as one of the most reliable reconstructions based on the number of modern data points available in the proxy record. However, the Spearman Rank Coefficient between reconstructed ENSO and precipitation was only -0.0278 (not significant). However, the reconstructed precipitation has reduced variability compared to observed annual precipitation (see Chapter 3), which may weaken the relationship between the two variables. Although the relationships between climate cycles are complex, understanding if ENSO (and PDO, MJO and other climate cycles) variability was different in the past climate could be a key link for reconstructing paleoclimate, and it would be beneficial to further analyze these relationships in future studies.